CHANNEL MODELING FOR VEHICULAR VISIBLE LIGHT COMMUNICATION

A Dissertation

by

Hossien Eldeeb

Submitted to the
Graduate School of Sciences and Engineering
In Partial Fulfillment of the Requirements for
the Degree of

Doctor of Philosophy

in the
Department of Electrical and Electronics Engineering

Özyeğin University
December 2021

Copyright © 2021 by Hossien Eldeeb

CHANNEL MODELING FOR VEHICULAR VISIBLE LIGHT COMMUNICATION

Approved by:

Professor Murat Uysal, Advisor
Department of Electrical and
Electronics Engineering
Özyeğin University

Assistant Professor Kadir Durak
Department of Electrical and
Electronics Engineering
Özyeğin University

Associate Professor Cenk Demiroğlu
Department of Electrical and
Electronics Engineering
Özyeğin University

Associate Professor Ertuğrul Başar
Department of Electrical and
Electronics Engineering
Koç University

Date Approved: 28 December 2021

Professor Serhat Erküçük
Department of Electrical and
Electronics Engineering
Kadir Has University

To My Beloved Parents, My Lovely Wife, and My Wonderful Children

ABSTRACT

The demand for vehicular communication systems has increased since they are considered the key enabling technology for Intelligent Transportation Systems (ITSs). Vehicular communications allow information sharing between the vehicles and the infrastructures, which have great potential in improving road safety, traffic flow, and passenger comfort along the road. The resulting vehicular connectivity forms are Vehicle-to-Vehicle (V2V), Vehicle-to-Infrastructure (V2I), Infrastructure-to-Vehicle (I2V), and Vehicle-to-Pedestrian (V2P), commonly referred to as Vehicle-to-Everything (V2X) communication. Most of the research efforts and standardization activities on V2X communication have focused on Radio Frequency (RF) technologies. However, limited RF bands allocated for V2X networks can suffer high interference levels in heavy traffic, and channel congestion might be particularly problematic for delay-sensitive safety functionalities. To address such issues, Visible Light Communication (VLC) has been proposed as an alternative or complementary vehicular access solution to RF-based V2X communications.

VLC is based on the principle of modulating the intensity of the Light-Emitting-Diode (LED) and enables the dual use of LED for both illumination and communication purposes. The ubiquitous availability of LED-based streetlights, traffic lights, and automotive exterior lighting positions VLC as a potential wireless connectivity solution for vehicular networks. Vehicular VLC has received increasing attention recently in several aspects such as physical layer design, upper layer network protocols, and integration with RF-based solutions for hybrid systems. As in any other communication system, channel modeling plays a critical role in VLC system design and optimization. Earlier results in the literature have focused on indoor channel modeling. Those results do not apply to vehicular VLC systems since they exhibit inherently different characteristics to indoor counterparts. For example, the ideal Lambertian model, used for indoor

LED luminaries, fails to match the illumination characteristics of automotive Headlights (HLs), Taillights (TLs), traffic lights, and streetlights. In addition, the effects of road reflectance, road type, weather conditions, the orientation of the user/vehicle equipment and infrastructures, receiver aperture size, and the sunlight might strongly affect the link performance of vehicular VLC systems. Despite the increasing attention on indoor VLC channel models, there is a lack of realistic vehicular VLC channel models.

Motivated by these, we provide in this dissertation a comprehensive channel modeling study for different vehicular VLC links. In the first part of this dissertation, we explain our channel modeling approach, which builds upon advanced non-sequential ray tracing features of OpticStudio software. This approach allows the integration of any realistic light source radiation pattern. It can handle a large number of reflections for better accuracy. Since this is a simulation-based channel modeling methodology, it must be validated, at least once, against the measurements in a real scenario. Therefore, we carry out measurements and simulations for the same cases to validate our channel modeling approach considering both the Line of Sight (LoS) and the Non-Line of Sight (NLoS) cases.

Such a realistic channel modeling approach is then adopted to model the V2V VLC channel when two vehicles travel in the same lane and by utilizing the Headlights (HLs) of the source vehicle as wireless transmitters. The most recent proposed channel path loss model was a linear function of transmission distance applicable only for ranges less than 20 meters. Therefore, we propose a new path loss expression that takes the form of a negative exponential function and provides an excellent match to simulation results for large transmission ranges and under different weather conditions. This expression is then utilized to derive the achievable transmission distance for a targeted data rate while satisfying a given value of Bit Error Rate (BER). We then consider V2V based Taillights (TLs) and derive a new path loss model that works for measured TL radiation patterns of different commercial car models. Utilizing the derived path loss model, we further derive a closed-form expression for the maximum transmission distance under the target BER value. Furthermore, the Root-Mean-Square (RMS) delay spread is investigated by

considering different V2V density scenarios. In the above points, the effect of both the lateral shift between the two vehicles, the exact geometry of the vehicle's HLs, and the receiver aperture on the path loss model of the V2V system is excluded. Therefore, to address such shortcoming, we develop a closed-form path loss expression for the V2V VLC system as a function of link distance, lateral shift between the two vehicles, weather type, transmitter beam divergence angle, and receiver aperture diameter.

While several vehicular VLC efforts investigated the V2V link channels while only a few attentions were paid to V2I/I2V channels, and by considering very idealistic assumptions. Motivated by this, we consider the I2V VLC links where the traffic lights and streetlights are deployed as wireless transmitters. First, we model the I2V based on a commercial traffic light and derive a closed-form expression of the path loss model as a function of both longitudinal and lateral shift distances. Then, we model the I2V system with street light transmitters and derive a closed-form expression for channel path loss as a function of pole spacing, the height of both the lighting pole and the vehicle, the longitudinal and lateral distance between the vehicle and the pole, and the aperture size of the Photodetector (PD). The effect of these transceiver and infrastructure parameters on the system average error rate performance is also investigated considering the mobility of vehicular communication, which makes the path loss no longer deterministic. We further model the reverse channel link, i.e., the V2I system, where the vehicle communicates with an infrastructure pole deploying its HLs as transmitters, and three PDs located within the traffic pole to act as receivers. Based on the Channel Impulse Responses (CIRs), obtained from the ray tracing, we introduce an expression for the achievable capacity considering the effect of propagation environment and the LED non-linear characteristics.

In most V2V and I2V VLC works, the most common underlying assumption is using one or two PDs. That might be sufficient for establishing a connection between two vehicles cruising in the same straight lane or between the vehicles and infrastructure with clear LoS. To position VLC as a strong candidate for vehicular connectivity, it

is essential to realize multi-directional reception in various deployment scenarios supporting V2V and I2V links. To address this of practical relevance, we investigate the channel modeling of multi-directional coverage for vehicular VLC systems in different road types and traffic scenarios. We quantify the capability of receiving signals in several cases including the V2V connectivity (with HLs and TLs) and the I2V connectivity (with traffic and streetlights). We further quantify the contribution of individual PDs to elaborate on the usage cases of each PD.

In the last part of this dissertation, we explore the vehicular VLC as a wireless connectivity solution to enable outdoor broadcasting for public safety systems. We utilize the ubiquitous streetlights as wireless transmitters taking into account the fundamental differences imposed by the outdoor medium and lightning infrastructure. These include the effect of the asymmetrical pattern of streetlights, the orientation of the user equipment, the weather condition, and the solar irradiance. We consider two broadcasting scenarios; VLC broadcasting in the roadway and VLC broadcasting in the sidewalk path, and obtain the received Signal-to-Noise Ratios (SNRs) for all links under the mobility condition.

ÖZETÇE

Akıllı ulaşım sistemleri (ITS'ler) için anahtar etkinleştirici teknoloji olarak kabul edildiklerinden, araç iletişim sistemlerine olan talep artmıştır. Araç iletişimi, araçlar ve yol boyunca altyapılar arasında bilgi paylaşımını sağlar. Böyle gelişmiş bir bağlantı çözümü, geleceğin AUS'lerinin ana hedefleri olan yol güvenliğini, trafik akışını ve yolcu konforunu iyileştirmede büyük potansiyele sahiptir. Ortaya çıkan araç bağlantı biçimleri, araçtan araca (V2V), araçtan altyapıya (V2I), araçtan yayaya (V2P), genellikle araçtan her şeye (V2X) iletişim olarak adlandırılır. AUS'lerin pratik uygulamaları son derece sağlam, ölçeklenebilir ve güvenilir V2X çözümleri gerektirdiğinden, araç iletişimine yönelik araştırma çalışmaları ve standardizasyon faaliyetleri sürekli artmaktadır. Bu çabaların çoğu şimdiye kadar radyo frekansı (RF) teknolojileri etrafında toplanmıştır. Bununla birlikte, V2X ağları için ayrılan sınırlı RF bantları, yoğun trafikte yüksek düzeyde parazite maruz kalabilir ve kanal tıkanıklığı, gecikmeye duyarlı güvenlik işlevleri için özellikle sorunlu olabilir. Bu tür sorunları ele almak için, RF tabanlı V2X iletişimine alternatif veya tamamlayıcı bir araç erişim çözümü olarak görünür ışık iletişimi (VLC) önerilmiştir.

VLC, ışık yayan diyotun (LED) yoğunluğunu modüle etme ilkesine dayanır ve hem aydınlatma hem de iletişim amaçları için LED'in ikili kullanımını sağlar. LED tabanlı sokak lambaları, trafik ışıkları ve otomotiv dış aydınlatmasının her yerde bulunması, VLC'yi araç ağları için potansiyel bir kablosuz bağlantı çözümü olarak konumlandırıyor. Araç VLC, fiziksel katman tasarımı, üst katman ağ protokolleri ve hibrit sistemler için RF tabanlı çözümlerle entegrasyon gibi çeşitli yönlerden son zamanlarda artan bir ilgi görmüştür. Diğer iletişim sistemlerinde olduğu gibi, kanal modelleme VLC sistem tasarımı ve optimizasyonunda kritik bir rol oynar. Literatürdeki daha önceki sonuçlar, iç mekan kanal modellemesine odaklanmıştır. Bu sonuçlar, iç

mekan benzerlerinden doğal olarak farklı özellikler sergiledikleri için araç VLC sistemleri için geçerli değildir. Örneğin, iç mekan LED armatürleri için kullanılan ideal Lambertian modeli, otomotiv HL, TL, trafik ışıkları ve sokak ışıklarının aydınlatma özellikleriyle uyuşmamaktadır. Ek olarak, yol yansıması, yol tipi, hava koşulları, kullanıcı/araç ekipmanı ve altyapılarının oryantasyonu, alıcı açıklığı boyutu ve güneş ışığının etkileri, araç VLC sistemlerinin bağlantı performansını güçlü bir şekilde etkileyebilir. İç mekan VLC kanal modellerine artan ilgiye rağmen, gerçekçi araç VLC kanal modellerinde eksiklik var.

Bunlardan motive olarak, bu tezde, iyi kurulmuş bir kanal modelleme yaklaşımı kullanan farklı araç VLC bağlantıları için kapsamlı bir kanal modelleme çalışması sunuyoruz. Bu tezin ilk bölümünde, OpticStudio yazılımının gelişmiş sıralı olmayan ışın izleme özelliklerine dayanan böyle bir kanal modelleme yaklaşımını açıklıyoruz. Bu yaklaşım, herhangi bir gerçekçi ışık kaynağı radyasyon modelinin entegrasyonuna izin verir. Daha iyi doğruluk için çok sayıda yansımayı işleyebilir. Bu simülasyon tabanlı bir kanal modelleme metodolojisi olduğundan, gerçek bir senaryodaki ölçümlere karşı en az bir kez doğrulanmalıdır. Bu nedenle, hem Görüş Hattı (LOS) hem de Görüş Dışı (NLoS) durumları göz önünde bulundurarak kanal modelleme yaklaşımımızı doğrulamak için aynı durumlar için ölçümler ve simülasyonlar gerçekleştiriyoruz.

İki araç aynı şeritte seyahat ettiğinde ve kablosuz vericiler olarak kaynak aracın HL'lerini kullanarak V2V VLC kanalını modellemek için böyle iyi kurulmuş gerçekçi bir kanal modelleme yaklaşımı benimsenmiştir. En son önerilen kanal yolu kaybı modeli, yalnızca 20 metreden daha kısa mesafeler için geçerli olan iletim mesafesinin doğrusal bir fonksiyonuydu. Bu nedenle, geniş iletim aralıkları için V2V kanal modellemesini araştırıyoruz ve negatif üstel fonksiyon şeklini alan ve geniş iletim aralıkları ve farklı hava koşulları altında simülasyon sonuçlarıyla mükemmel bir eşleşme sağlayan yeni bir yol kaybı ifadesi öneriyoruz. Bu ifade daha sonra, belirli bir bit-hata oranı (BER) değerini karşılarken, hedeflenen bir veri hızı için ulaşılabilir iletim mesafesini türetmek için kullanılır. Araç VLC'sinde hem HL'ler hem de TL'ler optik vericiler olarak kullanılabilir, ancak araç VLC'sinde bildirilen çoğu çalışma HL'lere

dayalı vericilere odaklanmıştır. Bu nedenle, V2V tabanlı TL'leri dikkate alıyoruz ve farklı ticari araba modellerinin ölçülen TL radyasyon modelleri için çalışan yeni bir yol kaybı modeli türetiyoruz. Türetilmiş yol kaybı modelini kullanarak, ayrıca, hedef BER değeri altındaki maksimum iletim mesafesi için kapalı biçimli bir ifade türetiyoruz. Ayrıca, farklı V2V yoğunluk senaryoları dikkate alınarak RMS gecikme yayılımı incelenmiştir.

Yukarıdaki noktalarda, hem iki araç arasındaki yanal kaymanın, aracın HL'lerinin tam geometrisinin hem de alıcı açıklığının V2V sisteminin yol kaybı modeli üzerindeki etkisi hariç tutulmuştur. Bu nedenle, bu tür eksiklikleri gidermek için, V2V VLC sistemi için bağlantı mesafesinin, iki araç arasındaki yanal kaymanın, hava tipinin, verici ışın sapma açısının ve alıcı açıklık çapının bir fonksiyonu olarak kapalı biçimli bir yol kaybı ifadesi geliştirdik. Önerilen model daha sonra sistem performansını analiz etmek için kullanılır. Birkaç araç VLC çalışması, V2V bağlantı kanallarını araştırırken, V2I/I2V kanallarına sadece birkaç çalışmada yer verildi ve çok idealist varsayımlar dikkate alındı.

Bundan yola çıkarak, HL'lere/TL'lere ek olarak trafik ışıklarının ve sokak ışıklarının kablosuz vericiler olarak yerleştirildiği I2V VLC bağlantılarını düşünüyoruz. İlk olarak, ticari bir trafik ışığına dayalı olarak I2V'yi modelliyoruz ve hem uzunlamasına hem de yanal kaydırma mesafelerinin bir fonksiyonu olarak yol kaybı modelinin kapalı biçimli bir ifadesini türetiyoruz. Önerilen model daha sonra hibrit I2V-V2V sistemi için optimum güç tahsisini elde etmek için kullanılmaktadır. Daha sonra, I2V sistemini sokak ışık vericileri ile modelliyoruz ve alıcı-verici ve altyapı parametrelerinin bir fonksiyonu olarak kanal yolu kaybı için kapalı formda bir ifade elde ediyoruz. Bunlar, direk aralığını, hem aydınlatma direğinin hem de aracın yüksekliğini, araç ile direk arasındaki uzunlamasına ve yanal mesafeyi ve PD'nin açıklık boyutunu içerir. Bu alıcı-verici ve altyapı parametrelerinin sistem ortalama hata oranı performansı üzerindeki etkisi, yol kaybını artık deterministik olmaktan çıkaran araç iletişiminin hareketliliği de dikkate alınarak araştırılmıştır. Aracın HL'lerini verici olarak dağıtan bir altyapı direği ile iletişim kurduğu ters kanal bağlantısını, yani V2I sistemini ve hareket etmesi

için trafik direği içinde, sarı, kırmızı ve yeşil LED armatürlerinin bitişiğinde bulunan üç PD'yi modelliyoruz. Kablosuz alıcılar olarak Işın izlemeden elde edilen CIR'lere dayanarak, yayılma ortamının etkisi ve LED'in doğrusal olmayan özellikleri dikkate alınarak ulaşılabilir kapasite için bir ifade sunuyoruz.

Çoğu V2V ve I2V VLC çalışmasında, en yaygın temel varsayım bir veya iki PD kullanmaktır. Bu, aynı düz şeritte seyreden iki araç arasında veya araçlar ile altyapı arasında net LOS ile bağlantı kurmak için yeterli olabilir. VLC'yi araç bağlantısı için güçlü bir aday olarak konumlandırmak için, V2V ve I2V bağlantılarını destekleyen çeşitli dağıtım senaryolarında çok yönlü alımı gerçekleştirmek esastır. Bunu başarmak için yeterli sayıda gerekli PD'nin ne olduğu açık bir soru olarak kalmaktadır. Bu tür pratik uygunluk sorusunu ele almak için, farklı yol tiplerinde (yani, çok şeritli, kavisli yollar), kavşaklarda (yani, T-şekilli, Y-şekilli kavşaklar) araç VLC sistemleri için çok yönlü kapsamın kanal modellemesini araştırıyoruz. , ve trafik senaryoları (yani, aynı veya farklı şeritlerde seyir, şerit değişikliği vb.). V2V bağlantısı (ön ve arka yönlerde) ve I2V bağlantısı (trafik ve sokak lambaları ile) dahil olmak üzere çeşitli durumlarda sinyal alma kapasitesini ölçmek için bir kanal modelleme çalışması yürütüyoruz. Her bir PD'nin kullanım durumlarını detaylandırmak için bireysel PD'lerin katkısını daha da nicelleştiriyoruz.

Bu tezin son bölümünde, kamu güvenliği sistemleri için dış mekan yayınını mümkün kılmak için bir kablosuz bağlantı çözümü olarak keşfederek araç VLC'sinin pratik bir uygulamasını ele alıyoruz. Dış ortam ve aydınlatma altyapısının dayattığı temel farklılıkları dikkate alarak her yerde bulunan sokak ışıklarını kablosuz vericiler olarak kullanıyoruz. Bunlar, sokak lambalarının asimetrik düzeninin etkisini, kullanıcı ekipmanının yönünü, hava durumunu ve güneş ışınımını içerir. İki yayın senaryosu ele alıyoruz; Karayolunda VLC yayını ve kaldırım yolunda VLC yayını ve hareketlilik koşulu altındaki tüm bağlantılar için alınan SNR'yi alın.

ACKNOWLEDGEMENTS

I want to express my appreciation to my advisor, Prof. Murat Uysal, for his wisdom, friendship, encouragement, support, patient guidance, invaluable insights, and suggestions during this experience as a Ph.D. student and research assistant. The work of the thesis would not be possible without his consistent support and guidance. I also had a great chance to work with him. I will never forget his support and help in providing numerous opportunities to learn and develop as a researcher.

I am truly grateful to the members of my dissertation committee, Assoc. Prof. Ertuğrul Başar, Asst. Prof. Kadir Durak, Assoc. Prof. Cenk Demiroğlu, and Prof. Serhat Erküçük for their time serving on my committee and carefully reviewing my dissertation. I would also like to thank the Vision project coordinator, Prof. Ali Khalighi for his support and guidance.

My warmest gratitude goes to my parents, who always supported me unconditionally throughout my life. I would like to lovingly thank my wife, Hasna, for her unconditional love, unrestricted kindness, and unlimited patience. I would thank her family (her mother and brothers: Hossam and Hatem) for their continuous support. I would like to thank my siblings: Ahmed and Walaa, and my friends at Giza-North Power station. I would love to thank my wonderful children: Joumana, Mohamed, and Malek. Some special words of gratitude go to all of my colleagues and friends in the CT&T Lab, particularly Dr. Mohammed Amassie, for their endless help and motivation.

This work was supported by the European Unions Horizon 2020 MSC ITN (VISION) under the Marie-Sklodowska Curie grant agreement number 764461. I would like to thank the project managers, Céline Auger and Melanie Dorier for their support and making this possible. Thanks Vision's supervision team, Volker Jungnickel, Stanislav Zvanovec, Zabih Ghassemlooy, Rafael Perez Jimenez, Luis Nero Alves, Gerhard Maierbacher, Emrah Kinav, and Bastien Bechadergue for their responsive reviews. I also thank all Vision's ESRs for the constructive collaborations.

ACRONYMS

APD	Avalanche Photodiode
BER	Bit Error Rate
C-V2X	Cellular-V2X
CFR	Channel Frequency Response
CIR	Channel Impulse Response
DC	Direct Current
DSRC	Dedicated Short-Range Communication
D2D	Device-to-Device
DD	Direct Detection
EGC	Equal Gain Combining
5G	Fifth Generation
Gb/s	Gigabits Per Second
HL	Headlight
IR	Infrared
I2P	Infrastructure-to-Pedestrian
I2V	Infrastructure-to-Vehicle
ITS	Intelligent Transportation System
IM	Intensity Modulation
LiFi	Light Fidelity
LED	Light-Emitting-Diode
LoS	Line of Sight
MIMO	Multiple-Input Multiple-Output
NLoS	Non-Line of Sight
O-LED	Organic-LED
PC	Phosphor-Converted

PIN	positive-intrinsic-negative
PD	Photodetector
PAM	Pulse-Amplitude Modulation
RF	Radio Frequency
RGB	Red-Green-Blue
RMS	Root-Mean-Square
SNR	Signal-to-Noise Ratio
SISO	Single-Input Single-Output
S2V	Streetlight-to-Vehicle
S2P	Streetlight-to-Pedestrian
TL	Taillight
VNA	Vector Network Analyser
V2X	Vehicle-to-Everything
V2I	Vehicle-to-Infrastructure
V2P	Vehicle-to-Pedestrian
V2V	Vehicle-to-Vehicle
VLC	Visible Light Communication

TABLE OF CONTENTS

LIST OF TABLES

LIST OF FIGURES

CHAPTER I

INTRODUCTION

1.1 Visible Light Communication

Visible light communication (VLC) is a novel fast-growing emerging technology that uses the unlicensed visible light spectrum (between 380 THz and 790 THz) as the communication medium [1–3]. VLC enables the data transmission by modulating information on the intensity of the Light Emitting Diodes (Light-Emitting-Diodes (LEDs)) achieving the dual functionality, that is, illumination and data transmission [4, 5]. Comparing with other conventional light sources, LEDs have attractive features include longer life expectancy, higher level of brightness, lower power consumption, higher tolerance to humidity, and less heat generation lighting [6–8]. VLC technology has a great potential in complementing or even substituting the existing radio frequency (RF) communication technologies in several application such as Device-to-Device (D2D) communications [9], indoor networking [10], vehicular networks [11, 12], medical applications [13], Internet access in airplane cabins [14], and positioning systems [15]. In VLC systems, three main parts should be considered: VLC Transmitter, VLC Receiver, and VLC Channel.

VLC Transmitter: The function of VLC transmitters is modulating the intensities of lighting sources (LEDs) at very high frequencies. As a result, the human eyes cannot perceive any difference in illumination compared to that when there is no modulation [16]. Consequently, VLC transmitters become able to achieve the dual functionality, i.e., illumination and data transmission simultaneously. VLC transmitters are affected by several factors including the intensity profile, spectral distribution, LED non-linearity characteristics, LED electrical-to-optical conversion efficiency. In VLC systems, different types of LEDs can be deployed including the Phosphor-Converted (PC) LED, the multi-colour LED, i.e., Red-Green-Blue (RGB) LED), the

Organic-LED (O-LED), and the Micro-LED (μ-LED) [17–20]. Each of these LEDs has different characteristics that make them proper for a specific application. O-LEDs can be considered the lowest cost one but with a significant limitation on the bandwidth (i.e., $\leq$ 1 MHz) [21]. On contrast, μ-LEDs provide a very large bandwidth (i.e., $\geq$ 300 MHz), however, their intricacy and cost are the bottleneck [22]. Generally, the most commonly used types are the PC LEDs and RGB LEDs. RGB LEDs have the ability to transmit the modulated data through three different color channels leading to a higher throughput with three times comparing with the single-channel LED. However, due to the cost-effectiveness and the simplified implementation of PC LEDs with respect to the RGB ones they are the most preferred type for producing white light [22]. Together with the LED source, a driver circuit is used to modulate the data using the emitted light and by controlling the flowing current through the LED [23].

VLC Receiver: The other critical element for realization of VLC system is the VLC receiver where the light detection is achieved by using the photodetectors (PDs). PDs are available either as stand-alone devices or in the form of an image sensor (camera sensor) which consists of a matrix of multiple PDs. Image sensors are existing in many of mobile devices such as smartphones however they can achieve a very limited data rates for VLC signals (i.e., a few kpbs) [24]. In contrast, the non-imaging PDs have the ability to receive the VLC signals with higher data rates [25], i.e., reaches to hundred of Mbps, hence, they are widely used for VLC systems. There are also several types of PDs, deployed in the VLC receivers, including the positive-intrinsic-negative positive-intrinsic-negative (PIN) PD, the Avalanche Photodiode (APD)), the photo-conductor, and the metal-semiconductor-metal PD. The most widely adopted ones are the PIN and APD PDs since their characteristics make them able to meet the VLC system requirements [22]. Together with the PD, which converts the incident optical power into electrical current, the VLC receiver contains an impedance amplifier device to amplify that current before reaching to the equalizer. Furthermore, the received rays at the VLC receiver pass first through an optical concentrator (to focus the rays on the sensitive area of the PD) and an optical filter to reduce the effect of the ambient light noise.

VLC Channel: In VLC, as any other communication system, the medium/space between the VLC transmitter and the VLC receiver is denoted by the VLC channel. In which, several factors should be considered which differ from indoor and outdoor VLC applications. One important issue in indoor applications is the impact of the interference [26,27]. It can be caused either by the reflections from walls and objects inside,i.e., inter-symbol-interferences or by the neighbouring users, i.e., co-channel interferences. In outdoor applications, in addition to the interference, many other environmental factors should be further considered [28]. These include the attenuation due to the atmospheric weather conditions, the blockage due to the user density and mobility, and the noise either from the sunlight or from the artificial light sources. It can be further noted that the intensity profile of the light source is a critical factor in characterizing the VLC channel since it affects the interactions of the emitted rays with the environmental elements during its paths until reaching the PD. Many of indoor luminaries have a uniform radiation pattern that can be described by the ideal Lambertian model. However, that holds untrue for the light sources with non-uniform radiation patterns, i.e., asymmetrical pattern, as in outdoor luminaries. Furthermore, the area and the number of equipped PDs plays an important role in VLC channel as it affects the total number of captured rays and hence the total amount of collected power.

1.2 Vehicular VLC and Motivation of Research

In the last decade or so, there have been extensive research efforts in the context of Intelligent Transportation Systems (Intelligent Transportation Systems (ITSs)) which are a critical component of future smart cities [29,30]. ITSs aim to improve road safety, traffic flow, and passenger comfort by enabling the information sharing between the vehicles and infrastructures [31]. As a milestone of future generation ITSs, fully autonomous vehicles are being considered by major automakers as well as Google, Uber, and Tesla. One of the keys enabling technologies for such advanced transport solutions is vehicular communication in the form of Vehicle-to-Vehicle (V2V), Vehicle-to-Infrastructure

(V2I), Vehicle-to-Pedestrian (V2P), and Infrastructure-to-Pedestrian (Infrastructure-to-Pedestrian (I2P)), commonly referred to as Vehicle-to-Everything (V2X) communication [32].

Since practical implementation of ITSs require highly robust, scalable, and reliable V2X connectivity solutions, the research efforts and standardization activities on V2X communication are continuously increasing. Most of these efforts have been so far centered around the RF technologies. For example, dedicated short-range communication (Dedicated Short-Range Communication (DSRC)) is already commercially available by some auto manufacturers [33] while Cellular-V2X Cellular-V2X (C-V2X) fifth generation (Fifth Generation (5G)) chipsets are being produced [34]. The current market penetration of V2X solutions is relatively low and therefore, the allocated RF bands might be sufficient at the time being. In the near future, however, high interference levels can be experienced in limited RF bands particularly in high-density traffic scenarios. Channel congestion will result in longer delays and degrade the packet rate.

To address such issues, VLC has been proposed as an alternative or complementary vehicular access solution to RF-based V2X communications [11, 28, 35]. VLC is based on the principle of modulating the intensity of the light-emitting-diode (LED) and enables the dual use of LEDs for both illumination and communication purposes. The ubiquitous availability of LED-based street lights, traffic lights and automotive exterior lighting positions VLC as a potential wireless connectivity solution for vehicular networks [36, 37]. In addition to interference immunity, VLC has the potential to achieve very high data rates on the order of Gigabits Per Second (Gb/s) with off-the-shelf LEDs [38] or even more with custom design LEDs [39]. With such attractive merits, vehicular VLC has received an increasing attention recently and several topics such as physical layer design [40], upper layer network protocols [12] and integration with RF-based solutions for hybrid systems [41] have been studied in the recent literature [42].

As in any other communication system, channel modeling is critical for the design, analysis and optimization of VLC systems. Earlier results in the literature have focused

on indoor channel modelling [43, 44]. Those results are obviously not applicable to vehicular VLC systems which exhibit inherently different characteristics in comparison to indoor counterparts. Initial works on V2V VLC and/or I2V VLC assume the ideal Lambertian model [45–48]. While this model can be well suited for many indoor LED luminaries, it fails to match with the illumination characteristics of automotive HLs, TLs, traffic lights, and street lights with their asymmetrical intensity distributions [28, 49]. For example, the vehicle headlights are designed to provide an adequate road illumination on the movement direction minimizing glare of oncoming traffic, and backward reflections to the driver [42,50]. On the other side, the street lights are designed to focus the light into the road surfaces increasing the illuminated area in the two directions of the road (i.e., around the light pole) which results in a substantially different distribution pattern [49]. Considering that in a vehicular VLC system the outdoor lighting module is the transmit antenna, any modification of the antenna pattern naturally affects the communication performance [51]. In addition to, the effects of road reflectance, road type, weather conditions, orientation of the user/vehicle equipment/infrastructures, receiver aperture size, and the sunlight might strongly affect the link performance of vehicular VLC systems.

Existing V2V VLC Channel Models: In V2V VLC systems, both HLs and TLs of the vehicle can be employed as the optical transmitters. There is already a growing number of works on V2V VLC channels [1, 52–64]. Earlier works mainly built upon some ideal, yet unrealistic assumptions. For example, some works [1, 52–55] considered the ideal clear weather condition and the Lambertian illumination pattern which might be valid for indoor light sources, but do not capture the asymmetrical intensity distribution of vehicle HLs and/or TLs. In an attempt to address such shortcomings, a piecewise Lambertian channel model was proposed in [56], which estimated the received power of the scooter TL for short distance up to 10 m. On the other side, the intensity patterns for HLs were measured in [57–59] and then used in the performance analysis. The work in [60] further presented a closed-form path loss expression for V2V based HLs as a function of distance under the assumption of clear weather condition.

In [61], the link asymmetry problem of V2V was identified with a significant difference in the received power for incoming and outgoing links.

Another important concern is the effect of road surface on V2V VLC systems. There are some attempts to to address this by considering both dry and wet asphalt roads as in [57, 59]. However, these works were built on the assumption of fixed reflectance values for both the road surface and vehicle coating. Such an assumption can be justified for infrared wavelengths; however, in the visible light band, reflectance is wavelength-dependent and this should be considered for a precise channel modelling.

A critical factor that needs to be further taken into account in V2V VLC channel modelling is the impact of weather conditions. Some efforts to address this issue were reported in [62,63] where the effect of artificially generated rain and fog on the received optical signal was quantified for a TL LED using a laboratory chamber. Recently, in [64], a V2V link with HLs acting as transmitters was considered and a linear path loss expression was developed for clear, rain and fog conditions. This is however valid only for very short link ranges up to 20 m.

Existing I2V VLC Channel Models: The topic of I2V VLC communications was widely adopted in the open literature where traffic lights [46, 65–72] or street lights [73–81] are used as VLC transmitters. Earlier I2V works assumed the ideal Lambertian model for the traffic lights [46, 65, 66] or the street lights [73–76]. While Lambertian model is a good model for indoor luminaries, such a model fails to match with the illumination characteristics of streetlights with their asymmetrical intensity distribution [28, 49]. In addition, most of these works consider only LOS component while reflected rays from the road were not considered. The impact of road reflection is discussed in [77, 78] but a fixed reflectance value is assumed for simplicity. This however does not hold for visible light spectrum where wavelength-dependent reflectance should be assumed for a realistic modelling. The focus of [77] is implementing a Light Fidelity (LiFi) system prototype while the focus of [78] is introducing an architecture of hybrid VLC and RF system. The works in [73–75], further assumed the reception from streetlights located only at one side of the road to calculate the SNR [73, 74] or

to develop a handover technique [75]. The reception from the street lights located on both sides of the road was then considered in [76] again under the LoS assumption. The focus of [76] is introducing a channel estimation method based on a decision feedback.

In an attempt to consider the asymmetrical pattern of street lights, the authors in [79, 80] used ray tracing to obtain the CIR for an I2V VLC system where the radiation pattern of LED street lamp was imported from the Dialux library. This work considered only a single street light located at a specific distance from the car in static conditions and again assumed fixed reflectance value for road surface. The focus of [79] is calculating the SNR at different optical bands while the focus of [80] is comparing the delay time for V2I and V2V cases. The wavelength-dependent reflectance of the road surface together with asymmetrical pattern of a commercial street light was more recently considered in [81] where a specific I2V scenario with a fixed pole height, a fixed spacing between poles, and a fixed aperture PD was considered.

In summary, while the most recent introduced V2V channel path loss model in [64] considered the asymmetrical pattern of the vehicle HLs while it is only valid for relatively short distance (up to 20 m). Also, while the recent works in [79–81] considered the effect of the asymmetrical pattern of the infrastructure in channel modeling, they present only numerical results and do not provide any I2V channel path loss models. A closed form path loss expression provides critical insight into system design and performance analysis. In an effort to fill these research gaps, we propose in this dissertation realistic channel path loss models for vehicular VLC links including V2V based on both HLs and TLs, and I2V based on both traffic and street lights. In our study, we adopt channel modeling approach based on non-sequential ray tracing which will be discussed in details in the next chapter.

1.3 Dissertation Outline

Motivated by these, to fill these research gaps, we provide in this dissertation a comprehensive channel modeling study for different vehicular VLC links including V2V based on both HLs and TLs, and I2V based on both traffic and street lights. In our study, we

adopt channel modeling approach based on non-sequential ray tracing which will be discussed in details in the next chapter of this dissertation. Therefore, the dissertation has five main parts that can be outlined as follow.

In the first part of this dissertation, we explain our channel modeling approach which builds upon advanced non-sequential ray tracing features of OpticStudio software. This approach allows the integration of any realistic light source radiation pattern and can handle a large number of reflections for better accuracy. Wavelength-dependent reflectance of surface coating for each material in the environment, as well as different types of reflections (specular, diffuse, or mixed) can be considered for a precise characterization. Then, since this is a simulation based channel modeling methodology, it has to be validated at least once against the measurements in a real scenario. Therefore, we carry out measurements and simulations for the same scenarios to validate our channel modeling approach considering both the LoS and the NLoS cases and in both indoor and outdoor environments. The obtained CIRs and Channel Frequency Responses (CFRs) of the two methods indicate a very good agreement validating the ray tracing approach.

In the second part of this dissertation, such a well established realistic channel modeling approach is adopted to model the V2V VLC channel when two vehicles travel in the same lane utilizing either the HLs or the TLs of the source vehicle as wireless transmitters. First, we propose a path loss expression for V2V based HLs, which takes the form of a negative exponential function, and provides an excellent match to simulation results for larger transmission ranges and under different weather conditions. This expression is then utilized to derive the achievable transmission distance for a targeted data rate.

Then, we consider V2V based TLs and derive a new path loss model works for measured TL radiation pattern of different commercial car models. Next, we estimate the performance of V2V VLC system in terms of the maximum transmission distance at a target BER. Furthermore, the RMS delay spread is investigated by considering different V2V density scenarios.

In the above points, the effect of both the lateral shift between the two vehicles, the

exact geometry of the vehicle HLs, and the receiver aperture on the path loss model of V2V system are excluded. Therefore, to address such shortcoming, we develop a comprehensive closed-form path loss expression for RF VLC system as a function of link distance, lateral shift between the two vehicles, weather type, transmitter beam divergence angle, and receiver aperture diameter.

In the third part of this dissertation, we consider I2V VLC links. First, we model the I2V based traffic lights transmitters taken into account the inherent characteristics of the commercial traffic lights same as the wavelength-dependent reflectance of the road, poles, and vehicle objects. We derived a new path loss model as function of both the longitudinal and lateral shift distances which is then used to investigate the received SNR performance of the I2V system. Then, the reverse channel link, i.e., V2I system, is considered. In which, the vehicle communicates with a traffic pole deploying its HLs as wireless transmitters while 3 PDs located within the traffic pole adjacent to yellow, red and green LED luminaries to act as wireless receivers. Based on the CIRs, obtained from the ray tracing, to model propagation environment as well as the effects of LED non-linear characteristics, we calculate the received SNR and achievable data rates for the V2I system.

Furthermore, we consider the I2V systems with street light poles located at both sides of the road. We introduce a comprehensive channel path loss model based on data fitting to CIRs obtained using our channel modeling approach and during the travel distance. The proposed closed-form path loss expression is a function of transceiver and infrastructure parameters. These include the spacing between the street light poles, the height of the street light poles, the height of the vehicle, both the longitudinal and lateral distance between the vehicle and the street light pole, and the aperture size of the PD. The derived channel path loss model is then utilized to investigate the performance of I2V VLC systems through the derivation of closed form BER expression taking into account the randomness of the channel path loss.

In the fourth part of this dissertation, we investigate the multi-directional coverage for Vehicular VLC Communication. Our motivation is that in most of RF and/or I2V

VLC works, the common underlying assumption is the use of one or two PDs. This is typically sufficient for establishing connection between two vehicles cruising in the same straight lane or between the vehicle and infrastructure with clear line-of-sight. To position VLC as a strong candidate for vehicular connectivity, it is essential to realize multi-directional reception in various deployment scenarios supporting both RF and I2V links. It remains an open question what is the sufficient number of required PDs to achieve this. To address this question of practical relevance, we investigate the channel modeling of a vehicular VLC system in different road types (i.e., multi-lane, curved roads), intersections (i.e., T-shaped, Y-shaped intersections) and traffic scenarios (i.e., cruising in the same or different lanes, lane change etc.). We conduct a channel modeling study to quantify the capability of receiving signals in different cases in a way to achieve the omni-directional coverage for both RF connectivity (in front and back directions) and both I2V connectivity (with traffic and street lights).

In the fifth part of this dissertation, we consider a practical application of vehicular VLC systems. We explore VLC as a wireless connectivity solution to enable the outdoor broadcasting for public safety systems utilizing the ubiquitous street lights as transmitters. In our channel modeling, We take into account the fundamental differences imposed by the outdoor medium and lightning infrastructure. These includes the effect of asymmetrical pattern of streetlights, orientation of the user equipment, weather condition, and the solar irradiance. Based on the ray tracing approach, we obtain the CIRs for the Streetlight-to-Pedestrian (S2P) and Streetlight-to-Vehicle (S2V) links. The obtained CIRs are then used to calculate the variance of the received signal at the PD. We then utilize the advanced features of OpticStudio and provide a realistic modeling for the solar irradiance calculating the variance of the received background noise at the PD. The received SNR is then obtained for both S2V and S2P links under the mobility condition.

1.4 Organization

The dissertation is organized as follow. Chapter 2 focuses on the explanation and validation of our channel modeling based on the non-sequential ray tracing, which is then utilized for the channel modeling in the following chapters, Chapter 3 focuses on the channel modeling for RF communication links, Chapter 4 focuses on the channel modeling for I2V communication links, Chapter 5 focuses on the channel modeling for multi-directional coverage including both RF and I2V cases. Toward a practical application of vehicular VLC systems, Chapter 6 focuses on exploring VLC as a wireless connectivity solution to enable the outdoor broadcasting for public safety systems. These chapters are organized as follow:

Chapter 2 has three sections. In Section 2.1, we provide an overview of existing VLC channel modeling methodologies. In Section 2.2, we explain our channel modeling approach which is based on non-sequential ray tracing features of OpticStudio. In Section 2.3, we investigate the accuracy of our channel modeling approach by comparing the results of CIRs and CFRs obtained from the simulation and the measurements at different scenarios.

Chapter 3 considers RF VLC channel modeling and has two sections. In Section 3.2, we derive closed form expressions for the channel path loss of RF in perfect alignment case based on the vehicle HLs (see Section 3.2.1) and the vehicle TLs (see Section 3.2.2) respectively. These expressions are then utilized to derive closed form expressions of the maximum achievable transmission distance for a targeted BER performance. In Section 3.3, we derive a comprehensive closed form expressions for the channel path loss of RF in non-perfect alignment case which is a function of link distance, lateral shift, weather type, transmitter beam divergence angle, and receiver aperture diameter.

Chapter 4 considers I2V channel modeling and has three sections. Section 4.2 investigates the channel modeling for I2V based traffic lights and derives a closed form path loss expression as function of longitudinal and lateral distances. In Section 4.3, we derive a closed form expression for the channel path loss of I2V based street lights

as a function of spacing between lighting poles, pole height, vehicle height, both longitudinal and lateral distance, and the aperture size of the PD. The derived model is then utilized to derive a closed form BER expression considering the randomness of the channel path loss. Section 4.4 investigates the channel modeling of V2I link and derives an expression for the achievable capacity considering the effect of propagation environment as well as the effects of LED non-linear characteristics.

Chapter 5 investigates the multi-directional coverage for vehicular VLC and it consists of three sections. In Section 5.2, we illustrate the vehicular VLC scenarios under consideration which include different road types (i.e., multi-lane, curved roads), intersections (i.e., T-shaped, Y-shaped intersections) and traffic scenarios (i.e., cruising in the same or different lanes, lane change etc.). In Section 5.3, we indicate the locations of the PDs around the vehicle to achieve the required omni-directional coverage for all previous scenarios. In Section 5.4, we quantify the capability of receiving signals in all scenarios considering both RF links (in front and back directions) and I2V links (with traffic and street lights). We further quantify the contribution of individual PDs to elaborate the main usage cases of each PD.

Chapter 6 discuss the VLC-based outdoor broadcasting application and it has two sections. In Section 6.2, we introduce the VLC broadcasting system, illustrate the streetlight type classifications, explain the sunlight modeling with OpticStudio, and present the SNR calculations. In Section 6.3, we present the broadcasting scenarios under consideration and discuss the numerical results.

CHAPTER II

CHANNEL MODELING APPROACH

2.1 Introduction

In this chapter, we explain the channel modeling approach based on non-sequential ray tracing features of OpticStudio [82], and investigate its flexibility and accuracy. Channel modeling is considered as an essential stage to evaluate the communication system design [83]. Generally, there are two ways to characterize VLC channels. The first one is based on the simulation while the second uses experimental measurements. While simulations can be reproduced on every personal computer, measurements are time-consuming, costly and specific for the particular measured scenario. While simulations are more generic, they have to be validated at least once against measurements in a real scenario.

Simulation methodologies for VLC channel modeling can be classified into two major approaches, i.e, deterministic [84–89] and stochastic methods [90–93]. Recursive calculation [84–87] and geometric-based models [88, 89] are the most widely used deterministic techniques, but are typically limited to simple geometries due to computational complexity. As a more flexible alternative to deterministic methods, non-sequential ray tracing can be employed [92, 93]. This stochastic approach allows for the evaluation of the impulse response for environments with complex geometries especially when a large number of reflections are considered. In a ray tracing study, the objects hit by the rays are defined by their physical properties and orientation towards the directions of rays. This allows the ray to be launched and then hit whatever object is in its path. As a result, the ray may be reflected, scattered, refracted, diffracted, or split into sub-rays.

Ray tracing studies were reported for both Infrared (IR) and VLC wavelengths [92–96]. Non-sequential ray tracing of OpticStudio [82] allows the integration of any

realistic light source radiation pattern and can handle a large number of reflections for better accuracy. The wavelength-dependent reflectance of surface coating for each material in the environment, which is particularly important at visible wavelengths, as well as different types of reflections (specular, diffuse or mixed) can be further taken into account for a precise characterization. VLC channel models developed through this approach were also adopted as reference channel models in IEEE 802.15.13 and IEEE 802.11bb [97, 98].

It can be further noted that experimental measurements are time consuming and require dedicated hardware and costly equipment. Therefore, the challenge is to characterize VLC channels with a realistic simulation methodology in away to reach a satisfactory matching between simulations and measurements. Afterwards, modelling of more complex scenarios becomes readily accessible. Towards this main objective, in this chapter, we carry out measurements and simulations in the same scenarios to validate our channel modeling approach. Our measurement system exploits multiple LEDs and PDs at both transmitter (Tx) and receiver (Rx) front-ends, and a standard Vector Network Analyser (VNA). In the simulation study, we utilize the same set-up, i.e., the radiation pattern of LEDs, the effect of the receiver directivity, wavelength-dependent reflectance of the walls and objects inside the room, etc. to allow one-to-one comparisons with measurement campaign.

Results of both ray tracing simulations and measurements have indicated a very good match in both frequency and time domains validating the ray tracing approach. The rest of this chapter is organized as follow. In Section 2.2, we explain our channel modeling approach based on the ray tracing methodology adopted in our study. In Section 2.3, we introduce the measurement methodology used to validate our channel modeling approach and compare the results of simulation and measurements.

2.2 Ray Tracing Methodology

In this section, we explain the major steps of the ray tracing approach. As shown in Fig. 1, we have three main steps that can be described as the following:

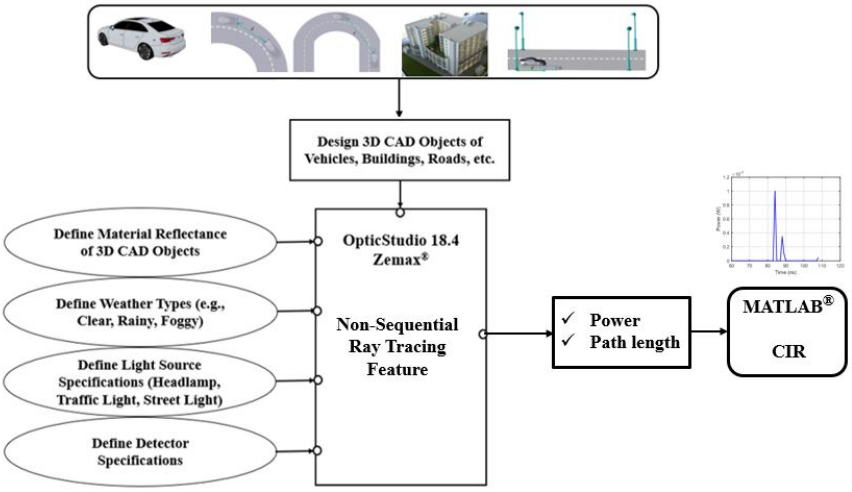

Figure 1: Main steps of ray tracing channel modeling approach.

Design: First, we design the 3D simulation model of the test environment under consideration in OpticStudio. Then, we design and import the CAD models of the objects inside, i.e., furniture, human beings, etc for indoor case and vehicles, poles, roads, etc in outdoor case. To arrive at the CAD model designs, we leverage a combination of built-in OpticStudio tools like Part Designer; external tools like SolidWorks, AutoCAD, Rhino, and others; importable designs from various online catalogs like TurboSquid, GrabCAD, and Free3D.

Define: Next, with the CAD files imported into OpticStudio [82], we define the specifications for the 3D environment and its CAD components. The coating materials of such CAD objects are defined in the simulation platform where the wavelength-dependent reflectance as well scatter fraction can be specified. Crucially, we specify parameters for the key system elements themselves—the transmitter and receiver. For the transmitter, we define the orientation and power, and identified the source type and radiation patterns using both imported sources and native sources from the built-in OpticStudio library. For the receiver, we specify the detector type and viewing angles, along with the sensitive area as required to provide the necessary quality of information. For simulating outdoor weather conditions in the 3D environment's atmospheric propagation medium, we use built-in OpticStudio volume physics tools that provided input parameters for key qualities of precipitation, including refractive index, radius,

and density of particles.

Analyze: When all definitions are applied, we specify the ray tracing parameters which include the number of rays and the maximum number of objects the light would touch—and then conduct the ray tracing analysis in OpticStudio [82]. At the end of the simulation process, OpticStudio produces an output file containing information about the simulated path length and power of each ray emitted from the light source and detected at the receiver. By importing the file into MATLAB, we compute the CIR by

$$h(t) = \sum_{i=1}^{N} P_i \delta(t - \tau_i) \tag{2.1}$$

where N is the number of rays received by the PD and δ is the Dirac delta function. Here, P_i and τ_i respectively denote the power and the propagation delay of the i^{th} ray received by the PD, $i = 1, \cdots, N$. After obtaining the CIR, we obtain various projected channel parameters such as channel channel delay spread, channel path loss, and channel frequency response.

One of the important channel parameters is path loss, which is critical for link budget calculations. With $H_0 = \int_0^\infty h(t)dt$ being the Direct Current (DC) channel gain, the path loss is given as

$$PL = -10\log_{10}(H_0) \tag{2.2}$$

Since multiple copies of the signal reach at the receiver through different paths, each of them has a different power level and path length. Hence, the channel is affected by temporal dispersion. The impact of multi-path dispersion is often characterized by the RMS delay spread which can be computed by

$$\tau_{rms} = \sqrt{\frac{\int_0^\infty (t - \mu_\tau)^2 h(t)^2 dt}{\int_0^\infty h(t)^2 dt}} \tag{2.3}$$

where μ_τ is the mean excess delay. It is well known that higher the value of RMS delay spread, lower is the data transmission rate. Another important parameter is the channel coherence bandwidth, B_c. Assuming a correlation level of 50% [83], the channel coherence bandwidth can be given by $B_{c,50\%} = 1/5\tau_{rms}$. From the CIR in Eq. (2.1), the channel frequency response can be then given by the help of Fourier transformation.

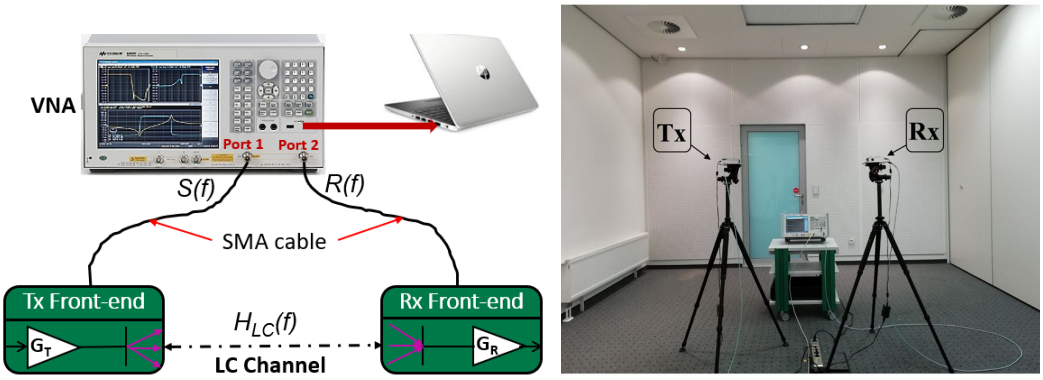

(a) (b)

Figure 2: Validation of ray tracing channel modeling approach (a) Channel measurement setup, (b) Test environment.

2.3 Experimental Validation

Measurement System: The channel measurement system (see Fig. 2.a) is based on frequency sweep technique using a standard Agilent two-port VNA (E5061B-3L5 model), capable of operating between 5 Hz and 3 GHz. At first, a 0 dB continuous-sinusoidal-signal, swept from 1 MHz to 200 MHz in steps of 200 kHz, is delivered to the optical Tx front-end. Then, Tx (consisting of multiple LEDs) radiates the signals through the propagation channel. A large amount of transmitted rays will be captured at the PD array of Rx kept at a particular configuration according to the effective sensitive area and FOV angle of the PD. In our set-up, the Tx front-end consists of four OSRAM OSLON SFH-4715AS LEDs which has the centroid wavelength at 850 nm [99]. Rx front-end is equipped with five HAMAMATSU-S6968 PDs with a high sensitivity around 850 nm. This combination of Tx and Rx arrays maximize the number of captured rays at the Rx which is critical during NLoS scenarios. The amplitude and phase of the received signal at the port 2 of VNA are compared with the transmitted ones and the corresponding frequency response of the VLC system is generated. The resultant response consists of frequency response of VLC channel, Tx and Rx front-ends. The effect of these front-end responses must be nullified then in order to characterize the VLC channel [100]. From this frequency response, a normalized CIR is calculated using inverse discrete Fourier transformation method.

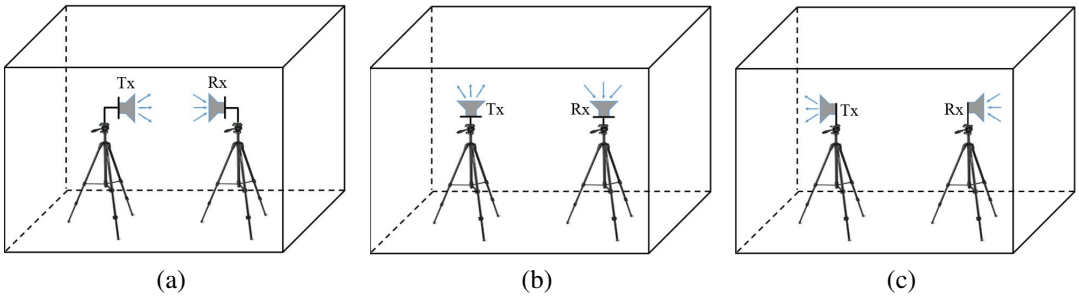

Figure 3: VLC scenarios for validation: (a) scenario I, (b) scenario II, (c) scenario III.

VLC Scenarios Under Consideration: As illustrated in Fig. 2.b, we performed the measurements in a small meeting room at HHI with a dimension of 5.7 m$\times$ 4.5 m$\times$ 3 m. Both Tx and Rx front-ends are deployed on a metal tripod at a height of 1.5 m and with a separation distance of d. In the measurements, three VLC scenarios (See Fig. 3) are considered as follows:

1. **Scenario I (LoS scenario):** Tx and Rx face each other maintaining a LoS link.

2. **Scenario II (NLoS with first order reflection):** Tx and Rx face towards the ceiling. The Rx in this case can capture the rays after the reflection, mostly from the ceiling which represents the first-order reflection rays.

3. **Scenario III (NLoS with high order reflections):** Tx and Rx face opposite directions. Hence the signalling takes place through the multiple reflections.

2.4 Results and Discussion

In this part, we present the simulation and experimental results of VLC channel characteristics. For all scenarios under consideration, the value of d varies between 1 m and 3 m with 0.5 m step size. Figs. 4 and 5 show the channel frequency response (amplitude) and the CIR of VLC channels obtained for three different scenarios under consideration. It is observed that results from simulation and experiments exhibit similar behaviour with having a deviation of 1-3 dB in amplitude and 1-4 radians in phase. One can notice also that the strongest peak of CIRs is observed at the same point in the experimental and simulated data.

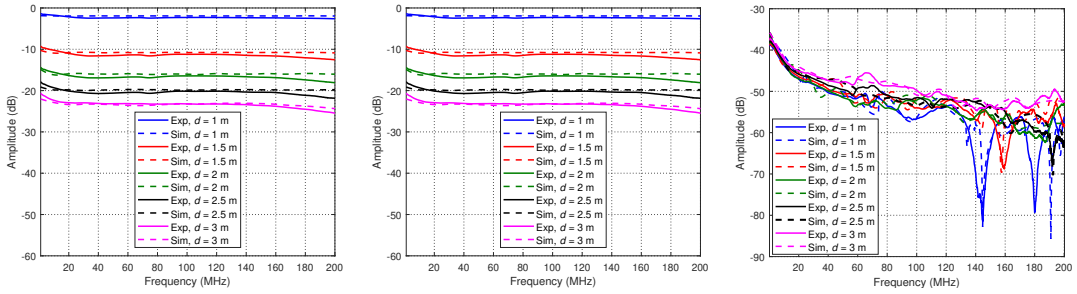

(a) (b) (c)

Figure 4: Validation results for frequency amplitude responses: (a) scenario I, (b) scenario II, (c) scenario III.

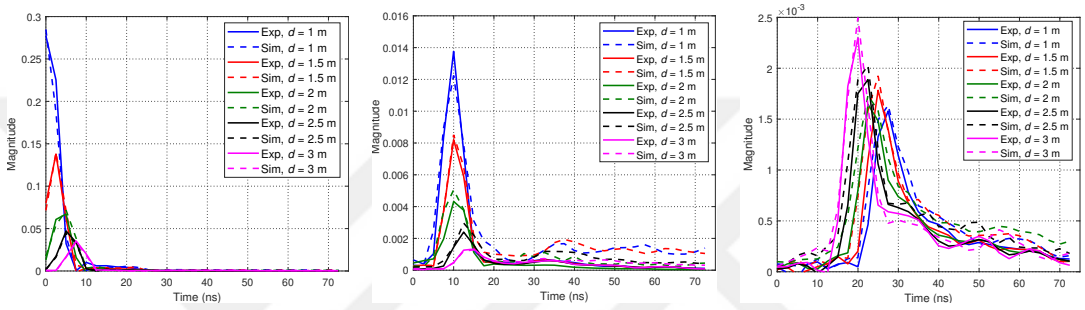

(a) (b) (c)

Figure 5: Validation results for CIRs: (a) scenario I (b) scenario II (c) scenario III.

In addition to our indoor verifications, it should be further emphasized that experimental validations of the data generated by this channel modeling approach have been demonstrated for different other VLC scenarios including indoor and outdoor scenarios. For example, in [101,102], this channel modeling approach is utilized for modeling different indoor Multiple-Input Multiple-Output (MIMO) VLC scenarios with furniture inside. The results are then compared with the measurements that are carried out using a channel sounder capable of measurements at frequencies of up to 250 MHz. The results of both methods indicated a very good agreement validating the ray tracing approach in indoor MIMO scenarios. In [103], this channel modeling approach is utilized to model the V2V VLC system, and the path loss results are compared with the experimental measurements proposed in [60]. The obtained ray tracing results provide a very good match with the measurement ones under the same vehicular VLC environment conditions validating the ray tracing approach in vehicular applications. The validation of this ray tracing approach is further documented in an IEEE 802.11-12/1234r0 standard

contribution [104]. In conclusion, the obtained results of both the ray tracing simulations and the measurements demonstrated that the ray tracing approach can create realistic channel models for both indoor and vehicular scenarios. In the next chapters, this channel modeling approach will be used for modeling the vehicular VLC channels.

CHAPTER III

CHANNEL MODELING FOR INTER-VEHICULAR COMMUNICATION

3.1 Introduction

In this chapter, we utilize the channel modeling approach described in Chapter 2 to model the V2V channels. It can be noted from our literature survey (See Section 1.2.1) that most of previous studies [1, 52–55] assume a simplifying, yet inaccurate, assumption in channel modeling that HLs and TLs have Lambertian profiles. Recently, a linear path loss model with asymmetrical HLs was introduced in [64], however, it is valid only for very short ranges up to 20 m. Therefore, there is a need for a new channel path loss of V2V with HLs, works for larger transmission ranges and under different weather conditions. Since in vehicular VLC, both HLs and TLs can be employed as the optical transmitters, a path loss model model for V2V with TLs is also required taken into account their asymmetrical intensity patterns. Besides the asymmetrical pattern effect, the lateral shift between the vehicles same as the receiver aperture size may affect the amount of collected power, and hence the system performance, which must be considered.

The rest of this chapter is organized as follow. In Section 3.2, we derive closed form expressions for the channel path loss of V2V in perfect alignment case based on the vehicle HLs (see Section 3.2.1) and the vehicle TLs (see Section 3.2.2) respectively. These expressions are then utilized to derive closed form expressions of the maximum achievable transmission distance for a targeted BER performance. In Section 3.3, we derive a comprehensive closed form expressions for the channel path loss of V2V in non-perfect alignment case which is a function of link distance, lateral shift, weather type, transmitter beam divergence angle, and receiver aperture diameter.

3.2 Perfect Alignment Case

Earlier studies on V2V VLC channel modeling [1, 52–55] assume that vehicle HLs and/or TLs have Lambertian profiles. It has been shown, however, in [64] and in [105] that HLs and TLs of commercial vehicles have asymmetrical patterns with a significant effect on the channel path loss. Therefore, we present in Section 3.2.1, a closed form expression for the channel path loss of V2V with HLs and derive the maximum achievable distance. In Section 3.2.2, we present a closed form expression for the channel path loss of V2V with TLs and derive the maximum achievable distance.

3.2.1 V2V Based Vehicle Headlights

Path Loss Model: In this section, we propose a closed-form path loss expression for V2V link with HLs transmitters and verify it through simulation results. The received optical power at a distance d can be written as

$$P_r = P_t G_e G_{att}, \tag{3.1}$$

where G_{att} represents the atmospheric attenuation and changes according to weather conditions. According to Beer-Lambert formula [106], it can be expressed as $G_{att} = \exp(-cd)$ where c is the extinction coefficient.

G_e is the geometrical loss due to spreading of the emitted optical beam along the distance between the transmitter and the receiver. To take into account the asymmetrical pattern of HL source, we propose the use of

$$G_e = A\left(\frac{1}{d^2}\right)^B, \tag{3.2}$$

where A represents the geometrical loss value at a reference distance of d_0 and B is the decaying factor. Replacing G_{att} and G_e in Eq. (3.1), we can express the path loss model as

$$P_r = P_t \underbrace{A d^{-2B} \exp(-cd)}_{\rho}, \tag{3.3}$$

where ρ is the optical channel coefficient. In order to determine A and B, we determine the received optical power at a reference distance $d_0 = 10$ m via ray tracing simulations

explained before. Let P_0 denotes the received optical power at $d_0 = 10$ m. We can then determine $A = P_0 d_0^{2B} \exp(c d_0) P_t$. Through our simulation results, the value of B is determined to be 0.87 for clear and rainy weathers while in case of foggy weather, it is determined to be 0.7. As a benchmark, we consider the linear path loss model of [64] which is given by

$$P_r = P_t (\alpha d + \beta), \tag{3.4}$$

where the values of α and β are given as (α, β) = (-0.44, -40.93), (-0.46, -40.90), and (-0.61, -40.46), respectively, for clear, rainy and foggy weathers.

Maximum Transmission Distance: Based on the derived path loss model in Eq. (3.3), we derive the achievable transmission distance for a targeted data rate while satisfying a given value of BER. Under the assumption of *L-ary* Pulse-Amplitude Modulation (PAM), the BER can be approximated by [107]

$$P_e \approx \frac{2(L-1)}{L\log_2(L)} Q\left(\frac{1}{L-1}\sqrt{\frac{(\eta\rho P_t)^2 \log_2 L}{N_0 R}}\right), \tag{3.5}$$

where L is constellation size, η represents the responsivity of PD, R is the data rate, and N_0 is the noise power spectral density. By rearranging Eq. (3.5), we get

$$R \approx \frac{(\eta P_t \rho)^2 \log_2 L}{N_0 (L-1)^2 Q^{-1}\left(\frac{P_e L \log_2 L}{2(L-1)}\right)^2} \tag{3.6}$$

Let R_t and $P_{e_{th}}$ respectively denote the targeted data rate and constraint BER. Solving Eq. (3.6) for ρ, we obtain

$$\rho \approx \left((L-1)\sqrt{\frac{N_0 R_\mathrm{t}}{(\eta P_t)^2 \log_2 L}}\right) Q^{-1}\left(\frac{P_{e_{th}} L \log_2 L}{2(L-1)}\right) \tag{3.7}$$

After some straightforward mathematical manipulations on $\rho = A d^{-2B} \exp(-cd)$, we can obtain d as

$$d = \frac{2B}{c} \mathrm{W}\left(\frac{c A^{\frac{1}{2B}}}{2B\rho^{\frac{1}{2B}}}\right), \tag{3.8}$$

where W(.) denotes Lambert-W function. By replacing Eq. (3.7) in Eq. (3.8), the achievable transmission distance for the given values of R_t and $P_{e_{th}}$ is obtained by

$$d = \frac{2B}{c} \mathrm{W}\left(\frac{c}{2B}\left(\frac{A_0 \eta P_t \sqrt{\log_2 L}}{(L-1)\sqrt{N_0 R_t} Q^{-1}\left(\frac{P_{e_{th}} L \log_2 L}{2(L-1)}\right)}\right)^{\frac{1}{2B}}\right) \tag{3.9}$$

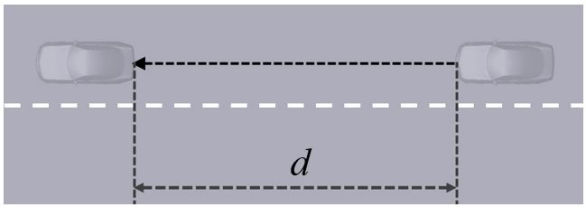

Figure 6: V2V scenario with HLs and perfect alignment.

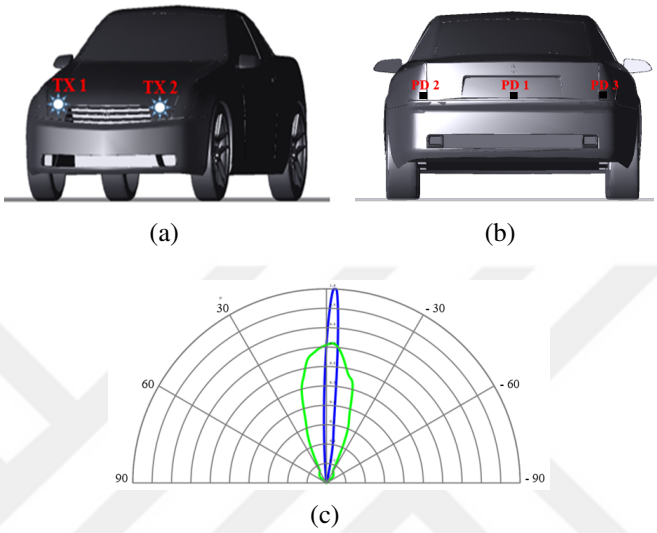

(a) (b)

(c)

Figure 7: V2V system model (a) Location of HLs on the source vehicle, (b) Location of PDs on the destination vehicle, and (c) Intensity profile of vehicle HLs

Simulation Results and Discussion: As illustrated in Fig. 6, we consider a V2V scenario in a two-lane highway road with a lane width of 3.75 m [108]. We assume that two cars are located at the center of the same lane and separated with an inter-vehicle distance of d. Following the specifications of [11], we assume "R2" type asphalt road which has mixed diffuse and specular reflection nature. We adopt Mie scattering to model clear, rainy and foggy weather conditions [106]. As illustrated in Fig. 7, we assume that cars are black-colored and modeled as CAD objects with dimensions of 4.6 m$\times$1.8 m$\times$1.3 m following Audi A5 Coupe specifications [109]. Headlamps of the first car serve as wireless transmitters. They are designed to provide an adequate road illumination without causing any glare for other road users, therefore they have asymmetrical intensity distributions patterns given in Fig. 7.c.

At the receiver side, we consider two cases: Case A) We assume a single PD (PD1) located at the center of the back of the car similar to [64], Case B) We assume the

Table 1: Simulation parameters for V2V system.

Transmitter	Type:	High-beam headlamp		
	Brand:	Philips Luxeon Rebel white LED		
	Power:	1 W		
	Light wavelength:	400 nm-700 nm		
Receiver	Type :	PN junction		
	Area :	1 cm^2		
	FoV:	180°		
	Responsivity:	0.28 A/W		
	Noise density:	10^{-22}		
Road	Type:	R2		
	Coating material:	Asphalt		
	Lane width:	3.75 m		
Vehicle	Length:	4.673 m		
	Width:	1.846 m		
	Height:	1.371 m		
	Coating material:	Black gloss paint		
Weather	Type:	Clear	Rainy	Foggy (Visibility of 50m)
	Particle index:	1.000277	1.33	1.33
	Size (μm):	10^{-4}	100	10
	Density (cm^{-3}):	10^{19}	0.1	124.6
	c (m^{-1}) :	1.5×10^{-5}	0.9×10^{-3}	0.078

deployment of two PDs (PD2 and PD3) installed under TLs as shown in Fig. 7.b. All simulation parameters are provided in Table 1.

In the following, we first confirm the accuracy of the proposed path loss expression through simulations. Then, we present numerical results for the achievable transmission distance under different weather types to achieve specified values of R_t and $P_{e_{th}}$.

In Fig. 8, we present the received power based on the path loss expression in (3.3) assuming single PD deployment (i.e., Case A) and considering clear, rainy and foggy weather conditions. As benchmarks, we provide simulation results and the linear path loss model in (3.4). It is observed that the linear model can match simulation results for only short transmission distances and deviates for distances larger than 20 m. On the other hand, the proposed expression in (3.3) provides a very good match to simulation results for a wider range [110]. Comparison of Figs. 8.a, 8.b, and 8.c further reveals that the rain has negligible effect on VLC link while fog introduces significant degradation.

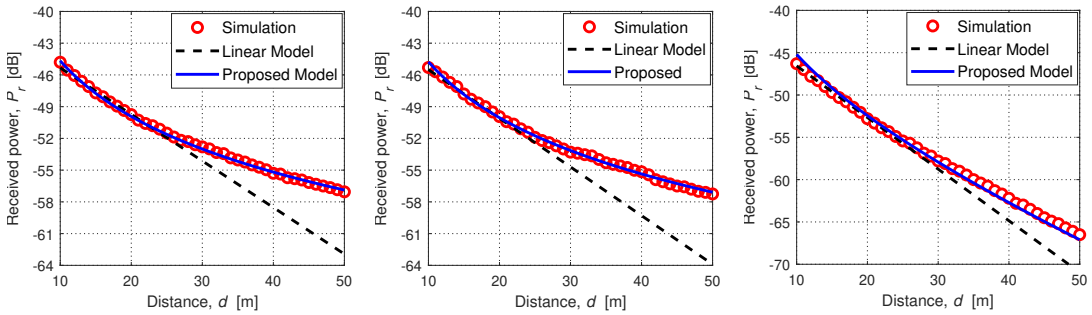

Figure 8: Path loss results for V2V with HLs and perfect alignment (a) Clear weather (b) Rain weather (c) Foggy weather.

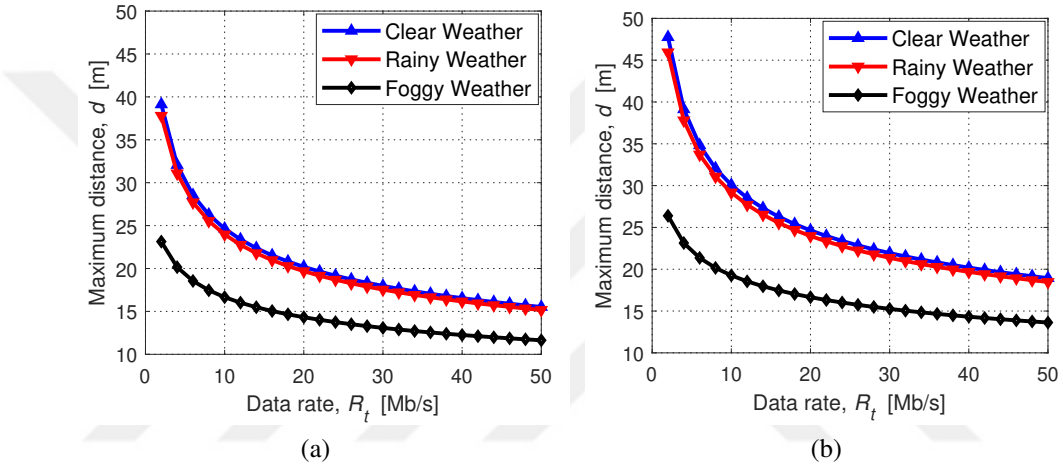

Figure 9: Achievable transmission distance versus the data rate for for V2V with HLs and perfect alignment (a) Case A (PD1) (b) Case B (PD2 and PD3).

As an example, consider $d = 30$ m. The received power in clear weather condition is -52.7 dB for the normalized unit power transmission. This reduces to -53.3 dB for rainy condition indicating a mere 0.6 dB degradation with respect to clear weather. It can be readily verified from Fig. 8.c that this further reduces to -57.9 dB for foggy weather and a degradation of 5.1 dB is observed.

In Fig. 9, we present the achievable transmission distance versus the data rate. We assume $P_{e_{th}} = 10^{-6}$ and 32-PAM. Assume a target data rate of $R_{\mathrm{t}} = 10$ Mb/s. In Fig. 9.a for single PD deployment, it is observed that the achievable transmission distance is 25 m for this data rate. This reduces to 24 m and 16.5 m respectively for rainy and foggy weathers. It can be readily verified from Fig. 9.b that using two PDs will increase the achievable transmission distance. The achievable transmission distances are obtained

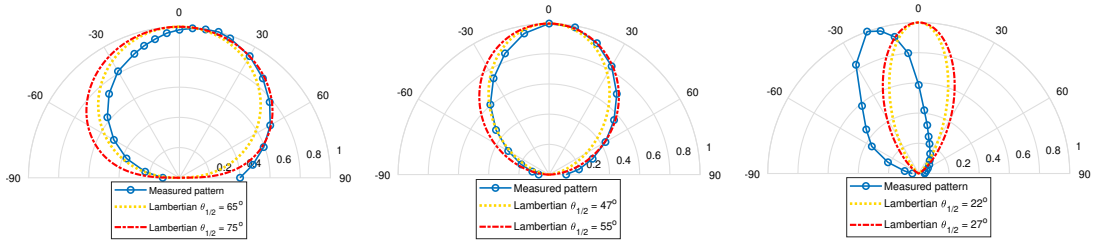

(a) (b) (c)

Figure 10: Measured and Lambertian patterns for TLs (a) BMW, (b) Audi, and (c) Nissan.

as 30.5 m, 29.3 m, and 19.5 m, respectively, for clear, rainy, and foggy weathers.

3.2.2 V2V Based Vehicle Taillights

While in vehicular VLC, both HLs and TLs can serve as the optical transmitters, while, most reported works on vehicular VLC have focused on HLs-based transmitters. There are only a few studies focused on the use of TLs in vehicular VLC [56,60,61]. Recently, the radiation pattern of a commercial's TL was measured [105], showing that TL has a non-symmetric pattern, which is different from the Lambertian model as shown in Fig. 10. This demonstrates the demand for a path loss model model for V2V with TLs taken into account such asymmetrical intensity pattern. Therefore, we incorporate the real measured radiation patterns for commercially available TLs from different automotive manufacturers i.e., BMW, Audi A5, and Nissan (see Fig. 10) using the 3D ray tracing platform, and derive a new path loss model. Then, we estimate the performance of VVLC through derivation the maximum transmission distance at a target BER. Furthermore, the RMS delay spread is investigated by considering different V2V scenarios.

Path Loss Model and Maximum Transmission Distance: In this section, we first propose a closed-form path loss expression for V2V link with TLs transmitters and verify it through simulation results. The proposed path loss model is an explicit function of d and the vehicle's TL, which is given by:

$$PL_i(d) = PL_{0,i} + 10\log_{10}\left(d^{-2\varepsilon_i}\right) - \zeta_i d,\ i \in \{a,b,c\} \tag{3.10}$$

where PL_0 is the reference PL at d_0 of 1 m. The values of ε_i and ζ_i are determined by

Table 2: TL Parameters from empirical measurements.

TL brand	θ**- left** (°)	θ**-right** (°)	P_t **(mW)**	ε_i	ζ_i
(a) BMW	65	75	111	0.809	0.074
(b) Audi	47	55	40	0.801	0.072
(c) Nissan	22	27	9	0.805	0.079

means of ray tracing simulation for each model as given in Table 2.

For non-return to zero on-off keying (NRZ-OOK) data format, the BER is given by:

$$\mathrm{BER}_i(d) = \frac{1}{2}\mathrm{erfc}\left(\frac{\sqrt{\gamma_i(d)}}{2\sqrt{2}}\right), \tag{3.11}$$

In Eq. (3.11), $\gamma_i(d)$ is the SNR and is given by:

$$\gamma_i(d) = \frac{(\eta R H_i(d))^2 P_t}{\sigma_n^2}, \tag{3.12}$$

where η is the electrical-optical conversion factor, R is PD's responsivity, σ_n^2 is the noise variance, P_t is transmit electrical power at the Tx, $H_i(d)$ is the channel DC gain at d. Substituting Eq. (3.12) in Eq. (3.11) and solving for $H_i(d)$, we have:

$$H_i(d) = 2\sqrt{2}\left(\sqrt{\frac{\sigma_n^2}{P_t\eta^2R^2}}\right)\mathrm{erfc}^{-1}(2\mathrm{BER_i})\cdot \tag{3.13}$$

$H_i(d)$ can also be obtained from Eq. (3.10) as:

$$H_i(d) = 10^{\left(\frac{PL_{0,i}}{10} + \log_{10}\left(d^{-2\varepsilon_i}\right) - \frac{\zeta_i}{10}d\right)}. \tag{3.14}$$

Using Eq. (3.14) and Eq. (3.13) and substituting for $\sigma_n^2 = N_0 B_w$, where N_0 is the noise power spectral density, and B_w is the noise bandwidth, the transmission range at the threshold BER ($\mathrm{BER_T}$) is expressed by

$$d_i = \frac{20\log_{10}e}{\zeta_i/\varepsilon_i}\mathrm{W}\left(\frac{\zeta_i/\varepsilon_i}{20\log_{10}e}\exp\left(\frac{\frac{PL_{0,i}}{10} - \log_{10}\left(2\sqrt{2}\left(\sqrt{\frac{N_0B_w}{P_t\eta^2R^2}}\right)\mathrm{erfc}^{-1}(2\mathrm{BER_T})\right)}{2\varepsilon_i\log_{10}e}\right)\right), \tag{3.15}$$

where W(.) denotes Lambert-W function.

Simulation Results and Discussion: We present the simulation results for path loss, delay spread, and achievable distance for R = 0.54 A/W, P_t = 10 W, N_0 = 10^{-22} W/Hz, B_w corresponds to 100 kHz, 1 MHz, and 5 MHz, and η = 0.5. We assume

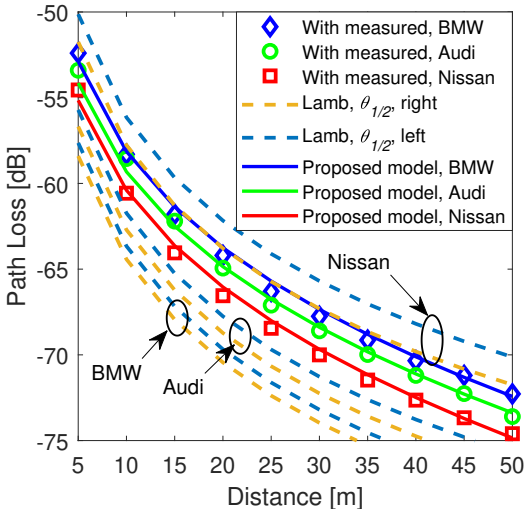

Figure 11: Path loss results for V2V with TLs and perfect alignment.

an asphalt road surface with the R2 type following the specifications of International Commission on Illumination [111]. R2 road type has a specular factor S_1 of 0.582 and an average luminance coefficient Q_0 of 0.07, which result in mixed diffuse and specular reflections [59]. For the vehicle, we assume gloss black paint as in [64]. The wavelength dependent reflectance of glossy black paint and the asphalt road surface are defined in [112, 113], respectively.

In Fig. 11, we present both the proposed path loss model in Eq. (3.10) and the widely used Lambertian model for the three TLs under investigation. The PL plots are obtained using ray tracing with the measured radiation pattern also included. It is observed that the proposed expression in Eq. (3.10) offers a very good match with the simulation results for the three TLs [114]. It is also observed that the path loss results are significantly different from those based on Lambertian model. For example, for Audi A5 ($i = b$) and for d = 25 m, the measured path loss is -67 dB, which is lower by $\sim$3 dB and $\sim$4 dB compared with Lambertian model with $\theta_{1/2}$ of 47° and 55°, respectively. Note that only Nissan TL ($i = c$) offers higher losses than the Lambertian model. This is due to Lambertian model is based on half-beam angle $\theta_{1/2}$, which are 22° and 27° for the left and right TLs in Nissan, respectively. However, these angles do not consider the orientation of the light profile that might be shifted with respect to the 0° direction, which is the case in Nissan TL. By considering the real pattern of the

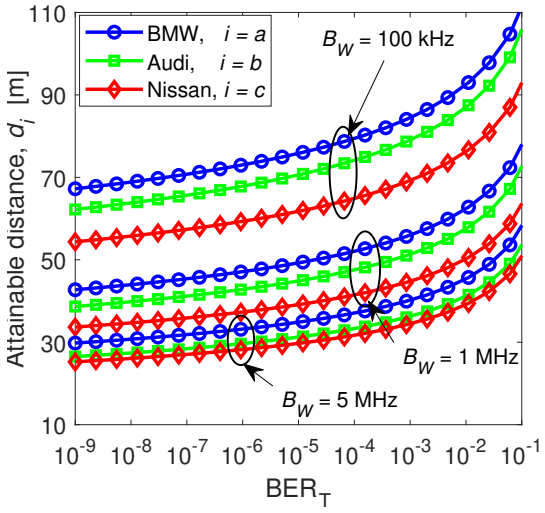

Figure 12: Achievable distance versus BER for V2V with TLs and perfect alignment.

light source, which is obtained by empirical measurements, a more realistic path loss can be determined. It is shown in Fig. 11 that, unlike BMW and Audi A5, the path loss based on the measured pattern for Nissan TL is higher than Lambertian by an average of 3 dB.

In Fig. 12, we show the attainable transmission distance d_i as a function of the target BER for three TLs. It is observed that, reducing B_w has a significant impact on d. This is because reducing B_w decreases the noise variance thus resulting in an increase in the received SNR. Therefore, d becomes larger, see Fig. 12. For example, for B_w = 1 MHz and a target BER of 10^{-3}, which is within the forward error correction BER limit, d_i values are ∼55, ∼51, and ∼44.5 m for BMW, Audi, and Nissan, respectively. These increase to 80, 75, and 66 m, respectively for 100 kHz.

To investigate the effect of reflections from neighboring vehicles, we consider a V2V system with the TLs of the front vehicle (i.e., BMW with $i = a$) and a single PD located in the front of the vehicle in behind are used as the transmitters and receiver, respectively. We consider three different scenarios and determine their root-mean-square (RMS) delay spreads (τ_{RMS}). The V2V scenarios under consideration are described as:

Scenario I: Two vehicles travel in a single-lane road and are separated by d. This is the ideal case since there are no neighboring vehicles as in Fig. 13.a.

Scenario II: A two-lane road with single-side neighboring vehicle is considered.

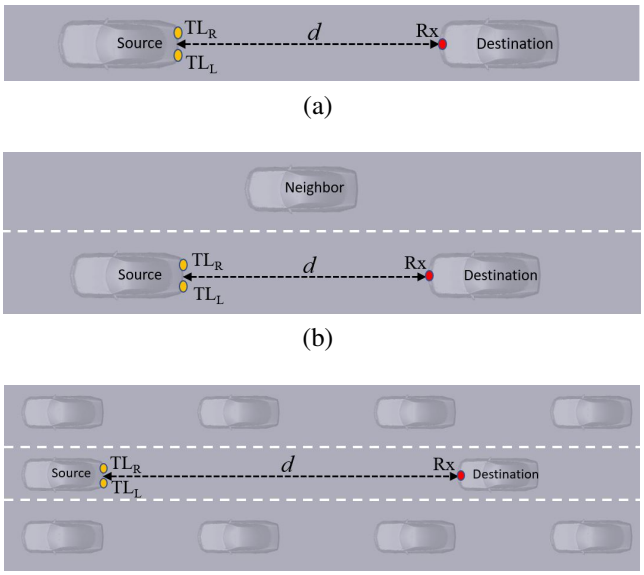

Figure 13: V2V scenarios with TLs and perfect alignment assuming BMW vehicle: (a) Scenario I, (b) Scenario II, and (c) Scenario III.

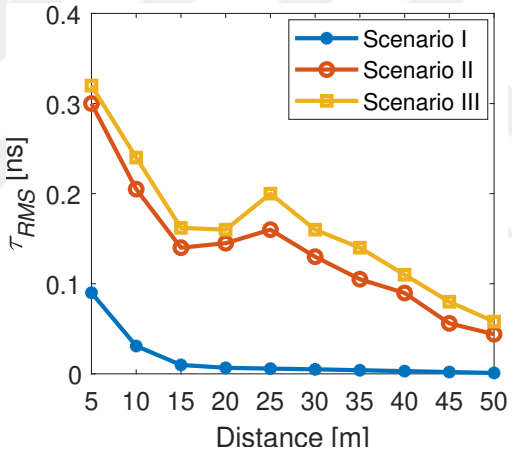

Figure 14: The delay spread versus the transmission distance for three V2V scenarios.

The two communicating vehicles are separated from each other by d. On the other side, the vehicle traveling at center of the adjacent lane is positioned at an equal distance between the two communicating vehicles, i.e., $d/2$, see Fig. 13.b.

Scenario III: A three-lane road with vehicles in all three lanes is considered, see Fig. 13.c.

Fig. 14 illustrates the RMS delay spread as a function of d for the three scenarios. It is observed in Scenario I that, there are increased levels of road reflections at shorter distances (i.e., $d \leq 15$ m) compared to longer distances. At $d \geq 15$ m, the delay spread becomes almost constant and negligible (i.e., NLoS paths becoming less important than

the LOS path). In scenarios II and III, the RMS delay spread becomes significant because of additional reflection-induced multipath components from the neighboring vehicles. For example, at d of 25 m, the RMS delay spread for scenarios I, II, and III are 6×10^{-3}, 0.15, and 0.2 ns, respectively. Notice that, the RMS delay spread depends on the geometry of the V2V system (i.e., location of the neighboring vehicles). When a reflecting object is located at a distance where the reflected rays have smaller angle of arrivals within the FoV of the Rx, significant power is received from the NLoS components, which reach the Rx at different times with respect to the LoS path. Hence, leading to higher RMS values. The reflected rays with larger arrival angles than the FoV, however, will not be captured by the Rx and hence do not affect the delay spread. Because of this, the delay spread might increase at some distances (i.e., d = 20 and 25 m), slightly reduces at others (i.e., d = 40 and 50 m), or sharply reduces at d = 10 and 15 m. This means that, when larger numbers of neighboring vehicles are considered, depending on the traffic scenario, the effect of the delay spread might be more and should be considered in the design of V2V systems.

3.3 Effect of Lateral Shift

The above V2V channel path loss models were built upon the assumptions that the receiver has a fixed area of 1 cm^2, the two vehicles follows each other with a perfect alignment, and the two HLs can be considered as a single transmitter. As a result, simplified path loss models were obtained, which required a small modification on the geometrical loss, while the well-known Beer-Lambert formula is assumed to represent the atmospheric attenuation loss. The resultant geometrical loss model was a function of reference path loss and the propagation distance (d), and it is inversely proportional to d^2. Deriving a path loss model considering the impact of the lateral shift between the two vehicles, the exact geometry of the vehicle HLs and the receiver aperture size, requires further modifications on the geometrical loss. In addition, increasing the receiver aperture size makes the well-known Beer-Lambert formula deviates to match with the

actual path loss results since it builds upon the implicit assumption that scattered/reflected photons cannot be captured by the receiver. Therefore, in this Section, we take into account the effect of all mentioned factors and present a closed-form path loss expression for the V2V VLC as a function of system and channel parameters. The proposed expression builds upon the summation of geometrical loss and attenuation loss. The obtained geometrical loss is also inversely proportional to d^2 but with different coefficients since both asymmetrical pattern of the two HLs and the geometry of V2V transmission are carefully taken into account. The attenuation loss term in the new expression can be considered as a modified version of the well-known Beer-Lambert model to consider such rays that could be received by the PD after some reflections/scattering. Based on extensive non-sequential ray tracing simulations, we obtain the CIRs for a given V2V scenario in various weather conditions, i.e., clear, rainy and foggy. Utilizing these CIRs, we propose a comprehensive path loss expression which is an explicit function of longitudinal distance, lateral shift, weather type, transmitter beam divergence angle, and receiver aperture size.

System Model: As shown in Fig. 15, we consider a single-lane road with a width of w_r. We assume that two vehicles follow each other in the same lane with a possible lateral shift of d_h. Each vehicle has a width of w_c and they are separated from each other with a longitudinal distance of d. The two high-beam HLs (denoted by TX1 and TX2) are adopted as wireless transmitters which are horizontally separated from each other with a distance of d_{tx}. A single PD (denoted by RX), placed at the center of the back of the other vehicle, acts as a wireless receiver. It has an aperture diameter of D_R and a viewing angle of FoV. L_i is the propagation distance from TXi to RX. Furthermore, the irradiance angle of TXi is given by θ_i while incident angle is defined by ϕ_i.

Path Loss Model: The path loss consists of two main components, i.e, attenuation loss and geometrical loss. Attenuation loss is a result of scattering and absorption while the geometrical loss [115] is a result of the fact that the transmitted beam spreads to a size larger than the receive aperture. The geometrical loss between the i^{th} transmitter

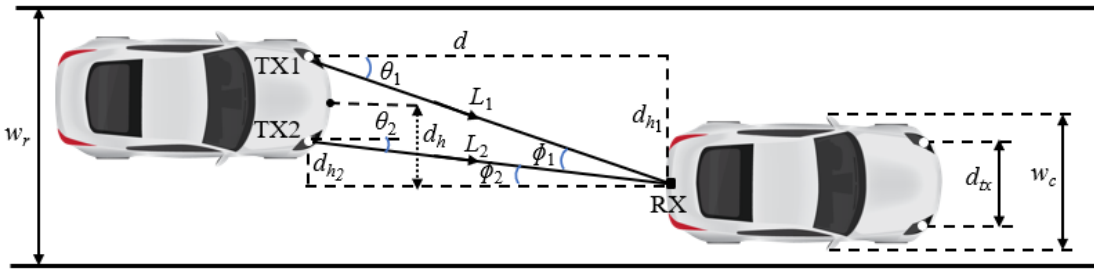

Figure 15: V2V scenario with lateral shift.

and the receiver can be expressed as

$$PL_{Geo_i} = 10\log_{10}\left(\frac{D_R(\cos(\theta_i))^{1/\varepsilon}}{\zeta L_i}\right)^2 \quad i = 1,2 \tag{3.16}$$

where we introduced two correction coefficients (ζ and ε) to take into account weather conditions and asymmetrical pattern of HLs. The values of these correction coefficients are determined through ray tracing simulation study.

The well-known Beer-Lambert formula defines the attenuation loss [106] and builds upon the implicit assumption that scattered photons cannot be captured by the receiver. In order to take into factor that some of the scattered rays could be received by the PD after some reflections, this can be modified as

$$PL_{\text{att}_i} = 10\log_{10}\left(\exp\left(-cL_i\left(\frac{D_R}{\zeta L_i}\right)^{\frac{\varepsilon}{2}}\right)\right), \tag{3.17}$$

where c stands for the extinction coefficient for a specific weather type and an additional term is introduced in the negative exponential that is proportional to the geometrical propagation of the light source. Based on Eq. (3.16) and Eq. (3.17), the path loss for the link between the i^{th} transmitter and the receiver can be expressed as

$$PL_i = 10\log_{10}\left(\left(\frac{D_R(\cos(\theta_i))^{1/\varepsilon}}{\zeta L_i}\right)^2 \exp\left(-cL_i\left(\frac{D_R}{\zeta L_i}\right)^{\frac{\varepsilon}{2}}\right)\right), \tag{3.18}$$

From the geometry of layout in Fig. 15, it can be readily checked that $L_i = \sqrt{d^2 + d_{h_i}^2}$, where $d_{h_i} = d_h \pm d_{TX}/2$ and $\theta_i = \arccos\left(d/L_i\right)$. Noting the use of dual transmitters and replacing L_i and θ_i within (3.18), we can obtain the overall path loss as

$$PL = PL_1 + PL_2 = 10\log_{10}\left(\frac{1}{2}\left(\sum_{i=1}^{2}\left(\left(\frac{D_R(d/\sqrt{d^2+d_{h_i}^2})^{1/\varepsilon}}{\zeta\sqrt{d^2+d_{h_i}^2}}\right)^2 \exp\left(-c\sqrt{d^2+d_{h_i}^2}\left(\frac{D_R/\zeta}{\sqrt{d^2+d_{h_i}^2}}\right)^{\frac{\varepsilon}{2}}\right)\right)\right)\right) \tag{3.19}$$

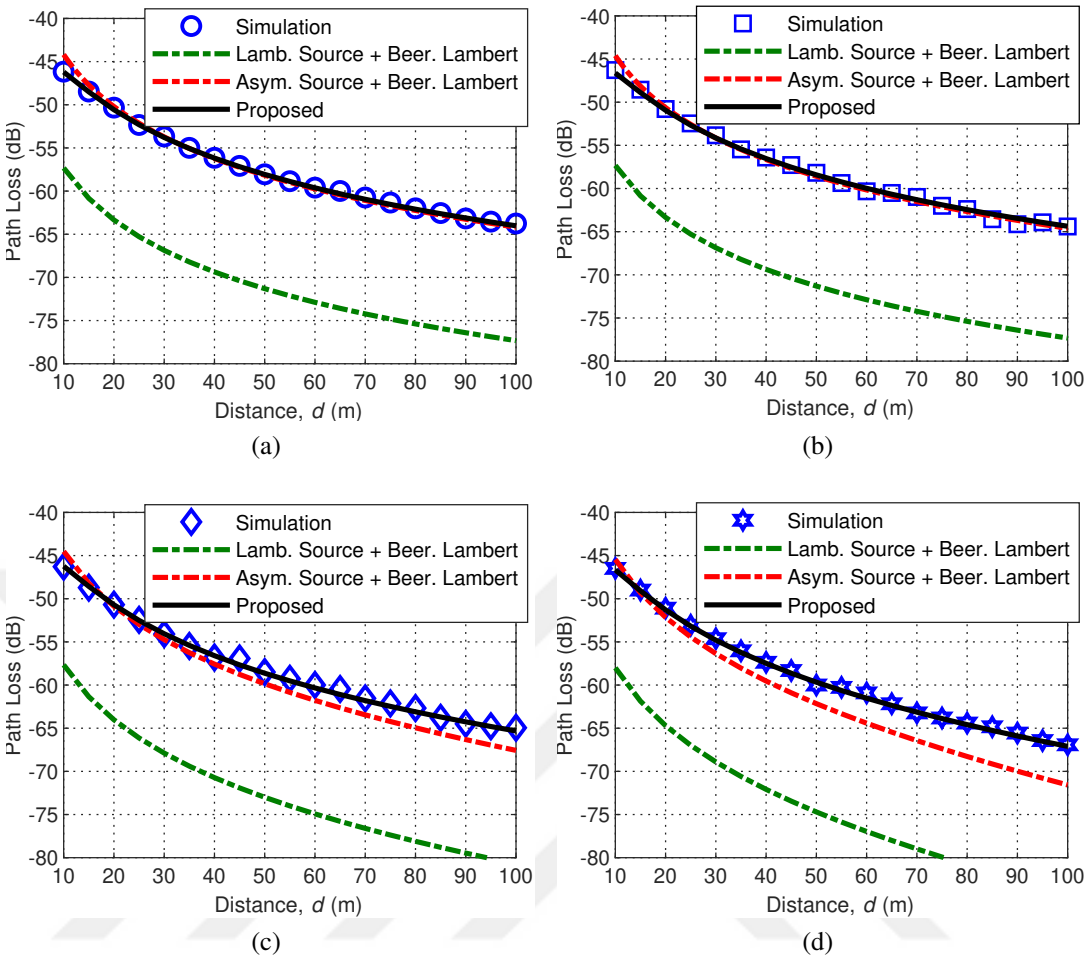

Figure 16: Comparison of proposed path loss expression with simulation results for different weather conditions (a) Clear weather (b) Rainy weather (c) Moderate fog, and (d) Thick fog.

Simulation Results and Discussion: The simulations are conducted for clear weather, rain, moderate fog (i.e., visibility of 500 m) [116] and thick fog (i.e., visibility of 250 m) [116]. In the following, we present the proposed path loss expression versus distance for the weather conditions under consideration along with simulation results. Corresponding ζ and ε values as well as weather condition parameters are given in [103]. In addition to simulations, we include two benchmarks as follows.

(a) The path loss calculated based on the assumption of Lambertian source and the Beer-Lambert formula.

(b The path loss calculated based on the assumption of the asymmetrical source and the Beer Lambert formula.

It is observed from Fig. 16 that our path loss model in Eq. (3.19) has excellent match

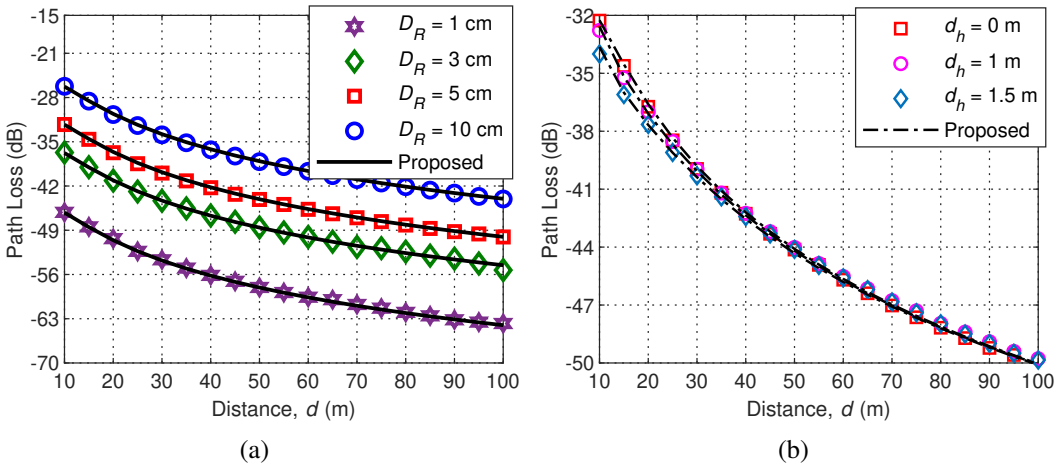

Figure 17: Comparison of proposed path loss expression with simulation results for (a) Different receiver aperture diameters and (b) Different lateral shifts.

with simulation results for all weather conditions [103]. In contrary, the benchmarks specified in (a) and (b) exhibit some deviations. Particularly, the path loss obtained by Lambertian source is a significant overestimation over the actual path loss compared to asymmetrical HLs. Beer-Lambert formula is a good fit with simulation results only for clear and rainy weathers and deviates for foggy conditions. Since the extinction coefficients of clear and rainy weathers are very small, the scattered rays can be ignored making Beer-Lambert formula valid for this case. In foggy weather conditions, the effect of scattering is significant. In this case, Beer-Lambert formula has a significant deviation from simulation. This deviation increases when visibility decreases.

In Fig. 17, we consider the clear weather condition and further investigate the validity of the proposed path loss model in (3.19) when either the receiver aperture or the lateral shift changes. In Fig. 17.a, we consider different values of receiver aperture diameter, i.e., $D_R = 1$ cm, $D_R = 3$ cm, $D_R = 5$ cm, and $D_R = 10$ cm and introduce the path loss results. It can be verified that the path loss expression in (3.19) maintains a very good match with all receiver aperture diameters under consideration. In Fig. 17.b, we assume fixed receiver aperture of $D_R = 5$ cm and investigate the effect of different lateral shift values, i.e., $d_h = 0$ m, $d_h = 1$m, and $d_h = 1.5$ m. It is observed that the lateral shift brings negligible loss with respect to perfect alignment case of $d_h = 0$ m. It is also observed that the obtained results from both the simulation and the proposed path loss

expression are in a good agreement.

To this end, we have modeled the V2V VLC channels based on both the HLs and the TLs transmitters. We also considered the effect of both the longitudinal and the lateral shift introducing a comprehensive path loss model for V2V VLC channel. In Chapter 4 on the following page, we model the I2V channel links where the traffic lights and the streetlights can act as the wireless transmitters.

CHAPTER IV

CHANNEL MODELING FOR INFRASTRUCTURE TO VEHICLE COMMUNICATION

4.1 Introduction

In Chapter 3 of this dissertation, we have derived path loss expressions for only V2V VLC links where HLs and/or TLs of the vehicle act as wireless transmitters and two vehicles communicate with each other. We have also derived closed-form expression for the maximum achievable distance while satisfying a pre-defined BER target and investigated the benefits of deploying dual PDs on the system performance. We have furthermore investigated the effect of various channel and system parameters on the V2V path loss including the longitudinal distance, lateral shift, weather type, and receiver aperture size.

In this chapter, we consider the I2V VLC links where in addition to HLs/TLs, the traffic lights and street lights are deployed as wireless transmitters. First, we model the I2V based commercial traffic lights, and derive a path loss model as function of longitudinal and lateral shift distances. Then, we model the I2V system with street light transmitters and derive a channel path loss expression as a function of pole spacing, height of lighting pole and vehicle, both longitudinal and lateral distance, and the aperture size of the PD. The effect of these transceiver and infrastructure parameters on the system average error rate performance is also investigated. We further consider the reverse channel link, i.e., V2I system, where the vehicle communicates with an infrastructure pole deploying its HLs as transmitters while 3 PDs located within the traffic pole to act as receivers. To model propagation environment as well as the effects of LED non-linear characteristics, we investigate the received SNR and achievable data rates.

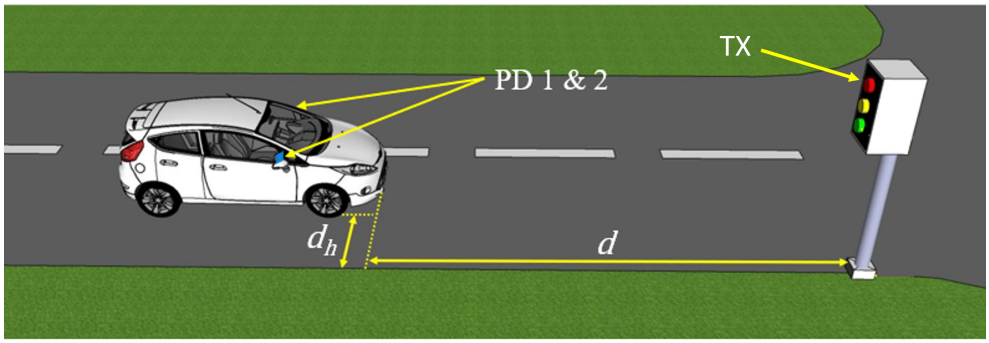

Figure 18: I2V scenario based traffic lights.

4.2 I2V Based Traffic Lights

System and Channel Model: As illustrated in Fig. 18, we consider an I2V VLC system in a typical two-lane road. A red traffic light works as a source and communicates with a vehicle which is assumed to be travelling at the right road-lane with a longitudinal separation distance of d with respect to the traffic light pole. The vehicle receives the signal from the traffic light using two PDs (PD 1 and PD 2), installed at the top of its mirrors, as shown in Fig. 18. We further define d_h which represents the horizontal shift between the vehicle and the traffic light pole.

For channel modelling, we utilize non-sequential ray tracing approach described in Chapter 1. In this method, a 3D simulation platform with CAD models of vehicles and traffic poles is constructed in OpticStudio software. Then, we define the coating material of CAD-object surfaces where the scatter fraction and the wavelength-dependent reflectance are specified. The light source specifications such as radiation pattern, optical power, orientations, and the number of emitted rays are further defined. Similarly, receiver specifications such as orientations, FoV angle, and aperture area are defined. After the 3D simulation platform is constructed, non-sequential ray tracing is performed to generate an output file including the power and the path length of each ray that reaches to the receiver.

Path Loss Model: The output information from the channel modeling approach is first proceed in MATLAB to obtain the CIRs. Assume that N_j is the total number of rays reaching the j^{th} PD for a given distance d. Let P_{ij} and τ_{ij} respectively denote the

Table 3: Values of a, b, c coefficients in Eq. (4.3)

Lateral shift	a	b	c
d_h = 0 m	-67.51	53.99	100.1
d_h = 1 m	-68.21	54.09	101.9
d_h = 2 m	-71.21	74.07	137.8

power and the propagation delay of the i^{th} ray, $i = 1,...,N_j$, received by the j^{th} PD, $j = 1,...,3$. The CIR at the j^{th} PD can be expressed as

$$h_j(t) = \sum_{i=1}^{N_j} P_{ij}\,\delta\left(t-\tau_{ij}\right), \tag{4.1}$$

where δ is the Dirac delta function. The total channel path loss can be then given as

$$PL = 10\log_{10}\left(\sum_{j=1}^{2}\int_0^{\infty} h_j(t)\,dt\right). \tag{4.2}$$

Then, based on the CIRs and path loss results obtained using the ray tracing approach, we propose a new expression for the channel path loss of I2V link based on the data fitting. The new path loss model is an explicit function of d and d_h, which is given by:

$$PL_{\text{I2V}} = 10\log_{10}\left(h_{\text{I2V}}\right) = a\,\exp\left(-\left(\frac{d-b}{c}\right)^2\right), \tag{4.3}$$

where h_{I2V} is the optical channel coefficient (i.e., path loss measured on a linear scale). In Eq. (4.3), a, b and c are coefficients obtained via ray tracing for each d_h value under consideration, by the use of data fitting MATLAB toolbox and (see Table 3).

Simulation Results and Discussion: To validate the proposed I2V path loss model in Eq. (4.3), we consider a commercial red traffic light with asymmetrical radiation pattern shown in Fig. 19, following [117]. The normalized unit power and a PD with area of 1 cm^2 are considered in the ray tracing simulations to present the path loss results. R2 type road with asphalt coating is considered. The car is modeled as black-colored CAD object with dimensions of Audi A5 Coupe model. The traffic pole is modeled as a CAD object with surface cover of galvanized steel metal. We further consider three I2V scenarios which are illustrated as the following:

- **Scenario I:** The car moves at the outer edge of the right lane with a horizontal shift of d_h = 0 m (distance between the right mirror and the traffic pole).

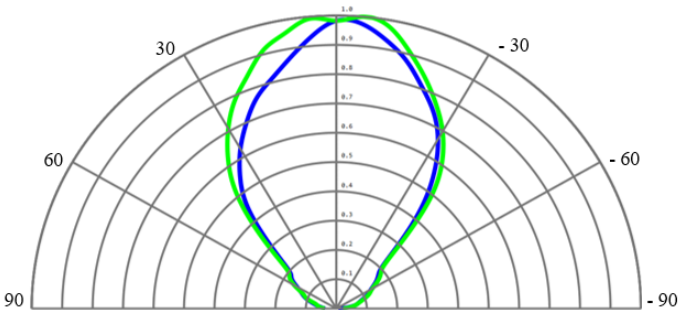

Figure 19: Intensity profile of OSRAM traffic light LED.

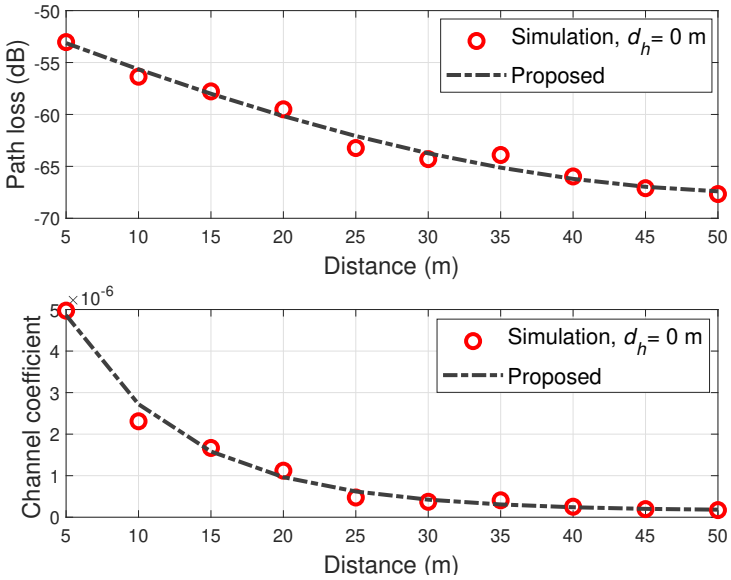

Figure 20: Path loss results for I2V with traffic light and perfect alignment.

- **Scenario II:** The car moves at the middle of the right lane which results in a d_h = 1 m with respect to the traffic pole.
- **Scenario III:** The car moves at the inner edge of the right lane which results in a d_h = 2 m with respect to the traffic pole.

In Fig 20, we consider the ideal I2V case (perfect alignment, i.e., d_h = 0 m), and present the results of the derived I2V path loss model versus ray tracing results. It observed that the path loss is significantly affected by distance. For example, consider d = 20 m, the path loss is given as -60 dB. This reduces to -67 dB for d = 50 m.

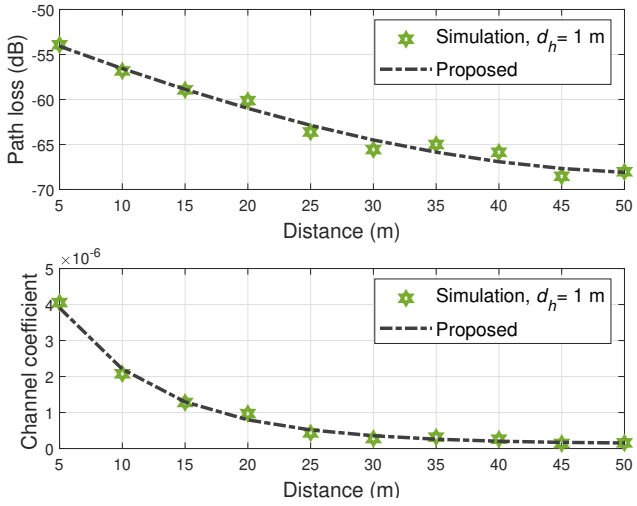

(a)

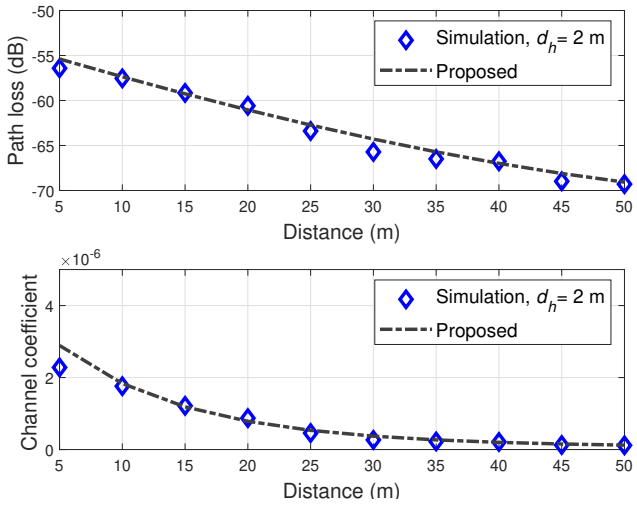

(b)

Figure 21: Path loss results for I2V with traffic light and lateral shift: (a) Scenario II and (b) Scenario III.

In Fig 21, we consider the I2V with lateral shift case (Scenario II, i.e., d_h = 1 m and Scenario III, i.e., d_h = 2 m), and present the results of the derived I2V path loss model versus ray tracing results. It is observed that the lateral shift impacts on the path loss results. For example, consider d = 50 m, the path loss is given for Scenario I, Scenario II, and Scenario III as -67.2 dB, -68.1 dB, and 69.3 dB, respectively. For all I2V scenarios under consideration, it is observed that the proposed path loss model provides a very good match with the simulation results either in linear or logarithmic scales [118].

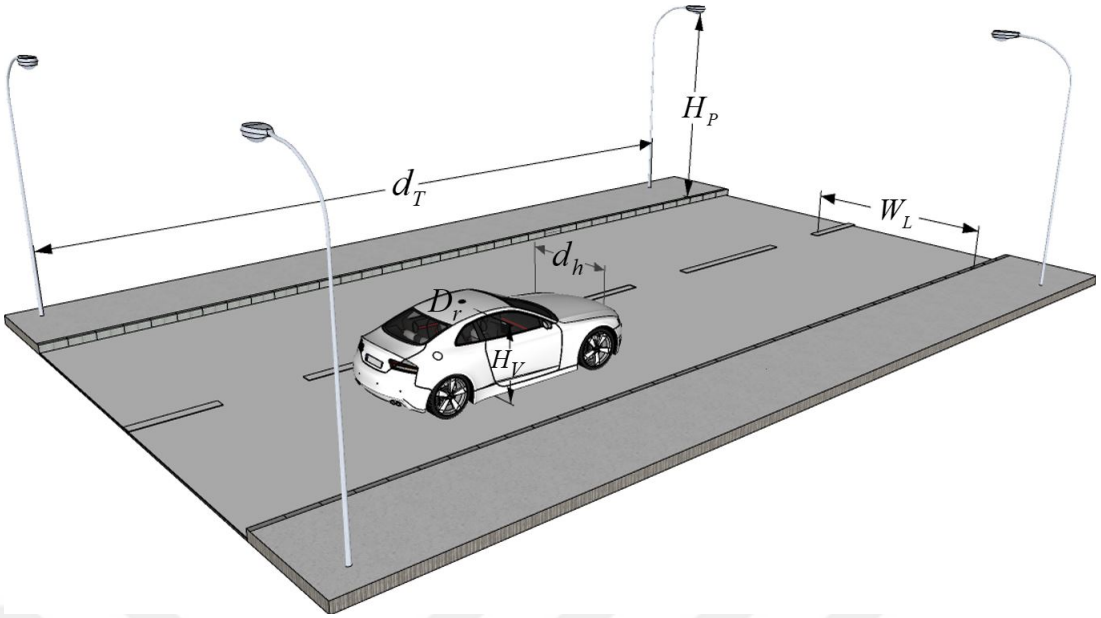

Figure 22: I2V VLC system with street lights.

4.3 I2V Based Street lights

System and Channel Model: As illustrated in Fig. 22, we consider an I2V VLC system with access points in the form of street lights. We assume a two-lane highway road with a total width of W_T and a lane width of W_L. The light poles have a height of H_P and are located at both sides of the road. On each side, they are uniformly separated from each other with a spacing of d_T. Each street light LED has an optical power of P_T and an electrical-to-optical conversion of η. The vehicle has a height of H_V and travels at a longitudinal distance of d with respect to the street light pole and has a possible lateral shift of d_h with respect to the road center. The vehicle is equipped with a PD located at its top. The PD has an aperture size of D_r, a responsivity of R, and a half field-of-view angle of FoV.

For channel modeling, we use the ray tracing approach explained and validated in Chapter 2, and applied for V2V VLC channels in Chapter 3. First, we construct the 3D propagation environment (including vehicles, street lights, road, etc.) in the OpticStudio 18.9 software. To precisely capture the interaction of the rays with the environment, we specify the optical characteristics of the road surface, streetlight poles, and vehicle coating by defining their wavelength-dependent reflectance values utilizing the built-in

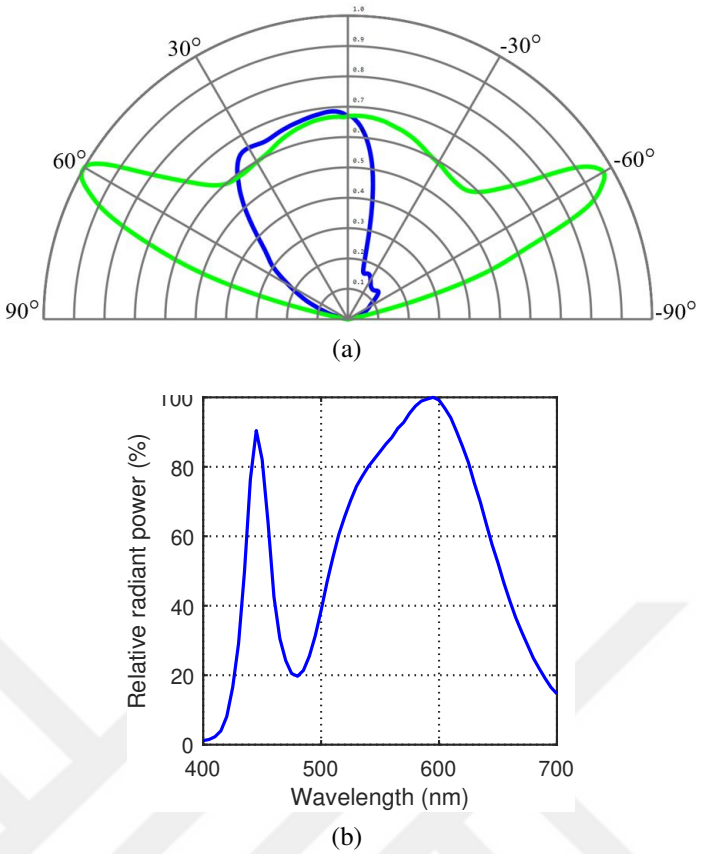

Figure 23: Optical characteristic of street light LED (a) Relative intensity distributions at both vertical and horizontal planes and (b) Relative spectral power distribution.

function "Table Coating" provided by OpticStudio tools. For transmitter modelling in the simulation platform, we create the photometric data (i.e., IES file) of the street light under consideration which contains the luminous intensity in all different planes. The photometric file is imported to the software along with the spectral power distribution of the LED (see Fig. 23). For receiver modeling, we specify the PD properties, i.e., FoV, aperture size.

After the simulation platform is constructed, we run non-sequential ray tracing. The output includes the received power and the path length information for each ray which is emitted from the light source and reaches the detector. Let P_{ij} and τ_{ij} respectively denote the power and the propagation delay of the i^{th} ray, $i = 1,2,\ldots,N_{rj}$, which is emitted from the j^{th} street light, $j = 1,2,\ldots,N_p$, and reached to the detector. The CIR at the PD is therefore expressed as

$$h(t) = \sum_{j=1}^{N_p} \sum_{i=1}^{N_{rj}} P_{ij}\,\delta(t-\tau_{ij}), \tag{4.4}$$

Table 4: Simulation parameters for I2V with street light transmitters.

Receiver	Aperture size (D_r)	1 cm, 2.5 cm, 4 cm		
	Field-of-view (FoV)	90°		
	Responsivity (R)	0.4 A/W		
	Noise density (N_0)	1×10^{-21} A^2/Hz		
	Bandwidth (B_w)	5 MHz		
Road	Type	R2		
	Material	Asphalt		
	Lane width	3.75 m		
Vehicle	Brand	Caterham R400	Audi A5	Mitsubishi Pajero
	Length	3.10 m	4.67 m	4.90 m
	Width	1.75 m	1.84 m	1.85 m
	Height	0.80 m	1.37 m	1.90 m
	Material	Black gloss paint		
Lighting pole	Material	Galvanized steel metal		
	Spacing (d_T)	15 m - 30 m		
	Height (H_P)	6 m - 10 m		
	Number of poles (N_P)	4		

where $\delta(t)$ is the Dirac delta function. We consider only the received signals from the four closest poles, therefore set $N_P = 4$, because the contribution from the other poles is too small and negligible. Based on Eq. (4.4), the path loss in dB is calculated similar to Eq. (4.2).

Path Loss Model: Based on the channel modeling approach described in the previous section, we obtain CIRs between the street lights and the moving vehicle at each 1 m over the traveling distance between two poles. The intensity pattern and relative spectral power distribution of streetlights used in simulations (Vestel Ephesus M4S [119]) are illustrated in Fig. 23. All simulation parameters are provided in Table 4. In our simulations, we assume that the optical power of each street light is unity. We can then scale the CIR for any given value of transmit power P_T to calculate the received power

(P_r) as $P_r = P_T\left(\int_0^{\infty} h(t)\,dt\right)$. The corresponding path loss is obtained based on Eq. (4.5) and presented in Fig. 24 for different combinations of H_P, D_r, H_V, d_T, and d_h values (See Table 5). Since the street lights are uniformly distributed along the road and with specific spacing distances, the vehicle on its way approaches a lighting pole and moves away from it. As a result, the received power exhibits a periodic pattern. In the following, we propose a closed form expression for I2V channel model to describe this sinusoidal behavior.

Let $2C_{\mathrm{P}}$ and C_{SA} respectively denote the peak-to-peak change of received power and the sinusoidal axis. The path loss is written as

$$h_{\mathrm{dB}} = C_{\mathrm{P}}\, z + C_{\mathrm{SA}}, \tag{4.5}$$

where $z = \cos\left(\left(2\pi/d_T\right) d\right)$ with d denotes the moving distance of the vehicle from one street light pole to the next one. C_P and C_{SA} in Eq. (4.5) are constants that can be calculated for a given scenario. Their values are influenced by the height of the lighting pole (H_P), the height of the vehicle (H_V), the distance between two lighting poles (d_T), lateral shift (d_h), and the diameter of the PD (D_r). Based on non-linear curve fitting [120], we obtain C_{P} and C_{SA} as Eq. (4.6) and Eq. (4.7), respectively.

$$C_{\mathrm{P}} = f\left(D_r, H_P, H_V, d_T, d_h, \mathbf{b}_1\right) - f\left(D_r, H_P, H_V, d_T, d_h, \mathbf{b}_2\right), \tag{4.6}$$

$$C_{\mathrm{SA}} = f\left(D_r, H_P, H_V, d_T, d_h, \mathbf{b}_1\right) + f\left(D_r, H_P, H_V, d_T, d_h, \mathbf{b}_2\right), \tag{4.7}$$

where in Eq. (4.6) and Eq. (4.7), $f\left(D_r, H_P, H_V, d_T, d_h, \mathbf{b}_i\right),\ i = 1,2$ is given by

$$\begin{aligned} f\left(D_r, H_P, H_V, d_T, d_h, \mathbf{b}_i\right) = {} & D_r\left(b_{i,1} + b_{i,2}\, d_h + b_{i,3}\, H_D + b_{i,4}\, d_T + b_{i,5}\, D_r\right) \\ & + d_T\left(b_{i,6} + b_{i,7}\, d_h + b_{i,8}\, H_D + b_{i,9}\, d_T\right) \\ & + H_D\left(b_{i,10} + b_{i,11} d_h + b_{i,12} H_D\right) \\ & + d_h\left(b_{i,13} + b_{i,14}\, d_h\right) \\ & + b_{i,15}, \end{aligned} \tag{4.8}$$

where $H_D = H_P - H_V + 1.371$ and $b_{i,j}$ denotes the j^{th} element of $\mathbf{b}_i$. It can be readily checked from Eq. (4.8) that each of transceiver and infrastructure parameters has different impact on the C_{P} and C_{SA} values. The values of C_{P}, C_{SA}, and $\mathbf{b}_i$ are determined

Table 5: System parameters for I2V with street light transmitters.

H_P (m)	d_T (m)	d_h (m)	D_r (cm)	C_P	C_{SA}
6	15	2	1	4.4679	-64.743
			2.5	4.2228	-56.289
7	18	2	2.5	4.4014	-57.255
	19	2	2.5	4.7492	-57.603
	21	2	2.5	5.3848	-58.245
	20	1	2.5	4.6165	-58.020
		1.5	2.5	4.8355	-57.970
		2	1	5.2054	-66.350
			2.5	5.0770	-57.930
			4	4.8720	-54.520
		2.5	2.5	5.3410	-57.920
8	22	2	1	4.9091	-66.863
			2.5	4.8620	-58.480
9	24	2	1	4.7461	-67.489
			2.5	4.7802	-59.141
10	30	2	1	5.1435	-68.704
			2.5	5.3062	-60.393

through data fitting and provided, respectively, in Table 5 and Table 6. It can be noted that the coefficient of $\mathbf{b}_i$ vector given in Table 6 are fixed for all system configurations.

To validate the proposed model in Eq. (4.5), we consider the pole height range as 6 m $\leq H_P \leq$ 10 m which is the typical pole height for streets in residential, commercial, and historical contexts [121]. Based on the pole height, the spacing range between the poles (d_T) is calculated which should be between 2.5-3 times the height [121]. Therefore, the spacing range of 15 m $\leq d_T \leq$ 30 m is considered. Also, different receiver apertures, i.e., D_r = 1 cm, D_r = 2.5 cm, and D_r = 4 cm are considered which are commercially available [122]. For the vehicle height (H_V), without loss of generality, we choose three values representing the lowest, average, and tallest height of current production cars which are given respectively as H_V = 0.8 m, H_V = 1.37 m, and H_V = 1.9

Table 6: Values of $\mathbf{b_i}$ coefficients in Eq. (4.8)

$\mathbf{b_1}$					
$b_{1,1}$	9.2155	$b_{1,6}$	-0.0632	$b_{1,11}$	-0.2078
$b_{1,2}$	3.8463e-04	$b_{1,7}$	0.0189	$b_{1,12}$	2.5373e-05
$b_{1,3}$	0.0161	$b_{1,8}$	0.0073	$b_{1,13}$	1.5592
$b_{1,4}$	0.0075	$b_{1,9}$	-0.0012	$b_{1,14}$	0.0208
$b_{1,5}$	-1.1290	$b_{1,10}$	-0.5359	$b_{1,15}$	-66.0693
$\mathbf{b_2}$					
$b_{2,1}$	10.0234	$b_{2,6}$	-1.6214	$b_{2,11}$	-0.0490
$b_{2,2}$	0.0480	$b_{2,7}$	0.0086	$b_{2,12}$	-0.2654
$b_{2,3}$	-0.0606	$b_{2,8}$	0.0334	$b_{2,13}$	-0.1189
$b_{2,4}$	-0.0083	$b_{2,9}$	0.0188	$b_{2,14}$	-0.0690
$b_{2,5}$	-1.0949	$b_{2,10}$	4.3667	$b_{2,15}$	-76.4639

m. For the lateral shift (d_h), we consider four possible values within the minimum and maximum limits according to the width of the car and the road-lane which are given as d_h = 1 m, d_h = 1.5 m, d_h = 2 m, and d_h = 2.5 m. In our simulation, we consider the received signals from the four closest poles (i.e., N_P = 4), because the contribution from the other poles is too small and negligible. Also, the coating materials for road, vehicles, and poles are considered as asphalt, black gloss paint, and galvanized steel metal which have reflectance values given in [112, 113]. We consider PDs with various values for FoV angles from 65° up to 90°. Relatively large FoV values are selected since a narrow FoV angle might be a significant impediment in vehicular VLC systems as it limits the mobility [28, 123]. On contrast, large FoV angle results in a higher tolerance to horizontal and vertical movements in real driving scenarios [42] and allows for reception from different directions.

In Figs. 24-27, along with the simulation results, we present the proposed path loss expression in Eq. (4.6). It is observed that the proposed model is in a good agreement with the simulation results for all H_P, H_V, d_T, D_r, and d_h values under consideration with a maximum difference of 0.45 dB.

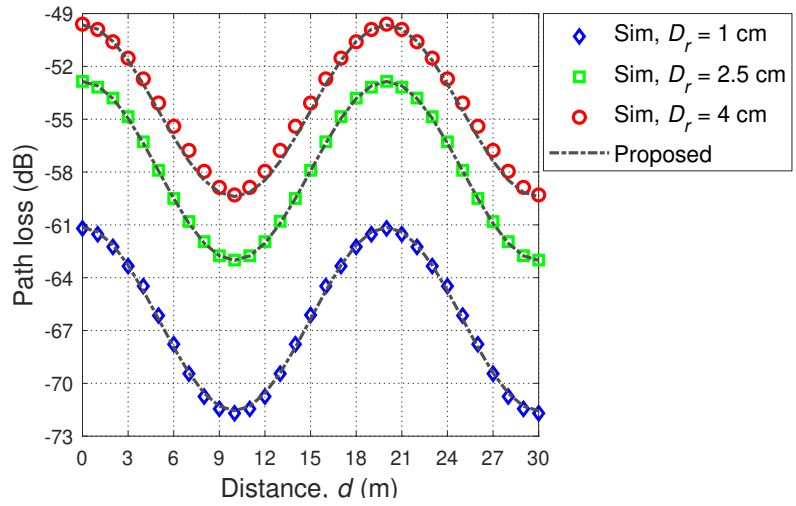

Figure 24: Path loss results at different sizes of receiver apertures (D_r) assuming H_P = 7 m, d_h = 2 m, H_V = 1.37 m, and d_T = 20 m.

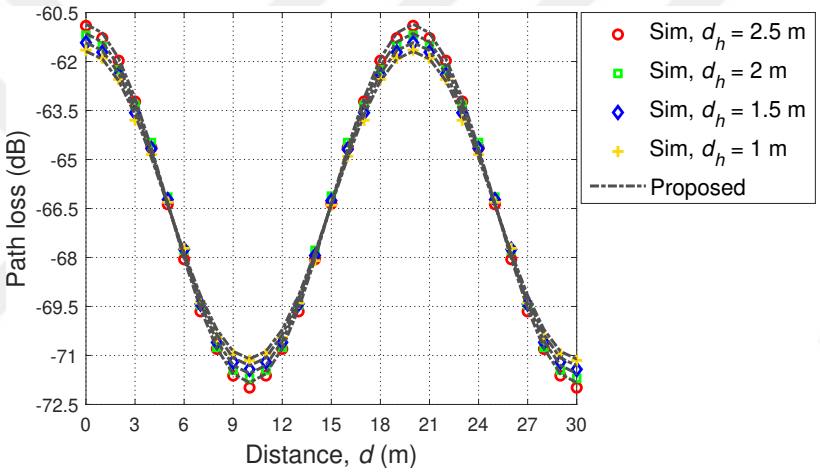

Figure 25: Path loss results at different lateral shifts (d_h) assuming H_P = 7 m, D_r = 1 cm, H_V = 1.37 m, and d_T = 20 m.

In Fig. 24, we assume fixed values of H_P = 7 m, H_V = 1.37 m, d_T = 20 m, and d_h = 2 m and investigate the effect of different receiver apertures, i.e., D_r = 1 cm, D_r = 2.5 cm, and D_r = 4 cm. It is observed that the path loss is significantly affected by the receiver aperture with a nonlinear relationship, which indicates that even a small decrease in the diameter can significantly increase the path loss. For example, consider the car moves at the middle between two lighting poles (i.e., d = 10 m). The path loss for D_r = 4 cm is -59.3 dB. This increases to -63 dB and -71.7 dB for D_r = 2.5 cm and D_r = 1 cm, respectively.

In Fig. 25, we assume fixed values of H_P = 7, H_V = 1.37 m, d_T = 20 m, and D_r

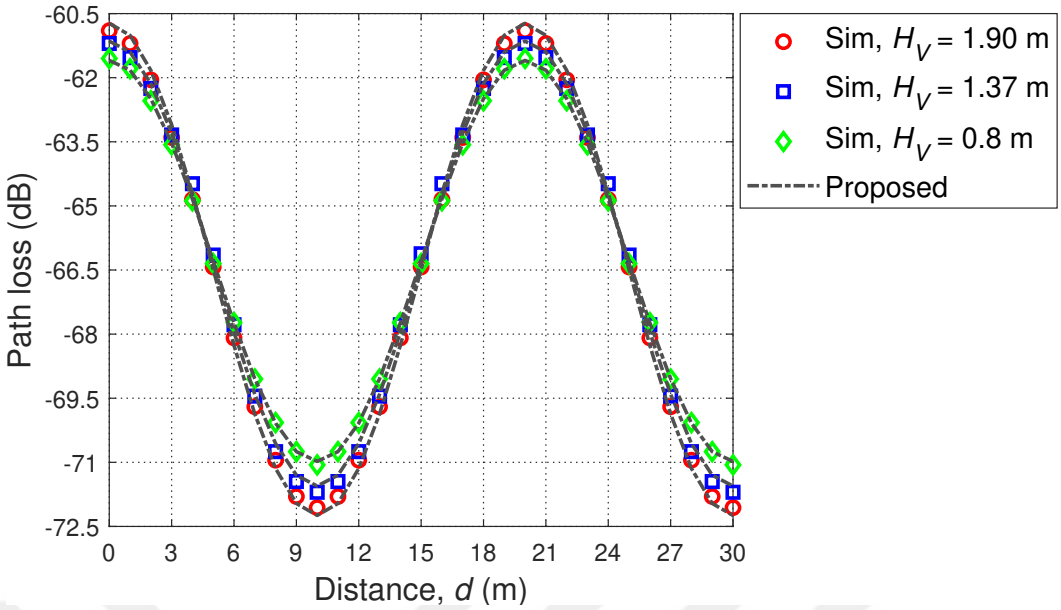

Figure 26: Path loss results at different vehicle heights (H_V) assuming $H_P = 7$ m, $d_h = 2$ m, $D_r = 1$ cm, and $d_T = 20$ m.

= 1 cm and investigate the effect of lateral shift, i.e., $d_h = 1$ m, $d_h = 1.5$ m, $d_h = 2$ m, and $d_h = 2.5$ m. It is observed that the impact of the lateral shift (d_h) is very small which is only visible when the vehicle is very close to either the light pole or to the middle between two poles. It is also seen that when d_h increases the path loss reduces at shorter distances (i.e., smaller d) and increases at larger distances (i.e., larger d). This is because at shorter distances, increasing d_h means that the vehicle becomes closer to the light pole where the maximum power can be received and hence a lower path loss occurs. At larger distance with larger d_h, the car becomes at the middle between two light poles located at one roadside (minimum power is received) and far away from the light poles located at the other roadside.

In Fig. 26, we assume fixed values of $H_P = 7$ m, $d_h = 2$ m, $d_T = 20$ m, and $D_r = 1$ cm and investigate the effect of car height, i.e., $H_V = 0.8$ m, $H_V = 1.37$, and $H_V = 1.9$ m. It is observed that the taller height of the car the lower path loss at shorter distances (i.e., ≤ 3 m) and higher path loss at larger distances. Closer to the lighting pole, the higher the car the more the collected power. This since the relatively small height difference between the PD and the streetlight pole and hence less propagation distance. At larger distance, however, taller car reduces the amount of collected powers from the streetlight

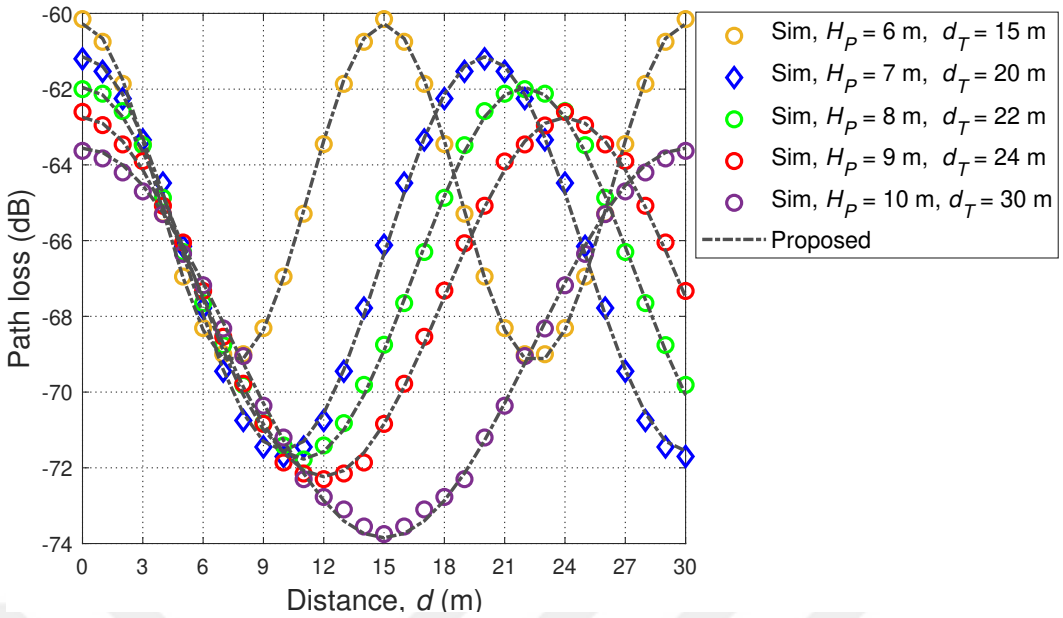

Figure 27: Path loss results at different pole heights (H_P) and spacing distances (d_T) assuming D_r = 1 cm, d_h = 2 m, and H_V = 1.37 m.

poles around the car. For example, consider the car is located under the light pole. The path loss is given for the lowest car height of H_V = 0.8 m as -61.6 dB. This reduces to -61.15 dB and -60.8 dB for H_V = 1.37 m and H_V = 1.9 m, respectively. When the car reaches the middle distance between two neighboring poles (i.e., d = 10 m), the path loss is given for H_V = 0.8 m, H_V = 1.37 m, and H_V = 1.9 m as -71 dB, -71.6 dB, and -72.1 dB, respectively.

In Fig. 27, we assume fixed values of D_r = 1 cm, H_V = 1.37 m, and d_h = 2 m and investigate the effect of pole heights, i.e., H_P = 6 m, H_P = 7 m, H_P = 8 m, H_P = 9 m, and H_P = 10 m with their corresponding spacing distance of d_T = 15 m, d_T = 20 m, d_T = 22 m, d_T = 24 m, and d_T = 30 m, respectively. It is observed the reverse effect comparing with the effect of the car height (H_V) where the smaller height of streetlights the lower path loss, particularly when the car moves closer to the lighting pole. This is due to the relatively shorter propagation distance and hence less attenuation. For example, consider the car location is under the lighting pole. The path loss for H_P = 10 m is -63.6 dB. This reduces for H_P = 9 m, H_P = 8 m, H_P = 7 m, and H_P = 6 m to -62.6 dB, -62 dB, -61.15 dB, and -60.2 dB, respectively.

Performance Results and Discussions: The proposed path loss model in Eq. (4.5)

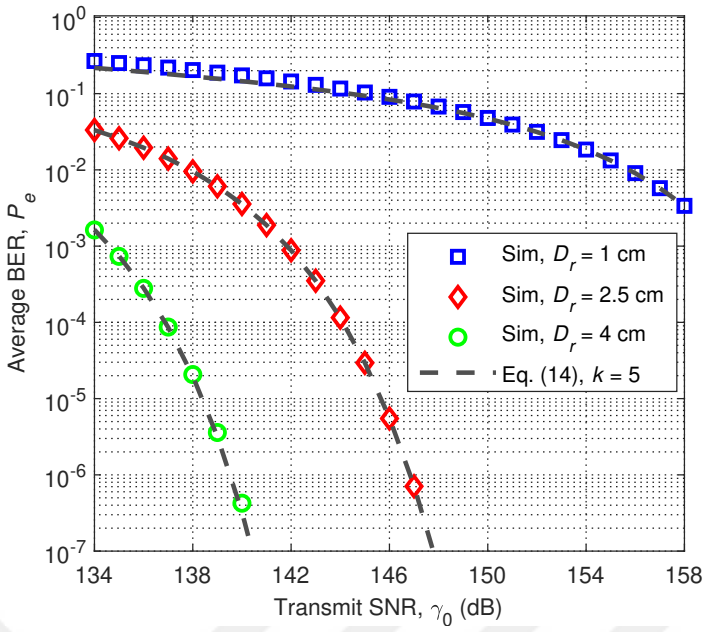

Figure 28: Effect of receiver aperture (D_r) on the average BER assuming $H_P = 7$ m, $d_h = 2$ m, $H_V = 1.37$ m, and $d_T = 20$ m.

exhibits a sinusoidal pattern which can be considered as large-scale fading [124]. This is utilized in [125] to derive an approximate closed-form average BER expression under the assumption of that unipolar M-ary PAM (M-PAM) is employed. By using Gauss-Chebyshev quadrature method of integration in [126, Eq. (25.4.38)], the average BER is given as [125, Eq. (14)]

$$P_e \approx \frac{M-1}{kM\log_2(M)} \sum_{j=1}^{k} \operatorname{erfc}\left(\sqrt{\frac{3}{(2(M-1)(2M-1))}\gamma_0}\, 10^{\left(0.1C_{\mathrm{P}}\cos\left(\frac{(2j-1)\pi}{2k}\right)+0.1C_{\mathrm{SA}}\right)}\right), \tag{4.9}$$

where k is the order of approximation. Here, we demonstrate the effect of transceiver and infrastructure parameters on the BER performance of the I2V system. Unless otherwise stated, we assume pole height of $H_P = 7$ m, pole spacing of $d_T = 20$ m, car height of $H_V = 1.37$ m, and lateral shift of $d_h = 2$ m. We consider a receiver with aperture of $D_r = 2.5$ cm and a FoV of 90°. We also consider PAM with $M = 4$, $N_0 = 1\times10^{-21}$ A^2/Hz [127, Chapter 19], and $B_w = 5$ MHz [128]. The values of η and R are considered respectively as 0.8 W/A and 0.4 A/W [129].

In our simulation, we consider the received signals from the four closest poles (i.e., $N_P = 4$), because the contribution from the other poles is too small and negligible. Also,

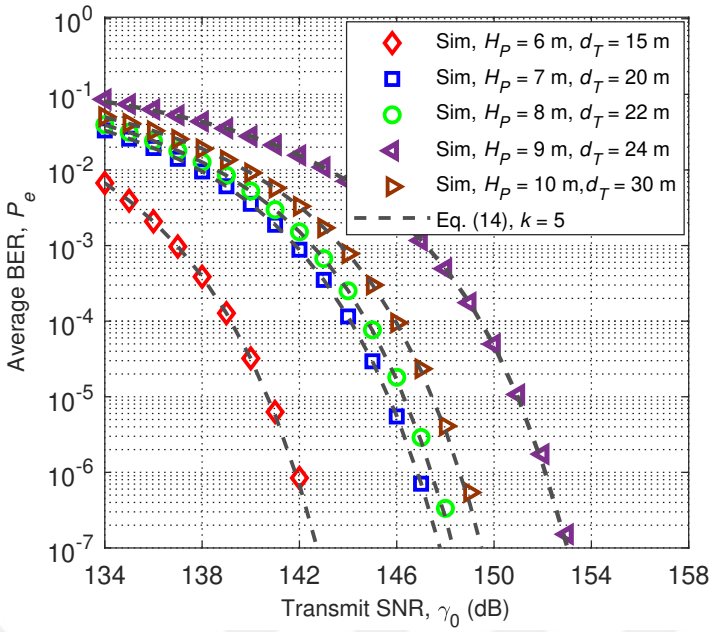

Figure 29: Effect of pole height (H_P) with corresponding spacing distance (d_T) on the average BER assuming $D_r = 2.5$ cm, $H_V = 1.37$ m, and $d_h = 2$ m.

the coating materials for road, vehicles, and poles are considered as asphalt, black gloss paint, and galvanized steel metal which have reflectance values given in [112, 113]. In the following, we present the effect of receiver aperture, pole height, car height, lateral shift, and spacing between poles on the average BER performance considering $k = 5$.

Fig. 28 illustrates the average BER for different values of receiver apertures (D_r) considering $H_P = 7$ m, $H_V = 1.37$ m, $d_T = 20$ m, and $d_h = 2$ m. It is observed that increasing the value of D_r has a significant improvement on the BER performance. This is due to the fact that the larger receiving area the larger number of photons that can be captured by the PD. For example, assume that an average BER of 10^{-3} is targeted. The required SNR value assuming $D_r = 1$ cm is 159 dB. This decreases to 141.9 dB and 135 dB for $D_r = 2.5$ cm, and $D_r = 4$ cm, respectively. One can notice that a PD with $D_r \leq 1$ cm might not be practical for I2V VLC with the system parameters under consideration. This is due to that I2V systems suffer a large SNR reduction when the vehicle becomes near the center between two streetlight poles with a significant impact on the average BER performance.

Fig. 29 illustrates the effect of pole height (H_P) with the corresponding spacing distance (d_T) on the average BER for fixed values of $D_r = 2.5$ cm, $H_V = 1.37$ m, and

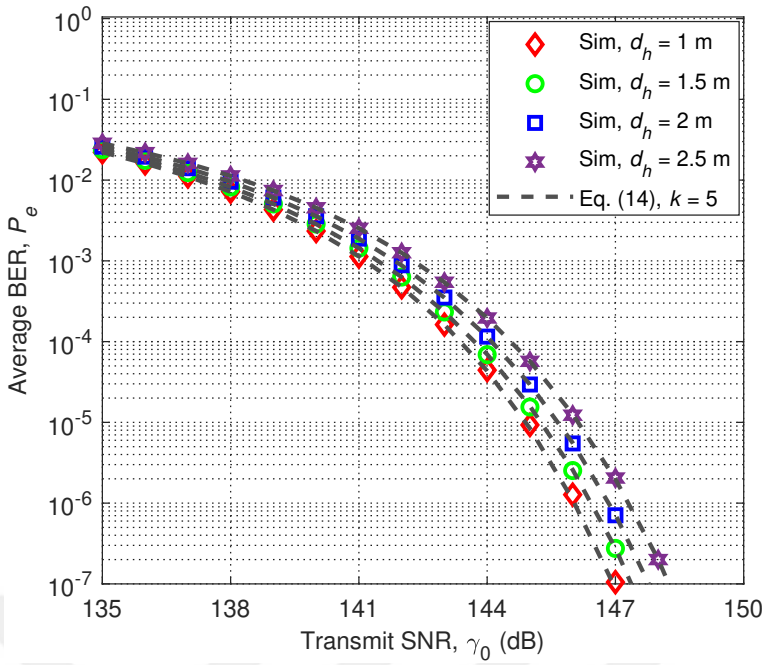

Figure 30: Effect of lateral shift (d_h) on the average BER assuming H_P = 7 m, D_r = 2.5 cm, H_V = 1.37 m, and d_T = 20 m.

d_h = 2 m. It is observed that decrease in H_P improves the average BER performance since the corresponding spacing distance reduces with decreasing H_P. For example, the required SNR value to achieve targeted BER of 10^{-3} for H_P = 10 m with d_T = 30 m is 147 dB. This decreases to 143.9 dB, 142.5 dB, 141.9 dB, and 137 dB for H_P = 9 m with d_T = 24 m, H_P = 8 m with d_T = 22 m, H_P = 7 m with d_T = 20 m, and H_P = 6 m with d_T = 15 m, respectively. A small change in the BER performance is observed between H_P = 7 m, H_P = 8 m, and H_P = 9 m while a large change is observed between either H_P = 7 m and H_P = 6 m or H_P = 9 m and H_P = 10 m. This is due to the relatively larger difference of the spacing distances in these cases where the path loss further increases particularly at the middle area between the poles. Note, the lowest value of the spacing distance is considered for H_P = 6 m (i.e., d_T = 15 m) while the highest one is considered for H_P = 10 m (i.e., d_T = 30 m) to illustrate the best and the worst cases, respectively.

Fig. 30 illustrates the effect of lateral shift (d_h) on the average BER performance for fixed values of H_P = 7 m, H_V = 1.37 m, D_r = 2.5 cm, and d_T = 20 m. It is observed that the effect of d_h is almost negligible where smaller d_h values lead to only slightly lower average BER. This is due to that when the vehicle becomes between two streetlight

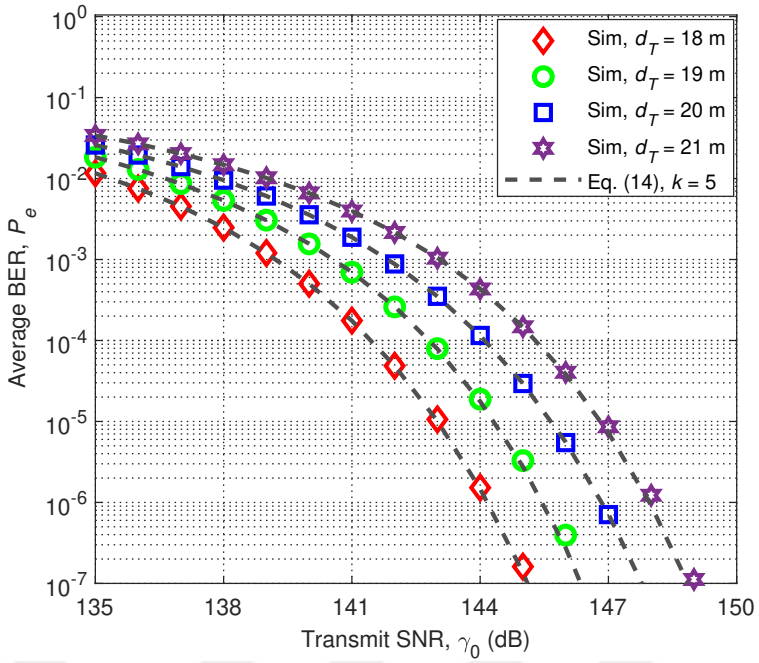

Figure 31: Effect of spacing distance between poles (d_T) on the average BER assuming H_P = 7 m, D_r = 2.5 cm, H_V = 1.37 m, and d_h = 2 m.

poles at one roadside, the smaller value allows the vehicle to collect slightly more power from the streetlights located at the other roadside.

Fig. 31 illustrates the effect of the spacing distance between the poles (d_T) on the average BER for fixed values of D_r = 2.5, H_P = 7 m, H_V = 1.37 m, and d_h = 2 m. It is observed that the longer spacing for the same pole height worsens the average BER performance. This is due to that the attenuation of the light signal as it travels through the air increases as long as the propagation distance increases. For example, the required SNR value to achieve a targeted BER of 10^{-3} for d_T = 21 m is 143 dB. This decreases to 141.9 dB, 140.5 dB, and 139.1 dB for d_T = 20 m, d_T = 19 m, and d_T = 18 m, respectively.

Finally, Fig. 32 illustrates the effect of car height (H_V) on the average BER performance for fixed values of H_P = 7 m, D_r = 2.5 cm, d_h = 2 m, and d_T = 20 m. It is observed that increase in H_V worsens the average BER performance. This is due to that when the taller car moves close to the middle distance between two light poles, the collected power from the streetlight poles around the car is less. For example, the required SNR value to achieve targeted BER of 10^{-3} for H_V = 0.8 m is 140.8 dB. This increases

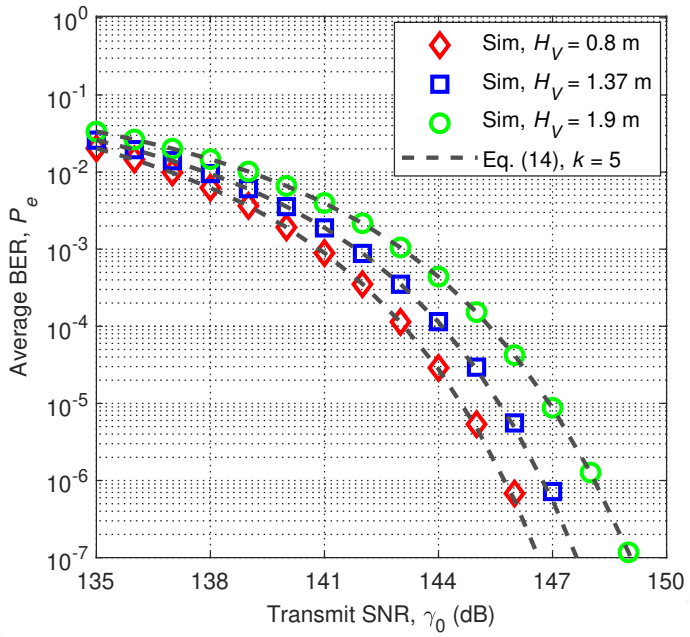

Figure 32: Effect of car height (H_V) on the average BER assuming H_P = 7 m, D_r = 2.5 cm, d_T = 20 m, and d_h = 2 m.

to 141.9 dB and 143.2 dB for H_V = 1.37 m and H_V = 1.9 m, respectively.

4.4 V2I Link and LED Front-end Effect

System and Channel Model: As illustrated in Fig. 33.a, we consider a V2I scenario in a two-lane road. We assume that the car moves at the right road lane with a separation distance of d with respect to the traffic light pole. We further define y_d which defines the horizontal shift between the car and the traffic light pole. As illustrated in Fig. 1.b, two high-beam LED HLs (denoted by Tx 1 and Tx 2) are used as VLC transmitters. These two LEDs are assumed to have an electrical-to-optical conversion of η and a total electrical power budget of P_e. Three photodetectors (PD-A, PD-B, and PD-C) are placed in the traffic light adjacent to yellow, red and green LED luminaries to act as wireless receivers. As illustrated in Fig. 33.b, PD-A is located at a height of h from the ground and a vertical separation of S is assumed between PDs. For channel modelling, we utilize non-sequential ray-tracing approach, described and validated in Chapter 2, used for modeling V2V VLC channels in Chapter 3, and recently applied for I2V link in Chapter 4. In this method, a 3D simulation platform with CAD models of cars and traffic poles is constructed in OpticStudio software. Then, we define the

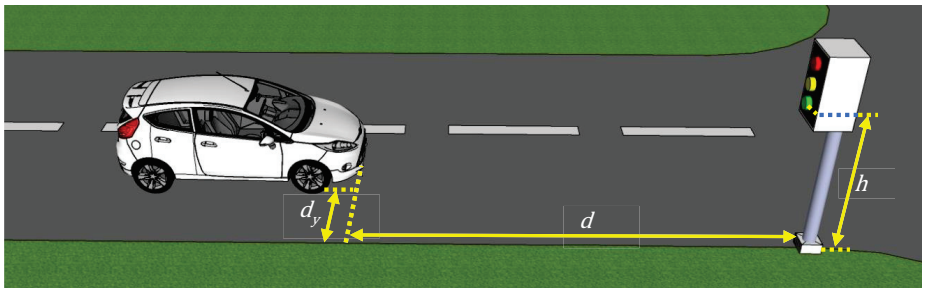

(a)

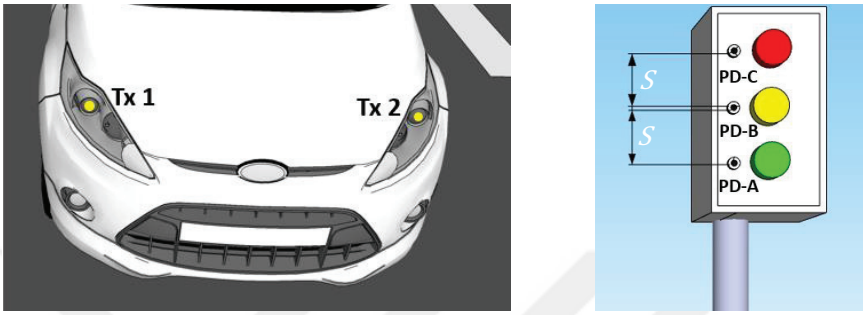

(b)

Figure 33: (a) V2I scenario under consideration and (b) Location of high-beam headlamps (transmitters) and photodetectors (receivers).

coating material of CAD-object surfaces where the scatter fraction and the wavelength-dependent reflectance are specified. The light source specifications such as radiation pattern, optical power, orientations, and the number of emitted rays are then defined. Similarly, receiver specifications such as orientations, FOV angle, and aperture area are defined.

After the 3D simulation platform is constructed, non-sequential ray tracing is executed to generate an output file including the power and the path length of each ray that reaches to the receiver. This information is proceed in MATLAB in order to obtain the CIR. Assume that N_j is the total number of rays reaching the j^{th} PD for a given distance d. Let P_{ij} and τ_{ij} respectively denote the power and the propagation delay of the i^{th} ray, $i = 1,2,...,N_j$ received by the j^{th} PD, $j = 1,...,3$. The CIR at the j^{th} PD can be expressed by

$$h_j^{\text{opt}}(t) = \sum_{i=1}^{N_j} P_{ij}\,\delta\left(t - \tau_{ij}\right), \tag{4.10}$$

where δ is the Dirac delta function. The corresponding frequency response is given by $h_j^{\text{opt}}(t) \xleftrightarrow{\text{FT}} H_j^{\text{opt}}(f)$. In addition to propagation environment, the LED characteristics might further introduce distortions. Let f_c denote the cut-off frequency of the LED. The

LED frequency response is typically given by [130]

$$H^{led}(f) = \frac{1}{1 + j\frac{f}{f_c}}. \tag{4.11}$$

Therefore, the effective frequency response at the j^{th} PD including the combined effects of both propagation channel and front-end effects is given by

$$H_j^{\text{eff}}(f) = H_j^{\text{opt}}(f) H^{led}(f) \xleftrightarrow{\text{IFFT}} h_j^{\text{eff}}(t). \tag{4.12}$$

The path loss can be then computed as

$$PL_j^{\text{eff}} = 10\log_{10}\left(\int_0^{\infty} h_j^{\text{eff}}(t)\, dt\right). \tag{4.13}$$

Achievable Data Rates: As a performance metric, we consider ergodic capacity which yields the maximum data rate that can be achieved in a communication system. For VLC systems with Intensity Modulation (IM)/Direct Detection (DD), the transmitted signal is typically constrained in both average and peak values [131]. The exact expression for ergodic capacity is still unknown for IM/DD systems. Consequently, different bounds on the capacity of optical channels are derived in the literature [132–134]. For example, it is shown in [134] that the gap between the exact and the lower bound can be neglected for high SNR values and the capacity can be approximated as

$$C \approx \frac{B}{2\ln(2)} \ln\left(1 + \frac{\exp(1)\,\gamma}{2\pi}\right), \tag{4.14}$$

where γ is the signal-to-noise ratio (SNR) and B is the bandwidth. SNR is given by

$$\gamma = \frac{\left(\eta R h_{DC}^{\text{eff}}\right)^2 P_{\text{e}}}{\sigma_n^2}, \tag{4.15}$$

where $h_{DC}^{\text{eff}} = \int_0^{\infty} h^{\text{eff}}(t)\, dt$ is the DC channel gain. $\sigma_n^2 = N_0 B$ is the noise variance and N_0 is noise power spectral density. Replacing Eq. (4.16) in Eq. (4.15), we have

$$C \approx \frac{B}{2\ln(2)} \ln\left(1 + \frac{\exp(1)\left(\eta R h_{DC}^{\text{eff}}\right)^2 P_{\text{e}}}{2\pi N_0 B}\right). \tag{4.16}$$

Simulation Results and Discussion: As shown in Fig. 33.a, we consider a V2I scenario in a two-lane road where R2 type road with asphalt coating is considered. The

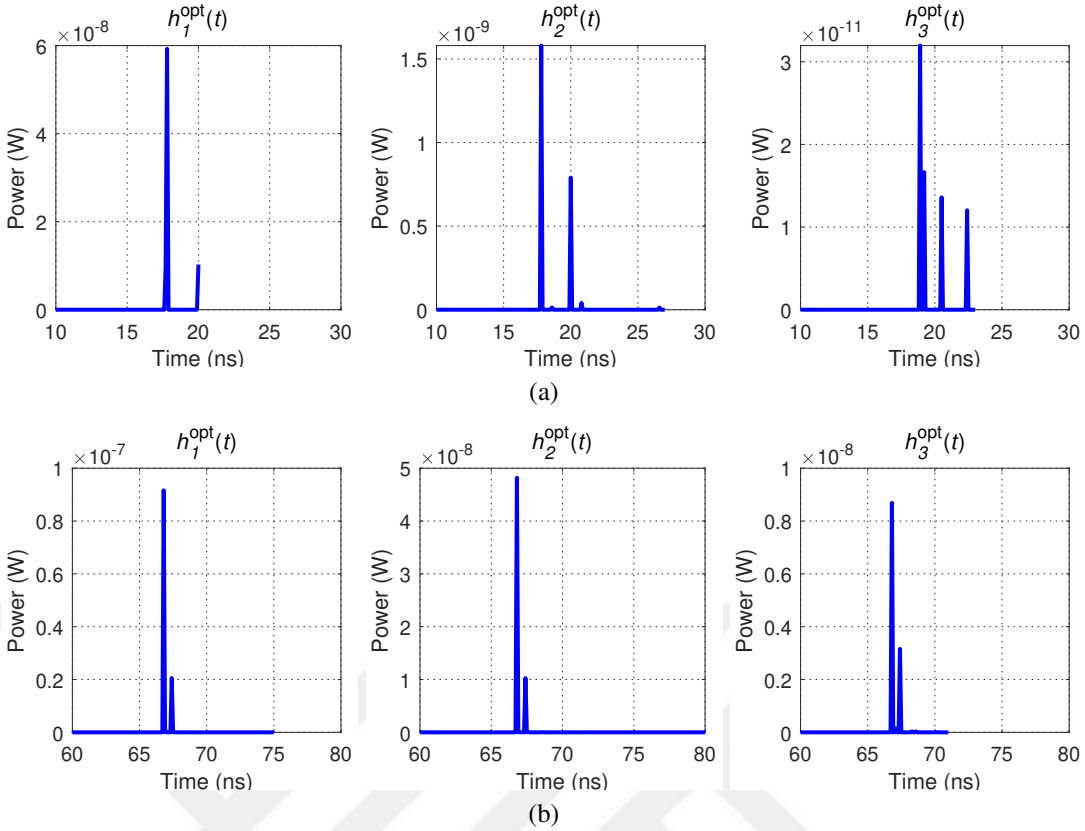

Figure 34: (a) CIR, and (b) corresponding frequency response for Nodes 1, 2, 3.

car is modeled as black-colored CAD object with dimensions of Audi A5 Coupe model [109]. The traffic pole is modeled as a CAD object with surface cover of galvanized steel. The values of h and S are assumed to be 2 m and 0.25 m, respectively. In our simulations, we use two Philips Luxeon Rebel white LEDs for car headlamps with P_e = 15 dBm, f_c = 20 MHz, and η = 0.5. We employ photodetectors each with an area of 1 cm^2, FOV angle of 90°, and responsivity of R = 0.28. In simulations, we first obtain CIRs under the assumption of unity transmission optical power. The CIRs can be then scaled for any given value of transmit power. We consider three scenarios:

- **Scenario I:** The car moves at the outer edge of the right lane with a horizontal shift of d_y = 0.25 m from the traffic pole.
- **Scenario II:** The car moves at the middle of the right lane which results in a d_y = 1 m shift with respect to the traffic pole and Scenario.
- **Scenario III:** The car moves at the inner edge of the right lane which results in a

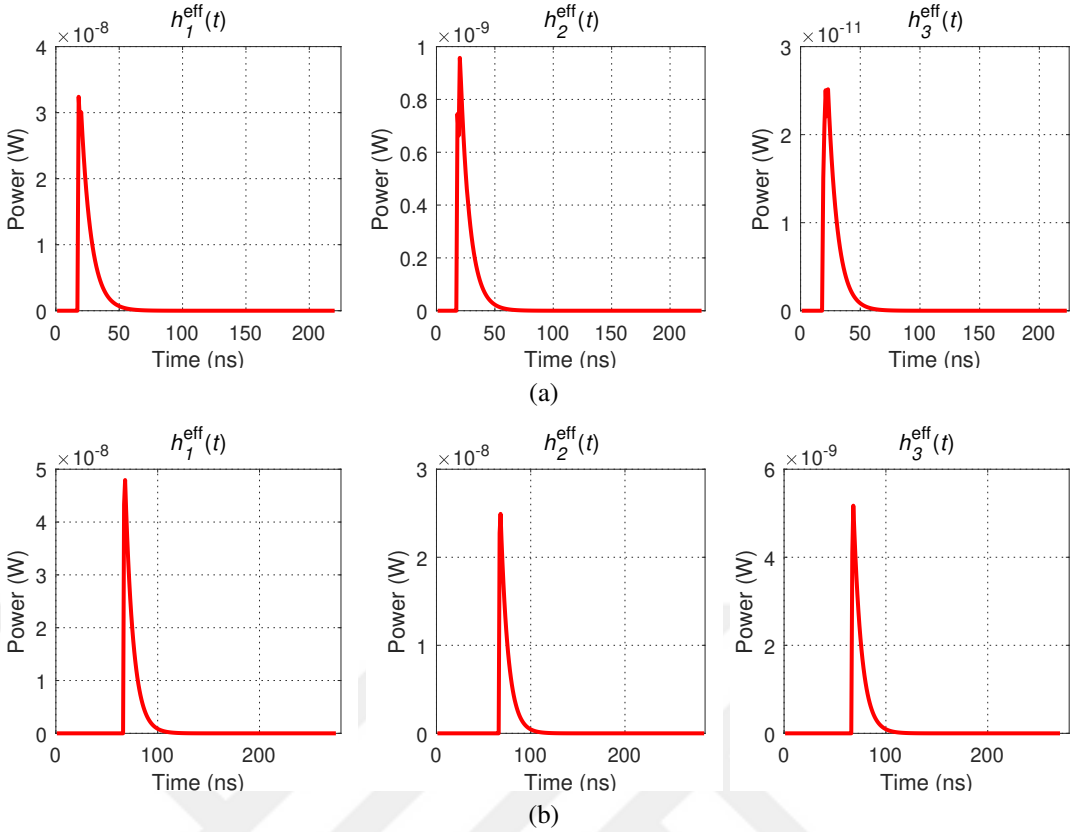

Figure 35: Effective CIRs for Scenario II at each PD assuming P_e = 15 dBm and f_c = 20 MHz (Right) d = 5 m (Left) d = 20 m.

d_y = 2 m shift with respect to the traffic pole.

In Fig. 34, we provide optical CIRs, i.e., $h_j^{\text{opt}}(t)$, $j = 1,...,3$ at distances of d = 5 m and d = 20 m for Scenario II. It can be observed that the CIRs have more than one peak where the highest peak comes from the right headlamp (Tx 1) and the second one comes from the left headlamp (Tx 2). This is due to the fact that signals with different travelling distances will have different arrival times. For example, consider d = 5 m and PD-A (see Fig. 34.a), the propagation distances from the right and left headlamps to the receiver are given, respectively, as 5.3 m and 6 m. It can be readily confirmed that the peak from the right headlamp occurs at 17.8 ns while the peak from the second headlamp is around 20 ns. It can be also observed that additional peaks are observed due to reflections from road. As seen from Fig. 34.b, as d increases, the distances between two peaks decreases and road reflections disappear.

In Fig. 35, we present the corresponding effective CIRs $h_j^{\text{eff}}(t)$, $j = 1,...,3$ for d = 5 m and d = 20 m assuming Scenario II. It is observed that the CIRs broaden in time due

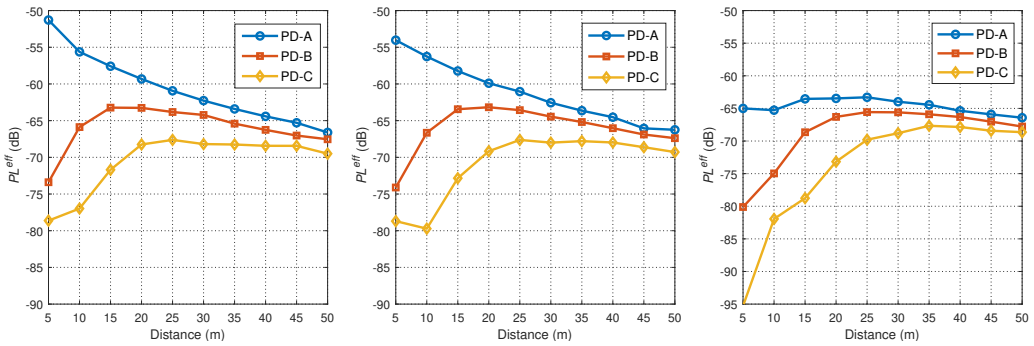

Figure 36: Path loss for (a) Scenario I (b) Scenario II (c) Scenario III for transmit power of P_e = 15 dBm and front-end bandwidth of 20 MHz.

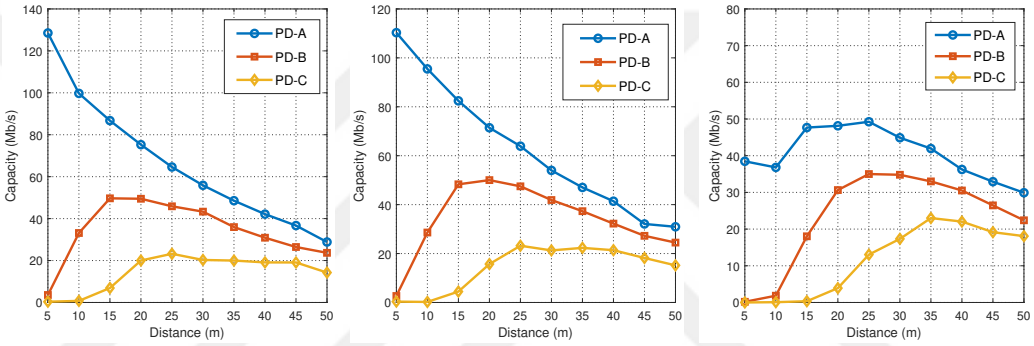

Figure 37: Achievable data rate versus distance at each PD for (a) Scenario I (b) Scenario II (c) Scenario III for transmit power of P_e = 15 dBm and front-end bandwidth of 20 MHz.

to the impact of low-pass nature of LED which dominates the overall characteristics. As a result, the effective CIR turns to be a single peak.

In Fig. 36, we present the path loss for all scenarios and three PDs under consideration. It is observed that PD-A achieves the highest channel gain while PD-C has the worst gain. This is due to the relatively large difference between its height and the height of car headlamps. For example, consider scenario I and a distance of d = 10 m. The channel gain using PD-A is recorded as PL_1^{eff} = -55.6 dB. This reduces to PL_2^{eff} = -65.8 dB and PL_3^{eff} = -76.9 dB for PD-B and PD-C, respectively. When the lateral shift (d_y) increases, the path loss further increases. For example, consider PD-A and a distance of d = 20 m. The path loss values for scenario I, scenario II, and scenario III are obtained respectively as -59.3 dB, 60.2 dB, and -63.5 dB.

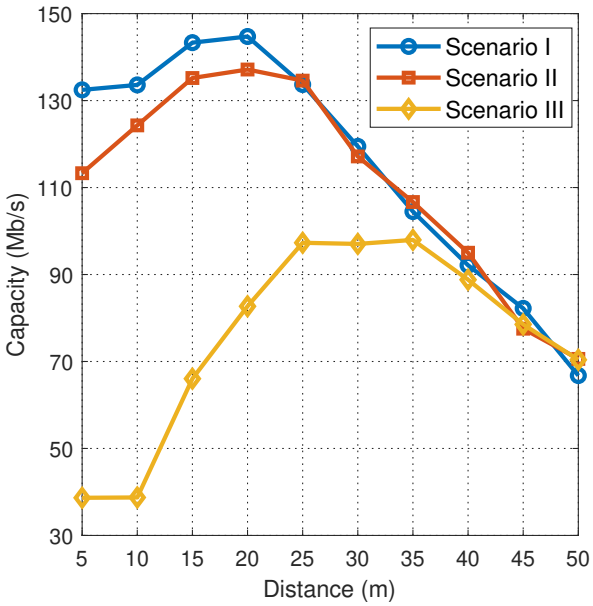

Figure 38: Achievable data rate versus distance for three photodetectors deployment case (equal gain combining).

In Fig. 37, the achievable data rates based on (4.17) are presented. Since the PD-A receives the highest gain with respect to other PDs, it can achieve the highest capacity for all scenarios under consideration. For scenario II and d = 30 m, the maximum data rate that can be supported with PD-A is 54 Mbps. This reduces to 41.8 Mbps and 21.3 Mbps respectively for PD-B and PD-C. It can be also noted that in shorter distances, the lateral shift dominates the overall characteristics. It is also observed that the capacity first increases with the distance until reaching the maximum value because of reducing the horizontal shift, d_y. Then, any increase in the distance results in decreasing of the capacity due to the effect of longitudinal distance, d.

So far, we assumed the employment of single photodetector. It is possible to take advantage of all three photodetectors. For this purpose, we employ equal gain combining. As observed from Fig. 38, the achievable data rate significantly increases due to combining.

To this end, we have investigated the channel modeling for V2V and I2V links and proposed closed-form expressions for the channel path loss under the common underlying assumption which is the use of one or two PDs. This is typically sufficient for establishing connection between two vehicles cruising in the same straight lane

or between vehicle and infrastructure with clear LoS. To position VLC as a strong candidate for vehicular connectivity, it is essential to realize multi-directional reception in various deployment scenarios supporting both V2V and I2V links. Therefore, it remains an open question what is the sufficient number of required PDs to achieve this. In Chapter 5 on the following page, we address this question of practical relevance by investigating the performance of a vehicular VLC systems in different road types and traffic scenarios.

CHAPTER V

MULTI-DIRECTIONAL COVERAGE FOR VEHICULAR COMMUNICATIONS

5.1 Introduction

In Chapter 3 and Chapter 4, we have investigated the channel modeling for the V2V and I2V links and proposed closed-form expressions for the path loss and maximum achievable distance for V2V links, and analyze the performance of I2V/V2I links. However, similar to the most of V2V and I2V VLC works [46, 56, 59, 64, 66, 71, 76, 79, 81, 103, 105, 110, 135–139], we considered the common underlying assumption which is the use of one or two PDs. This is typically sufficient for establishing connection between two vehicles cruising in the same straight lane or between the vehicle and infrastructure with clear LoS. To ensure reception in wider roads (i.e., two-lane) and curved roads, more PDs are typically required. For example, in [55], three PDs are deployed and, among three PDs, the one with maximum received power is chosen. In [140, 141], the performance of the V2V system is investigated utilizing an angle diversity receiver consisting of 4 and 3 PDs oriented in different directions. In [142], four PDs are used to prevent outages of a V2V system during lane change in a two-lane straight road.

In addition to aforementioned works which focus only on individual V2V or I2V links, there have been some sporadic efforts how to enable both V2V and I2V reception in the same time. For example, in [143], a receiver located at the vehicle's rooftop is utilized to receive the signals from the infrastructure and from the TLs of the front vehicle. These works, however, are limited to simple scenarios where two vehicles follow each other in single-lane or two-lane straight roads. To position VLC as a strong candidate for vehicular connectivity, it is essential to realize multi-directional reception in various deployment scenarios supporting both V2V and I2V links. Therefore, it remains an open question what is the sufficient number of required PDs to achieve this.

In this Chapter, we address this question of practical relevance by investigating the performance of a vehicular VLC system in different road types (i.e., multi-lane and curved roads), intersections (i.e., T-shaped and Y-shaped intersections) and traffic scenarios (i.e., cruising in the same or different lanes, lane change etc.). We conduct a channel modeling study based on non-sequential ray tracing approach, described and validated in Chapter 2, to quantify the capability of receiving signals in different cases. We first quantify the total received power versus distance for different scenarios under consideration. Our results reveal that deployment of nine PDs with carefully determined locations on the vehicle is sufficient to create the required quasi-omni-directional coverage for both V2V connectivity (in front and back directions) and I2V connectivity (with traffic and street lights). Then, we quantify the contribution of individual PDs to elaborate the main usage cases of each PD. We further investigate the effect of neighbor vehicles and possible blockage on the system performance.

The rest of this chapter is organized as follow. In Section 5.2, we describe our system model and vehicular scenarios under investigation. In Section 5.3, we illustrate the number and location of the Photodetectors on the connected Vehicle. In Section 5.4, we present the results of the total received power and the results of the contribution of individual PDs.

5.2 System Model and Vehicular Scenarios

Since the focus of this chapter is to investigate the placement and the number of PDs, we only consider the destination vehicle in V2V and I2V links. As illustrated in Fig. 39, the destination vehicle can receive signals from the front vehicle (where the TLs of the front vehicle serve as the transmitters) or from the preceding vehicle (where the HLs of the preceding vehicle serves as the transmitters). In I2V links, the wireless transmitters are street lights or traffic lights. The scenarios under consideration are summarized in Table 7. We consider V2V links in two-lane roads (Scenarios 1-3), multi-lane roads (Scenarios 4-6), T-shaped intersections (Scenarios 7 and 8), Y-shaped intersections (Scenarios 9 and 10), and curved roads (Scenario 11 and 12). We consider

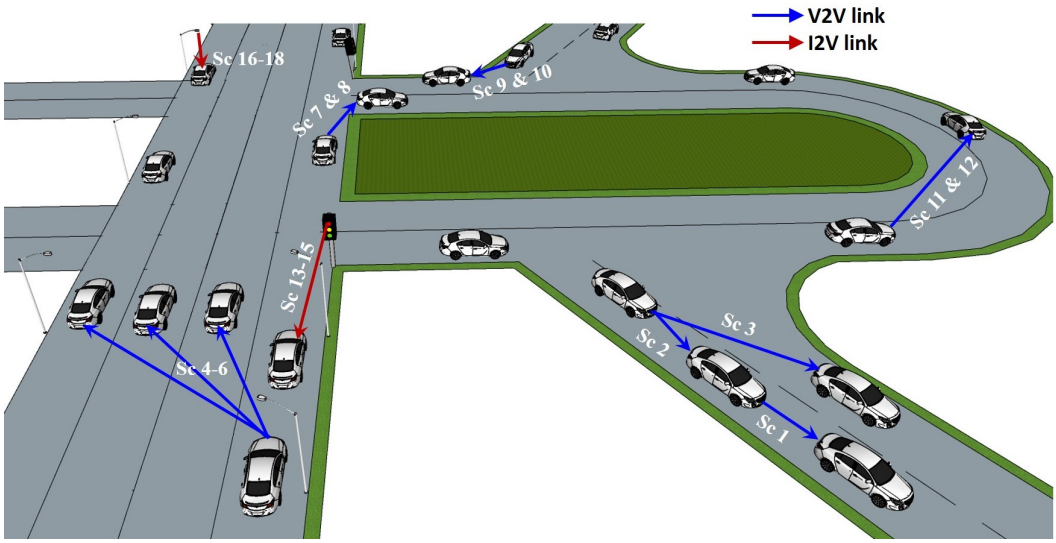

Figure 39: Full view of vehicular VLC scenarios.

I2V links either with traffic lights (Scenarios 13-15) or street lights (Scenarios 16-18). In the above scenarios, we have focused on cases where there are no neighbor vehicles or blockage nearby. Finally, in Scenarios 19-21, we investigate the effect of neighbors and possible blockage due to other vehicles in the same lane.

In Scenarios 1-3, we consider a straight road with two lanes each of which has a width of w_l. The vehicles are separated with a longitudinal distance of d and a lateral one of d_h.

- **Scenario 1 (Fig. 40.a):** In this ideal scenario widely assumed in the literature, the vehicles follow each other in the same lane and with a perfect alignment, i.e., $d_h = 0$.
- **Scenario 2 (Fig. 40.b):** The vehicles follow each other in the same lane but there is a misalignment between the vehicles. The maximum lateral shift between the two vehicles is $d_h = w_l - w_v$ where w_l denotes the width of the vehicle.
- **Scenario 3 (Fig. 40.c):** The two vehicles move in neighbor lanes and the source vehicle changes its lane approaching to the destination vehicle within the target lane.

In Scenarios 4-6, we consider a multi-lane road where each lane has a width of w_l.

Table 7: Vehicular scenarios under consideration.

Scenario	Road Design	Transmitter	Description
Scenario 1	Two-lane Straight road	HLs & TLs	The vehicles follow each other with a perfect alignment, i.e., $d_h = 0$.
Scenario 2	Two-lane Straight road	HLs & TLs	The vehicles follow each other in same lane but there is a misalignment, a maximum shift, i.e., $d_h = w_l - w_v$.
Scenario 3	Two-lane Straight road	HLs & TLs	The two vehicles are moving in neighbor lanes and the source vehicle changes its lane approaching to the destination one.
Scenario 4	Multi-lane Straight road	HLs & TLs	The source vehicle, located at center of 1^{st} lane, communicates with a destination one at center of 2^{nd} lane, i.e., $d_h = w_l$.
Scenario 5	Multi-lane Straight road	HLs & TLs	The source vehicle at center of 1^{st} lane , communicates with the destination one at center of 3^{rd} lane, i.e., $d_h = 2w_l$.
Scenario 6	Multi-lane Straight road	HLs & TLs	The source vehicle, located at the center of 1^{st} lane, communicates with destination one that travels at the center of the 4^{th} lane, i.e., $d_h = 3w_l$.
Scenario 7	T-Intersection	HLs & TLs	T-shaped road with $d_h \approx w_l/2$ between destination vehicle and intersection point.
Scenario 8	T-Intersection	HLs & TLs	Similar to scenario 4 but with shorter d_h value, i.e., $d_h \approx w_l/4$.
Scenario 9	Y-Intersection	HLs & TLs	Y-shaped road with $\theta = \sin^{-1}(2w_l/w_s)$ and $w_s \gg 2w_l$.
Scenario 10	Y-Intersection	HLs & TLs	Similar to scenario 9 but with larger angle, i.e., $w_s > 2w_l$.
Scenario 11	Curved-Road	HLs & TLs	Curved road with a large road radius, i.e., $R \gg w_l^3$.
Scenario 12	Curved-Road	HLs & TLs	Similar to scenario 11 but with shorter radius, i.e., $R \leq w_l^3$.
Scenario 13	Straight road	Traffic light	The vehicle moves at outer side of road lane, i.e., d_h is negligible with respect to w_l.
Scenario 14	Straight road	Traffic light	The vehicle moves at the center of the road lane, i.e., $d_h \approx w_l/4$.
Scenario 15	Straight road	Traffic light	The vehicle moves at the inner side of the road lane, i.e., $d_h \approx w_l/2$.
Scenario 16	Straight road	Streetlights	The vehicle moves at outer side of road lane, i.e., d_h is negligible with respect to w_l.
Scenario 17	Straight road	Streetlights	The vehicle moves at the center of the road lane, i.e., $d_h \approx w_l/4$.
Scenario 18	Straight road	Streetlights	The vehicle moves at the inner side of the road lane, i.e., $d_h \approx w_l/2$.

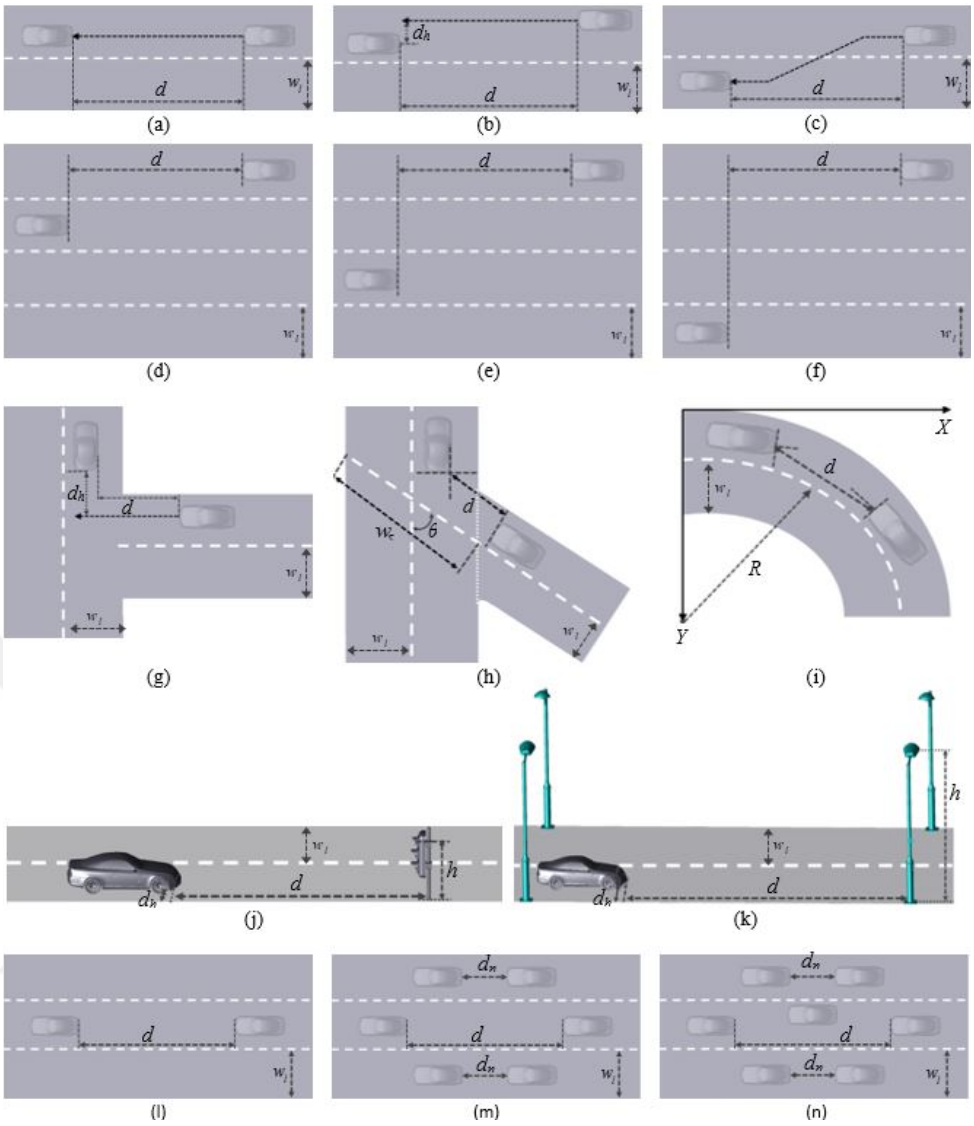

Figure 40: Vehicular VLC scenarios under investigation.

- **Scenario 4 (Fig. 40.d):** The source vehicle, located at the center of the 1^{st} lane, communicates with a destination vehicle that travels at the center of the 2^{nd} lane. This creates a lateral shift of $d_h = w_l$ between source and destination vehicles.

- **Scenario 5 (Fig. 40.e):** The source vehicle cruising at the center of the 1^{st} lane, communicates with a destination vehicle cruising at the center of the 3^{rd} lane, effectively resulting in a lateral shift of $d_h = 2w_l$.

- **Scenario 6 (Fig. 40.f):** The source vehicle cruising at the center of the 1^{st} lane, communicates with a destination vehicle cruising at the center of the 4^{th} lane, effectively resulting in a lateral shift of $d_h = 3w_l$.

In Scenarios 7 and 8, we consider T-shaped intersections.

- **Scenario 7 (Fig. 40.g):** In this scenario, the source and the destination vehicles are separated from each other with a longitudinal distance of d and there is a horizontal distance of $d_h \approx w_l/2$ between the source vehicle and the intersection point.

- **Scenario 8 (Fig. 40.g):** This scenario is similar to the previous one, but the destination vehicle is closer to the intersection, i.e., $d_h \approx w_l/4$.

In Scenarios 9 and 10, we consider Y-shaped intersections with an intersection angle of $\theta = \arcsin(2w_l/w_s)$ [144] where w_s denotes the intersection width.

- **Scenario 9 (Fig. 40.h):** In this scenario, the source and destination vehicles are separated with a longitudinal distance of d in a T-shaped intersection with a large intersection width, i.e., $w_s \gg 2w_l$.

- **Scenario 10 (Fig. 40.h):** This scenario is similar to the previous one but with relatively smaller intersection width, i.e., $w_s > 2w_l$.

In Scenarios 11 and 12, we consider a curved road with a radius of R where the vehicles are separated from each other with a distance of d.

- **Scenario 11 (Fig. 40.i):** In this scenario, we assume a large road radius, i.e., $R \gg w_l^3$.

- **Scenario 12 (Fig. 40.i):** In this scenario, we assume a relatively smaller road radius, i.e., $R \leq w_l^3$.

In Scenarios 13-15 (Fig. 40.j), we consider I2V link where the traffic light serves as the transmitter which has a height of h. The vehicle is assumed to be at a longitudinal distance of d with respect to the transmitter.

- **Scenario 13:** The vehicle moves at the outer side of the road lane, i.e., $d_h \ll w_l$.

- **Scenario 14:** The vehicle moves at the center of the road lane, i.e., d_h is comparable with w_l.

- **Scenario 15:** The vehicle moves at the inner side of the road lane with the maximum allowable lateral shift, i.e. $d_h = w_l - w_v$.

Scenarios 16-18 (Fig. 40.k) are identical to Scenarios 13-15 except the fact that the street light now serves as the transmitter. The vehicle moves between two street lights separated with a spacing of d_S where the vehicle can receive the data from the two poles.

In Scenarios 19-21, we consider a straight road with three lanes each of which has a width of w_l. The source and destination vehicles are in the middle lane and separated from each other with a longitudinal distance of d. There are also neighbor vehicles either in the same or different lanes.

- **Scenario 19 (Fig. 40.l):** This is the benchmark scenario where two connected vehicles follow each other in the middle lane of a three-lane road without any neighbor vehicles.

- **Scenario 20 (Fig. 40.m):** In this scenario, there are some neighbor vehicles in the other lanes. neighbor vehicles are assumed to travel in the middle of their lanes and are separated from each other with d_n

- **Scenario 21 (Fig. 40.n):** In this scenario, there is an additional neighbor vehicle which travels within the same lane and creates partial blocking to transmission between destination and source vehicles.

5.3 Location of the Photodetectors on the Vehicle

The number of PDs to be placed over the vehicle is the choice of system designer. It should be decided in such a way that omni-directional coverage should be ensured in various V2V and I2V scenarios while maintaining a reasonable cost. Considering most typical scenarios detailed above, we conjecture that 9 PDs would be enough to provide a quasi-omni-directional coverage. The locations of PDs are depicted in Fig. 41 and described as follows:

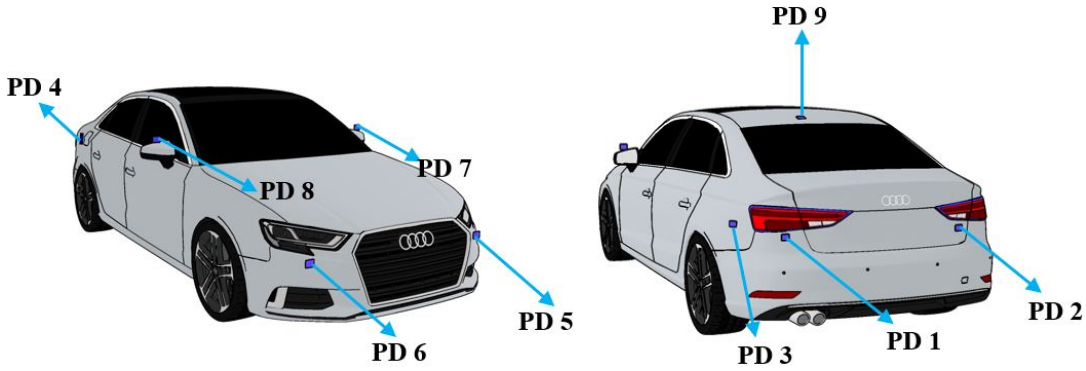

(a) (b)

Figure 41: Location of photodetectors on the destination vehicle a) Car front view b) Car back view.

- **At the back of the vehicle:** Two PDs (denoted as PD 1 and PD 2) are installed under the TLs. It is expected that they will be primarily useful to receive signals from HLs.
- **At the sides of the vehicle:** Two PDs (denoted as PD 3 and PD 4) are installed at the side-back of the vehicle and at the same height of PD 1 and PD 2. It is expected that PD 3 and PD 4 will be primarily useful when source and destination vehicles are in different lanes or in a curved road.
- **At the front of the vehicle:** Two PDs (PD 5 and PD 6) are installed under the HLs. They are positioned to receive signals from TLs of the front vehicle.
- **At the mirrors:** Two PDs (PD 7 and PD 8) are installed above the mirrors. They are expected to enable I2V links with traffic light transmitters. They might be also useful for V2V links in multi-lane or curved roads.
- **At the top of the vehicle:** A single PD (PD 9) is installed at the top of the vehicle. This is particularly useful for I2V links with street light transmitters.

We utilize the channel modeling approach described in Chapter 2 which is based on the non-sequential ray tracing features of OpticStudio. The main steps of this channel modeling methodology are illustrated in Fig. 1 (See Chapter 2). The output information, obtained from this approach, is imported into MATLAB in order to construct the CIR for each particular scenario.

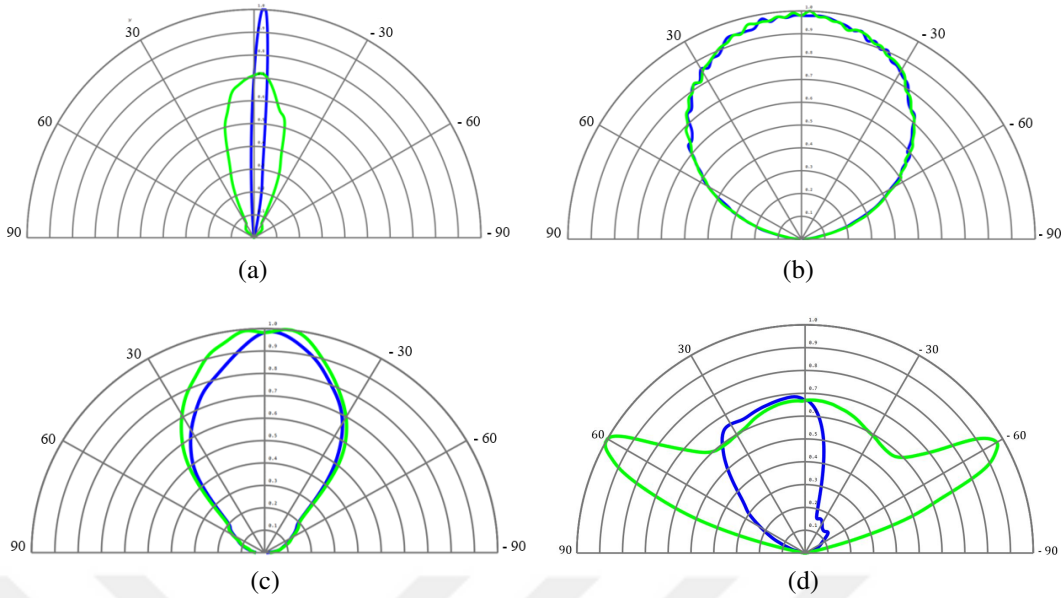

Figure 42: Radiation pattern of vehicular light sources in E-plan and H-plane. (a) Headlight (b) Taillight (c) Traffic light (d) Streetlight. For example, in (a), Blue line shows the intensity distribution of headlamp when one looks from side (e.g., from pavement) while the green line shows the pattern when one looks downward from top.

Consider the i^{th} transmitter and the j^{th} receiver. Let P_{ij}^{l} and τ_{ij}^{l} denote the optical power and the propagation delay of the l^{th} ray transmitted from the i^{th} LED and received by the j^{th} PD, respectively, $l = 1, \ldots, L_{ij}$. The normalized CIR for unit transmit power is given by

$$h_{i,j}(t) = \sum_{l=1}^{L_{i,j}} P_{i,j}^{l}\, \delta\left(t - \tau_{i,j}^{l}\right) \tag{5.1}$$

where $\delta(t)$ denotes the Dirac delta function. For a given transmit power of $\delta(t)$, the received optical power (in dB) at the j^{th} PD from the i^{th} transmitter can be then calculated as

$$Pr_{i,j} = 10\log_{10}\left(Pt_i \int_0^{\infty} h_{i,j}(t)\, dt\right) \tag{5.2}$$

The SNR is obtained as

$$\gamma = \frac{\left(\eta \sum_{j=1}^{N_r} Pr_j\right)^2}{N_0 B} \tag{5.3}$$

where η is the optical-to-electrical conversion ratio, N_r is the number of PDs, N_0 is the noise power spectral density, and B is the bandwidth. Let BER_{th} denote the targeted BER value. In order to avoid outage, the received SNR of the link should be higher than

Table 8: Simulation parameters for multi-directional coverage.

Receiver specifications	Area Field-of-view (FoV) Responsivity (η) Noise density (N_0) Bandwidth (B)	1 cm^2 90° 0.84 (A/W) 1×10^{-21} (A^2/Hz) 10 kHz, 10 MHz
Road specifications	Type Material Lane width (w_l) Road design	R2 Asphalt 3.75 m Straight, Intersections, Curved
Vehicle specifications	Length Width (w_v) Height Material	4.7 m 1.8 m 1.4 m Black gloss paint
Street light pole specifications	Material Spacing (d_S) Height (h)	Galvanized steel metal 20 m 7 m
Traffic light pole specifications	Material Height (h)	Galvanized steel metal 2 m

a threshold SNR value of γ_{th} calculated from BER_{th}. Under the assumption of OOK, the minimum required value of received optical power to avoid outage is obtained by [145]

$$Pr_{req} = \sqrt{\frac{N_0 B}{\eta^2}\left(Q^{-1}\left(BER_{th}\right)\right)^2} \tag{5.4}$$

5.4 Results and Discussion

5.4.1 Total Received Power

In this section, we present simulation results for vehicular scenarios under consideration based on non-sequential ray tracing. In our simulation study, Philips Luxeon Rebel white light LEDs [146] and Osram-TOPLED red light LEDs [147] are used for HLs and TLs, respectively. For street lights and traffic lights, Vestel Ephesus M4S [119] and Osram-OSLON [147] are utilized, respectively. The radiation patterns for HL, TL, traffic light, and street light are presented in Fig. 42. All simulation parameters are

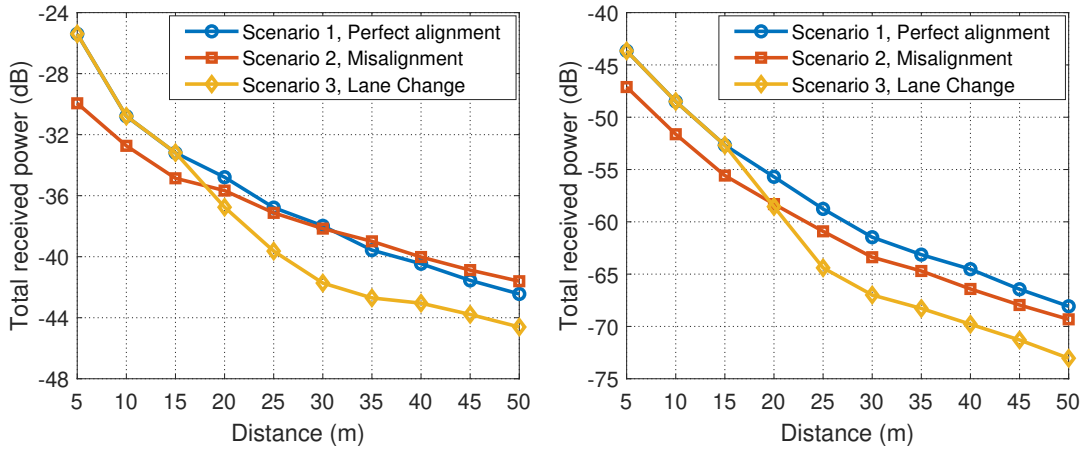

Figure 43: Total received power for V2V in straight road scenarios based on (a) HLs (b) TLs.

provided in Table 8. We further consider two different use cases:

- **Low-speed communication with B = 10 kHz:** This is sufficient for most safety applications [56,148]. From (4), it can be readily calculated that a received power of $Pr_{req} \geq -80$ dB is required to achieve $BER_{th} = 10^{-3}$.
- **High-speed communication with B = 10 MHz:** This is required to support higher data rates for infotainment applications such as video streaming [149,150]. This requires a received power of $Pr_{req} \geq -64.7$ dB.

In the following, we first present the total received power versus distance discussing what type of communications can be supported (Section 5.41). Then, in Section 5.4.2, we discuss the individual contributions of each PD to the total received power and highlight the main use case of each PD.

In Fig. 43, we present the received power versus distance for Scenarios 1-3 based on either HL transmitters (Fig. 43.a) or TL transmitters (Fig. 43.b). As expected, the received power takes its maximum value when two cars are in perfect alignment (i.e., Scenario 1). In Scenario 2, we assume that there is a misalignment of $d_h = 2$ m between the two vehicles. This misalignment is particularly effective at shorter longitudinal distances. For example, the received power for perfect alignment is -30.8 dB at d =

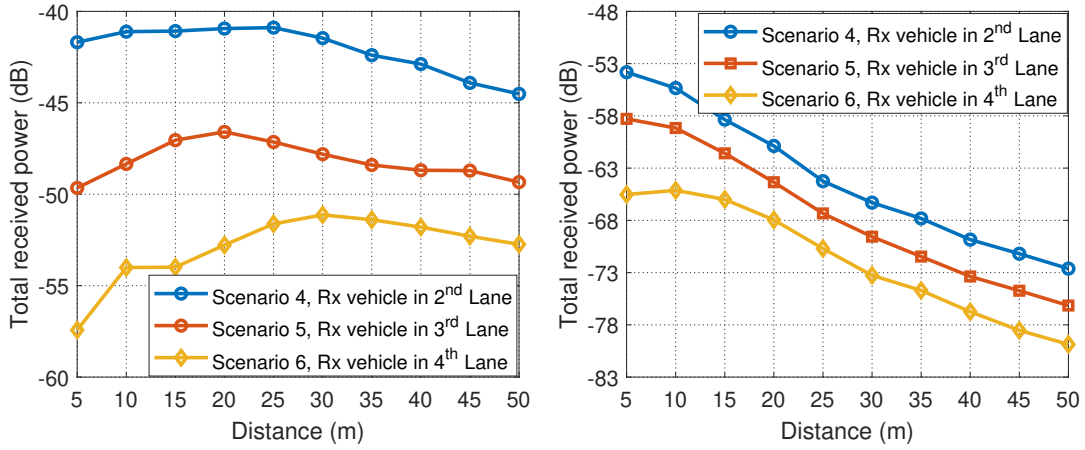

Figure 44: Total received power for V2V in multi-lanes scenarios based on (a) HLs (b) TLs.

10m under the assumption of HL transmitters (see Fig. 43.a). This reduces to -32.75 dB in the presence of misalignment. In Scenario 3, it is observed that the rate of change in the received power during the lane changing range (from 15 m to 30 m) is much higher than that in trailing period (from 30 m to 50 m). This is due to that during the lane switching, there is a change in both inter-vehicle distance (d) and lateral shift one (d_h). From Fig. 43, it can be concluded that the received power is sufficient (i.e., $Pr > -45$ dB) for both low- and high-speed communications in these three scenarios when HL transmitters are used to communicate with the preceding vehicle. On the other hand, with the use of TL transmitters, the received power (i.e., $Pr > -73$ dB) is sufficient only for low-speed communication.

In Fig. 44, we present the received power versus distance for Scenarios 4-6 based on either HL transmitters (Fig. 44.a) or TL transmitters (Fig. 44.b). It is observed that despite the relatively large horizontal displacements, two vehicles in different lanes can successfully communicate with each other. For example, the received power for Scenario 4 (i.e., source and destination vehicles are in neighbor lanes) is -40.9 dB at d = 25 m with HL transmitters. This reduces to -47.2 dB and -51.7 dB, respectively for Scenario 5 (i.e., source and destination vehicles are separated from each other with a lane), and Scenario 6 (i.e., source and destination vehicles are separated from each

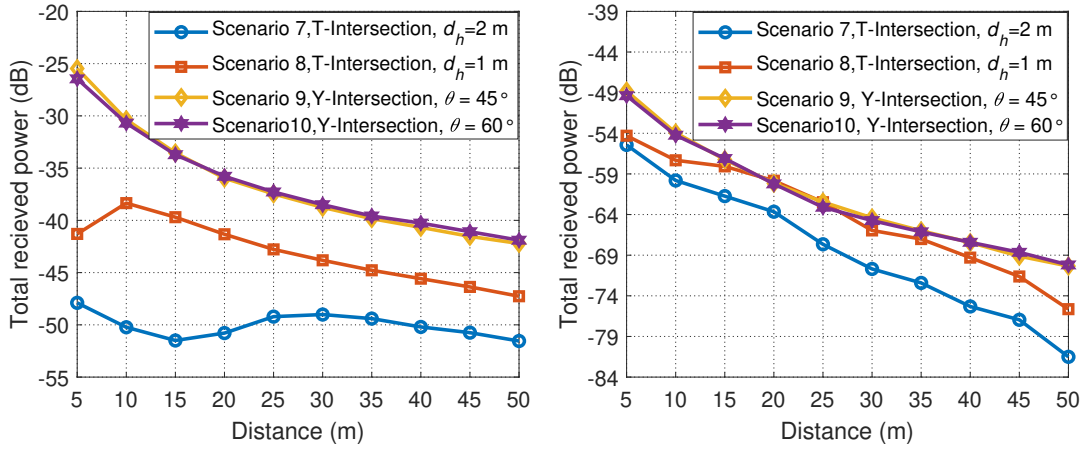

Figure 45: Total received power for V2V in intersection scenarios based on (a) HLs (b) TLs.

other with two lanes). It can be readily checked that both low- and high-speed communications can be supported when the HLs act as the transmitters. On the other hand, with TL transmitters, the received power is $Pr > -79.87$ dB and therefore satisfies the minimum level to support low-speed communication.

In Fig. 45, we present the received powers versus distance for Scenarios 7-10 where T- and Y-shaped intersections are considered. For T- shaped intersections (Scenarios 7 and 8), it is observed that the value of d_h (the distance between the destination vehicle and the intersection point) has a significant impact on the received power. For example, assuming d = 25 m and HL transmitters, the received power for d_h = 1 m is -42.7 dB. This reduces to -49.2 dB for d_h = 2 m. For Y-shaped intersections (Scenarios 9 and 10), an exponential decay in the received power with d is observed. It is also observed that the intersection angle θ has a little effect on the received power. For example, the received power for θ = 45° is -64.4 dB assuming TL transmitters and d = 30 m. This slightly reduces to -64.75 dB for θ = 60°. From Fig. 45, it can be concluded that the received power is sufficient (i.e., $Pr > -51.5$ dB) for both low- and high-speed communications in these four scenarios with HL transmitters. Based on the use of TL transmitters, the received power is sufficient (i.e., $Pr > -81.5$ dB) only for low-speed communication.

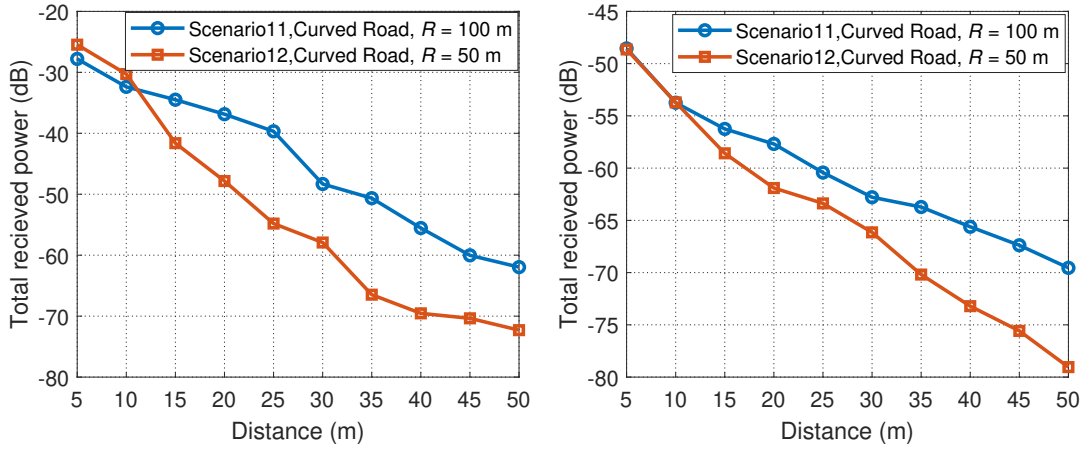

Figure 46: Total received power for V2V in curved road scenarios based on (a) HLs (b) TLs.

In Fig. 46, we present the received power versus distance for Scenarios 11-12 where a curved road is considered. It is observed that the received power significantly reduces when the road radius (R) decreases. For example, consider d = 40 m and HL transmitters. As observed from Fig. 46.a, the received powers for R = 100 m and R = 50 m are respectively -55.5 dB and -69.6 dB. It can be also observed that the received power much depends on the curve radius same as the propagation distance. At shorter radius together with larger distance, the received power is much reduced, and the system outage might occur particularly take place when high data rate is targeted. It can be readily checked that the received power in Scenario 11 is sufficient (i.e., $Pr > -61.9$ dB) for both low- and high-speed communications with HL transmitters while the received power in Scenario 12 remains lower than the minimum level of -64.7 dB. Based on the use of TL transmitters, the received power in these scenarios is sufficient (i.e., $Pr > -79$ dB) only for low-speed communication.

In Fig. 47, we present the received power versus distance for I2V scenarios based on either traffic light transmitters (Scenarios 13-15, Fig. 47.a) or street light transmitters (Scenarios 16-18, Fig. 47.b). It is observed from Fig. 47.a that the received power is affected by the particular position of the vehicle with respect to traffic light transmitter. As observed from Fig. 47.a, the received power at d = 10 m for d_h = 0 m (i.e., the

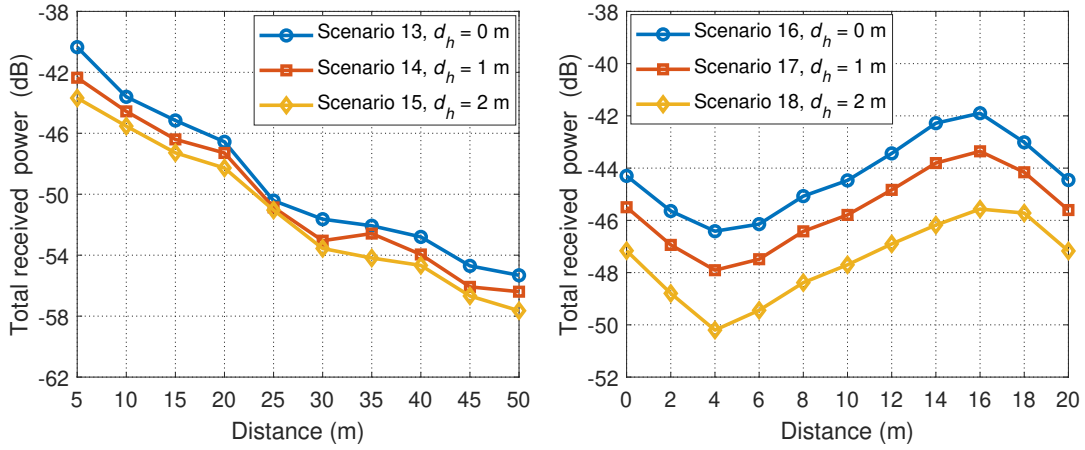

(a) (b)

Figure 47: Total received power for I2V scenarios based on (a) Traffic lights (b) Streetlights.

vehicle is located at the outer side of the road lane) is -43.6 dB. This reduces to -44.55 dB and -45.53 dB for d_h = 1 m and d_h = 2 m, respectively.

In Fig. 47.b, the street lights serve as transmitters where the vehicle moves between two street light poles separated with d_S = 20 m. Under the first pole, only PD 9 (located on the top of the vehicle) can collect a significant amount of the power. This is due to the fact that PDs 5-8 cannot see this transmitter, and PDs 1-4 (which are looking to the second pole) are still far. When the vehicle moves away from the first pole, the received power decreases. If the distance becomes sufficiently large ($d > 4$ m), the PDs 5-8 are now able to collect power. In particular PD 7 and 8 (located on the top of the mirrors) along with PD9 collect most of the power. When the vehicle approaches the second pole, the contributions of PDs 5-8 relatively decrease while there is some increase in received powers of PDs 1-4. In particular, PD 4 (located at same side of closer street lights) reaches its maximum value at d = 16 m. After that, it reduces to reach its minimum value when the vehicle arrives under the second pole (d = 20 m). At this point, a significant power is only collected again by PD 9. It can be readily checked that for all I2V scenarios under consideration, the received power is much higher than the required power to support both low- and high-speed communications.

In Fig. 48, we present the received power versus distance for Scenarios 19-21 where

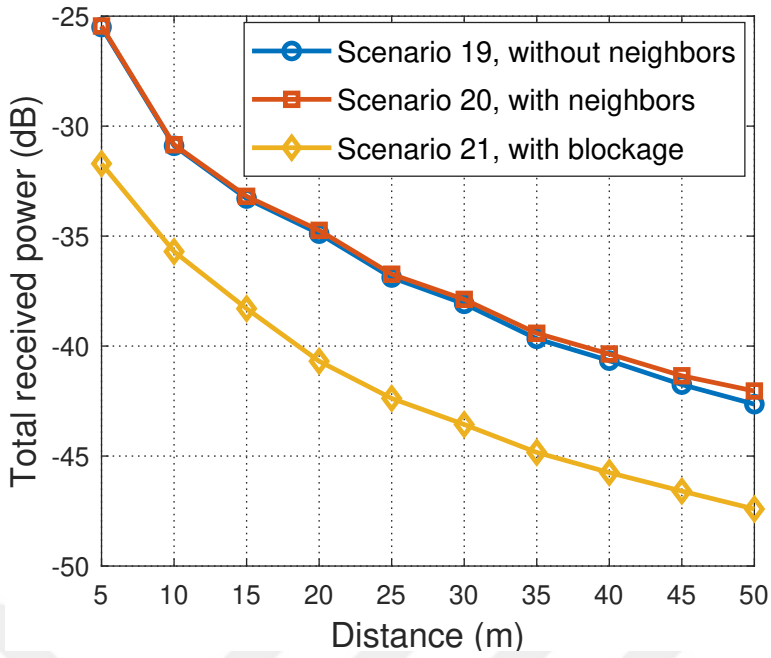

Figure 48: Total received power for V2V scenarios with neighboring vehicles.

the effect of neighbor vehicles and partial blockage are considered. In Scenario 20, it is observed that the received power slightly increases in comparison to the benchmark scenario (i.e., Scenario 19) as a result of receiving additional amount of power reflected from the neighbor vehicles. This is observed only at sufficiently large distances ($d \geq$ 40 m). The reason for that is at larger distances, the reflecting surface at the two sides of neighbor vehicles increases and hence the number of reflected rays reaching the PD increases. At shorter distances, the amount of received power from such reflections is negligible. In Scenario 21, a significant reduction in the received power is observed in comparison with Scenarios 19 and 20. This is due to the effect of partial blockage by the neighbor vehicle which travels in the same lane. For example, consider d = 50 m. The received power for scenario 19 is -42.6 dB. This increases to -42 dB and reduces to -47.4 dB for scenario 20 and 21, respectively. From Fig. 48, it can be further concluded that the received power is sufficient (i.e., $Pr >$ - 47.5 dB) for both low- and high-speed communications.

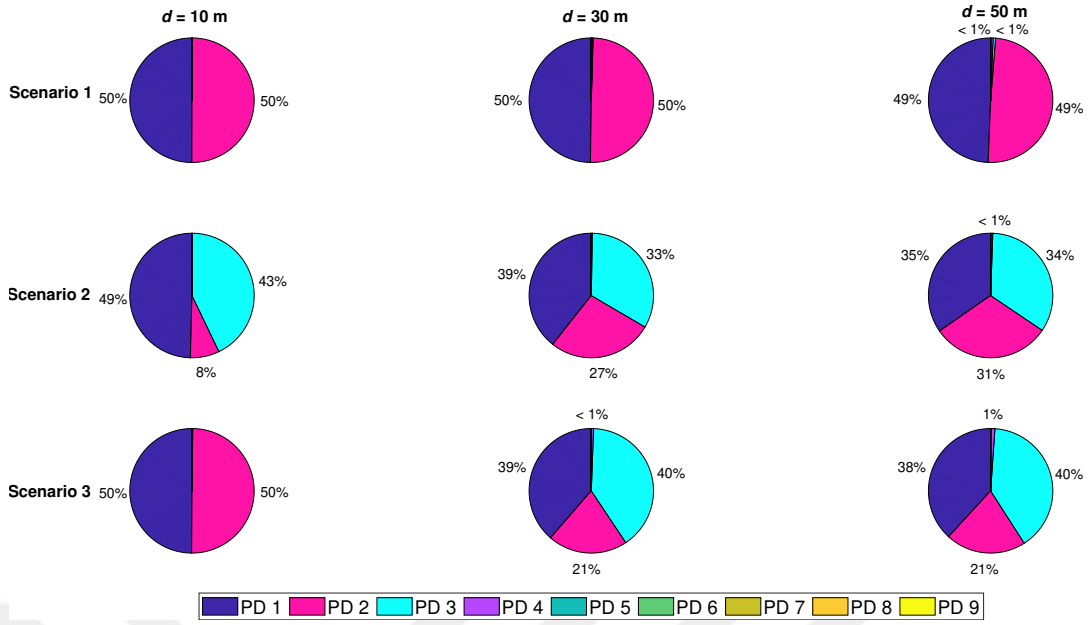

(a)

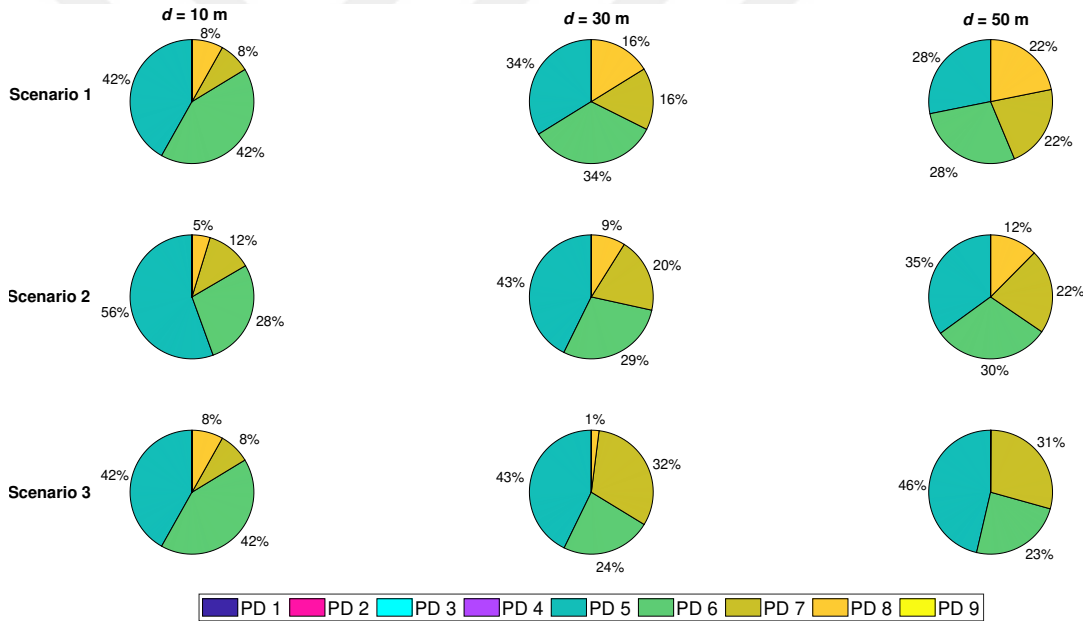

(b)

Figure 49: Contribution of each PD for V2V in straight road based on (a) HLs (b) TLs.

5.4.2 Individual Contribution of Each PD

In the previous section, we presented the total power versus distance for different scenarios under consideration. In this section, we quantify which PDs contribute at what extent to total received power.

In Fig. 49.a, we present pie charts for Scenarios 1, 2 and 3 based on HL transmitters. In Scenario 1 where two cars are perfectly aligned, the deployment of only two photodetectors in the back (i.e., PD 1 and PD 2) would be sufficient. These two PDs collect 98% or more of the total power based on the distance. For large distances, PD 3 and PD 4 collect a small amount as a result of road reflections if the distance between two vehicles is sufficiently large, e.g., about 2% at a distance of d = 50 m. In Scenario 2 when there is some displacement (towards the left-hand side) between two vehicles, it is observed that PD 1 and PD 3 (located on left-hand side of the destination vehicle) are primary receptors. The contribution of PD 2 increases with the increase in distance since the effect of lateral displacement becomes negligible for large distances. It should be noted that if the displacement is towards the right-hand side, PD 2 and PD 4 would be primary receptors. In Scenario 3, the lane change occurs from the left-hand side to the right-hand side. It is observed that within initialization range (from 10 m to 15 m), PD 1 and PD 2 can collect almost all power (i.e., 100%) due to the proper alignment between the two vehicles. However, during the lane change range (from 15 m to 30 m) and trailing range (from 30 m to 50 m), PD 3 collects the highest amount of received power (i.e., 40%) while the contributions of PD 1 and PD 2 are reduced.

In Fig. 49.b, we present pie charts for Scenarios 1, 2 and 3 based on TL transmitters. In Scenario 1 where two cars are perfectly aligned, PD 5 and PD 6 capture most of the received power if the distance is sufficiently small. When distance gets larger, the contributions of PD 7 and PD 8 are more pronounced since the height difference between the TL transmitters and PD 7 / PD 8 gets smaller. In Scenario 2 when there is some displacement (towards the left-hand side) between two vehicles, PD 5 and PD 6 remain as the primary receptors. However, in comparison to Scenario 1, the contribution of PD 6 is now reduced since it is located on the other side of the displacement. In Scenario 3, PD 5 and PD 6 collect most of the power within the initialization range (from 10 m to 15 m) while a small amount of received power is collected with PD 7 and PD 8. During the lane change range (from 15 m to 30 m) and trailing range (from 30 m to 50 m), PD 5, PD 6 and PD 7 collect almost all power and the contribution of PD 8 becomes

Figure 50: Contribution of each PD for V2V in multi-lane based on (a) HLs (b) TLs.

negligible.

In Fig. 50.a, we present pie charts for Scenarios 4, 5, and 6 based on HL transmitters. In these three scenarios, PD1 and PD 3 (located on the same side of the source vehicle) are the primary receptors. PD2 also contributes to the received power to some extent. With the increase in distance, the contribution of PD 2 increases. Because at sufficiently large distances, PD 2 is able to see both HLs of the source vehicle.

In Fig. 50.b, we present pie charts for Scenarios 4, 5, and 6 based on TL transmitters. In these three scenarios, PD5 and PD 7 (located on the same side of the source vehicle) are the primary receptors. PD 6 comes as the third largest contributor to the received power. Its contribution particularly becomes large for large distances. Finally, only a very small received power is collected by PD 8 as a result of road reflections if the distance between two vehicles is sufficiently large.

In Fig. 51.a, we present pie charts for Scenarios 7, 8, 9, and 10 based on HL transmitters. In Scenarios 7 and 8 where T-shaped intersection is considered, PD 3 collects most of the received power (e.g.,73% or more) due to its location on the side of intersection point. The rest of received power is collected by PD 1 and PD 2 and their contribution further decreases when either the longitudinal distance (d) or the horizontal one (d_h) increases. In Scenarios 9 and 10 where Y-shaped intersection is considered, PD 1 and PD 3 are the main receptors. For Scenario 9 where lower skew angle is considered (i.e., $\theta = 45°$), the contribution of PD 3 is approximately twice of PD 1 if the distance between the vehicles is sufficiently large. In Scenario 10 where a larger skew angle is considered (i.e., $\theta = 60°$), PD 1 is able to collect approximately same power amount of PD 3. In addition, PD 2 collects some power which increases when the distance gets larger.

In Fig. 51.b, we present pie charts for Scenarios 7, 8, 9, and 10 based on TL transmitters. In Scenarios 7 and 8 where T-shaped intersection is considered, PD 5 and PD 6 collect the highest amount of received power for shorter longitudinal distances. When the distance between two vehicles increases, the contribution of PD 7 much increases while the received power using PD 6 is significantly reduced because of its location on the other side of intersection point. A very small portion of received power is collected by PD 8 as a result of road reflections for sufficiently large distances. In scenarios 9 and 10 where Y-shaped intersection is considered, PD 5 collects the highest amount of received power for short distances. At larger distances, the contribution of PD 5 decreases while the contribution of PD 7 increases. Particularly at shorter distances, a significant amount of received power is collected by PD 6.

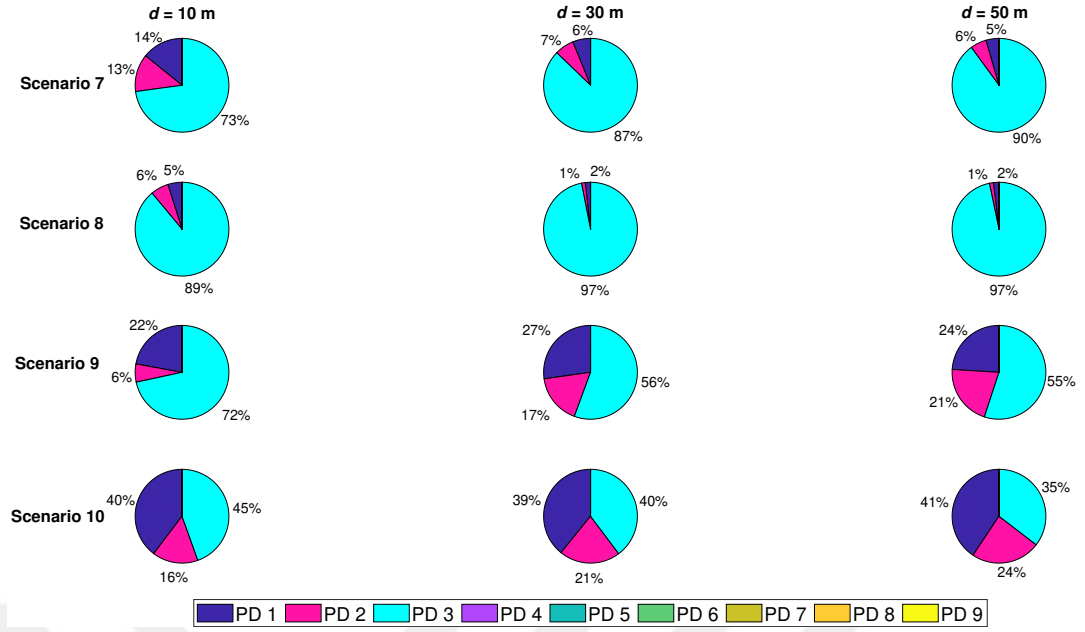

(a)

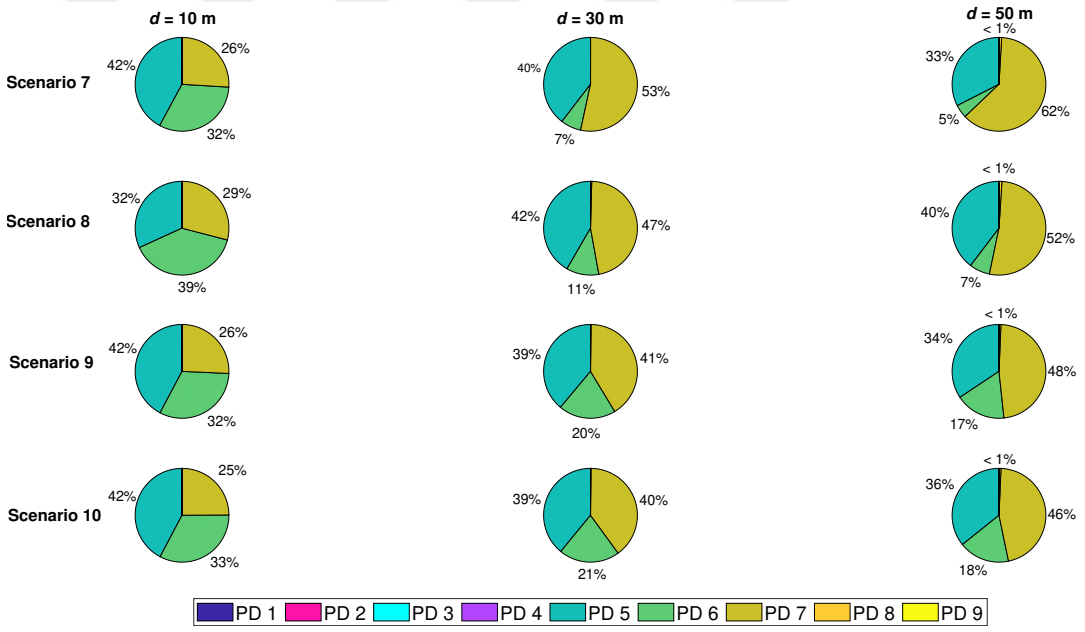

(b)

Figure 51: Contribution of each PD for V2V in intersections based on (a) HLs (b) TLs.

In Fig. 52.a, we present pie charts for Scenarios 11 and 12 based on HL transmitters. In Scenarios 11 and 12, curved roads with radii of R = 100 m and R = 50 m are considered, respectively. At shorter distances PD 3 collects the highest amount of received power (i.e., 69% at d = 10 m and Scenario 11) while contributions of PD 1 and PD 2 are somewhat limited. When the distance increases, the received power using PD 1 and PD 2 increases. For sufficiently large distance, the contribution of PD 2 becomes

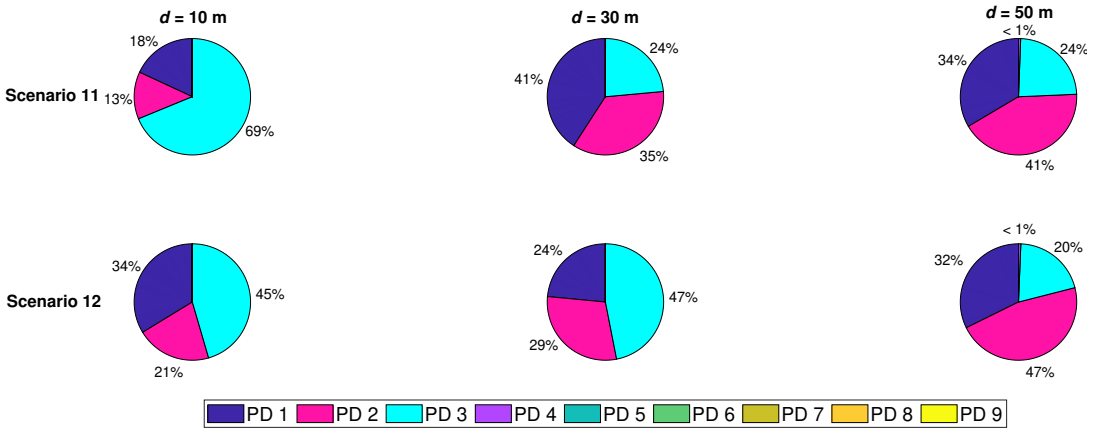

(a)

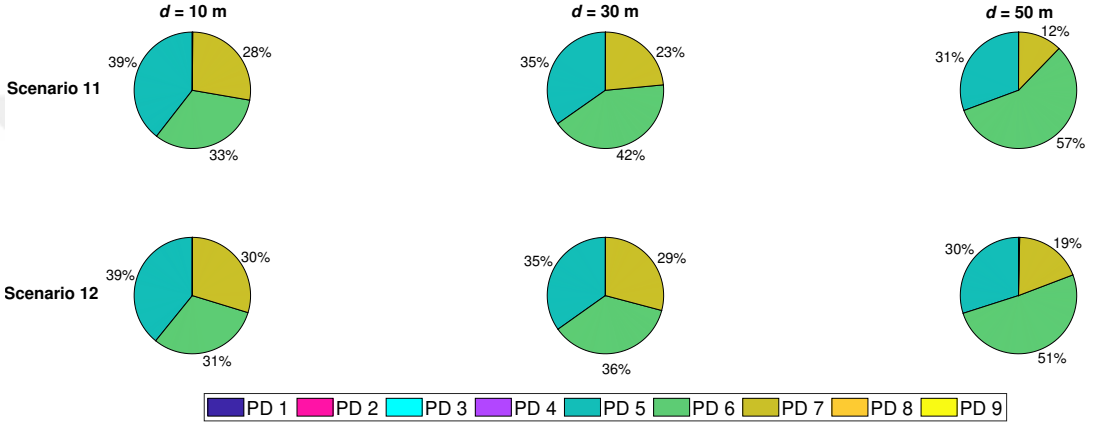

(b)

Figure 52: Contribution of each PD for V2V in curved road scenarios based on (a) HLs (b) TLs.

the maximum (41%) followed by PD 1 (34%) and PD 3 (24%). This is due to that with increasing the distance the direction of the source vehicle moves away from PD 3 and towards PD 2. In other words, the angle of arrival at PD 2 is smaller compared to PD 3.

In Fig. 52.b, we present pie charts for Scenarios 11 and 12 based on TL transmitters. In Scenarios 11 and 12, it is observed that PD 5 and PD 6 always collect the highest received powers (i.e., 70% or more based on the distance). The contribution of PD7 decreases with increase in distance.

In Fig. 53, we present pie charts for Scenarios 13-15 based on traffic light transmitters and for Scenarios 16-18 based on street light transmitters.

In Scenarios 13-15 (see Fig. 53.a), the traffic light is the transmitter. It is observed that PD 5 and PD 7, located at the right-hand side, collect the highest amount of received power, i.e., 59% and more. In Scenario 13 (d_h = 0 m), a small difference is observed

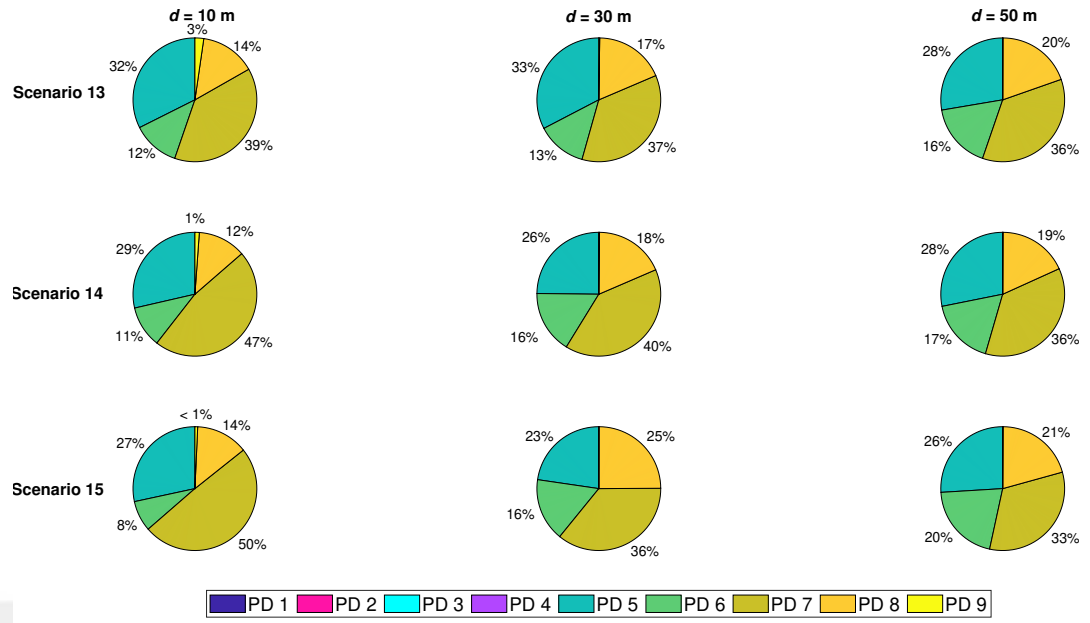

(a)

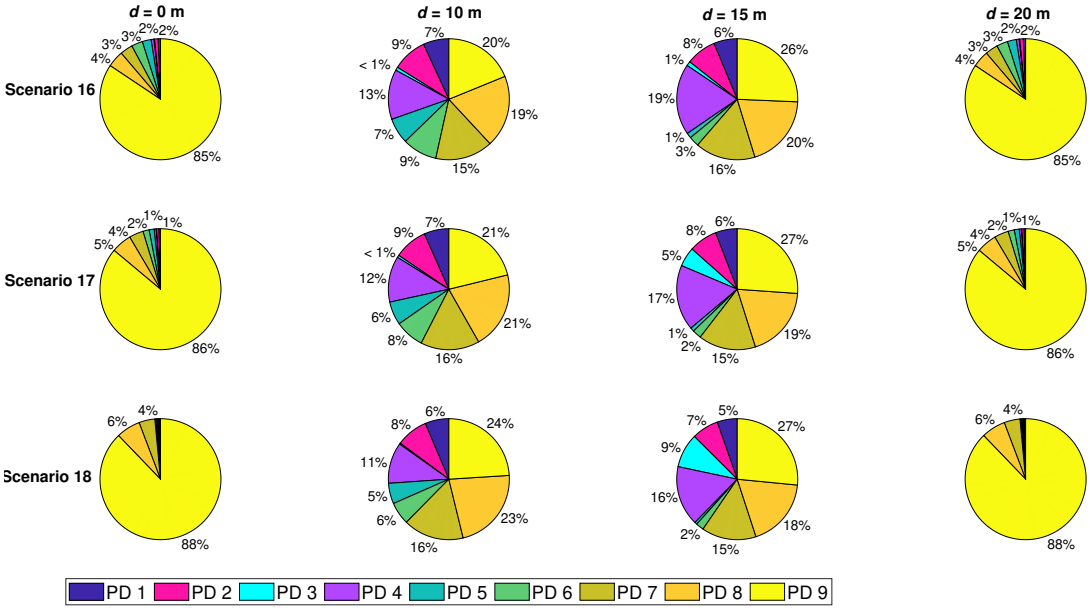

(b)

Figure 53: Contribution of each PD for I2V scenarios based on (a) Traffic lights (b) Streetlights.

between received powers of PD 5 and PD 7. In Scenarios 14 and 15 where d_h increases respectively to 1 m and 2 m, the difference gets larger particularly at shorter distances. It is further observed that contributions of PD 6 and PD 8 (located at the left-hand side) improve with the increase in distance.

In Scenarios 16-18 (see Fig. 53.b), the street lights are transmitters. At small distances, PD 9 located at the top of the vehicle is the primary receptor. As distance increases, all

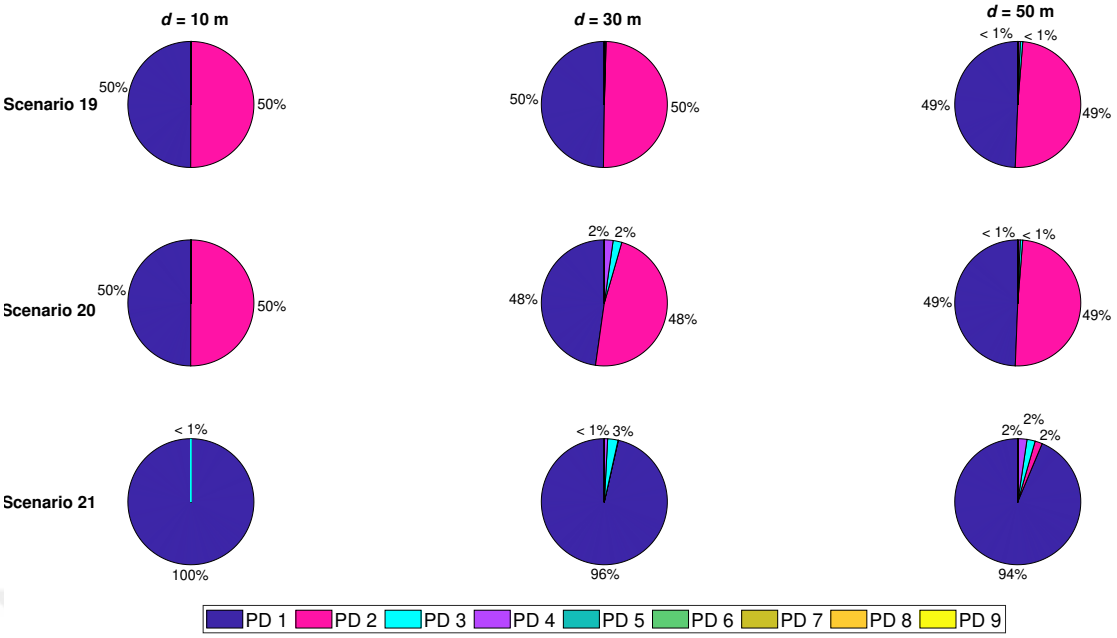

Figure 54: Contribution of each PD for V2V scenarios with neighboring vehicles.

9 PDs contribute at different levels to the received power although PD 9 always receives the highest received power.

In Fig. 54, we present pie charts for Scenarios 19, 20, and 21. In Scenario 19 and 20 where two vehicles follow each other in the middle lane with and without neighbor vehicles (i.e., no blockage), PD 1 and PD 2 are the main receptors. These two PDs collect 96% or more of the total power based on the distance. A small amount of received power is collected using PD 3 and PD 4 because of road reflections if the distance between two vehicles is sufficiently large. In Scenario 21 where partial blockage occurs, PD 1 becomes the primary receptor which collects 94% or more of the total power based on the distance. On the other side, the received power using PD 2 becomes negligible (i.e., only 2% due to reflections and at sufficiently larger distances). This is due to its location on the side of blockage vehicle. It should be noted that if the blockage vehicle is re-located at the left-hand side, PD 2 would be primary receptor.

Effect of Neighbor Vehicles on SINR: It should be emphasized that received power by its own might not be sufficient to evaluate the performance in Scenarios 19, 20, and

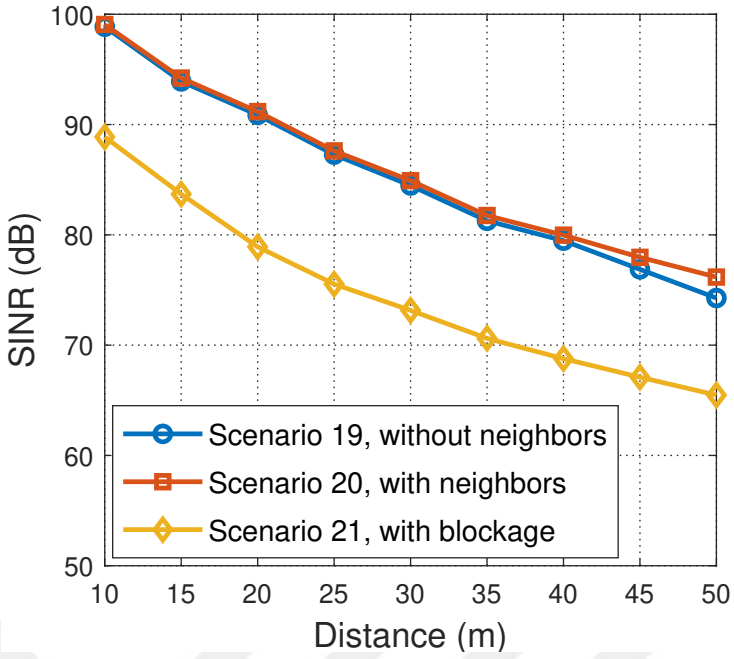

(a)

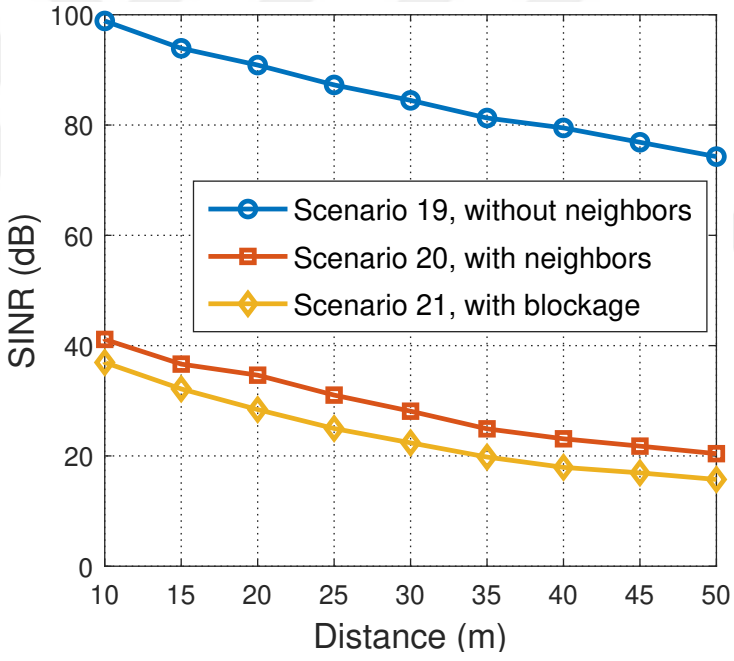

(b)

Figure 55: Effect of neighboring vehicles and blockage on the received SINR (a) Case A, i.e., inactive transmitters and (b) Case B, i.e., active transmitters.

21 where there are neighbor vehicles. In particular, we need to impose some assumption on the transmitters of the neighbor vehicles and accordingly calculate signal-to-interference-plus-noise ratio (SINR). In the first case, the neighbor vehicles are assumed to have inactive HLs transmitters. In this case, the HLs are used only for illumination purposes with no signal transmission. The received light from neighbors with inactive

transmitters is treated as shot noise in SINR calculation. In the second case where the transmitters are assumed to be active, the received lights from neighbor vehicles are considered as interfering signals in SINR calculation.

In Fig. 55.a, we present the SINR results for the case of inactive transmitters and assume high speed communication, i.e., $B = 10$ MHz. Similar to our earlier observations in Fig.11, the presence of neighbor vehicles in other lanes improves received SINR due to additional reflections. On the other side, when there is a blockage (i.e., Scenario 21) the received SINR is significantly degraded.

In Fig. 55.b, we consider the case of active transmitters and assume $B = 10$ MHz. It is observed in Scenario 20 that the received SINR value significantly reduces (i.e., ≥ 57 dB) with respect to Scenario 19. In Scenario 21, it is observed that the blockage vehicle further reduces the SINR values (i.e., ≤ 6 dB) with respect to Scenario 20. This is due to the fact that the blockage affects both the desired and the interfering signals. Despite the degrading effects of neighbor vehicles, the received power values are sufficient for both low-speed and high-speed communication use cases. In particular, the threshold SINR value required to achieve our target of $\text{BER}_{th} = 10^{-3}$ is given as $\gamma_{th} = 9$ dB. It is observed from Fig. 18 that SINR value of 15.7 dB is achieved at a distance of 50 m even in the case of heavy traffic described by Scenario 21.

CHAPTER VI

OUTDOOR BROADCASTING CHANNEL MODELING

6.1 Introduction

The previous chapters of this dissertation discuss the channel modeling of V2V and I2V links as well of the multi-directional receptions. The results demonstrate the ability of VLC technology to reuse the lightning infrastructures for communications purposes which makes VLC seems to be most appropriate for safety broadcasting applications. Unlike indoor VLC broadcasting systems which build upon LED ceiling luminaries, outdoor VLC systems use ubiquitous streetlights to broadcast safety messages for vehicles and pedestrian along the road. Outdoor lights with specific illumination requirements have radiation patterns which differ from their indoor counterparts [28, 81]. In addition to, the effects of weather conditions, orientation of the user equipment, and the sunlight might strongly affect the link performance of the outdoor VLC broadcasting systems.

While there is a growing number of works on investigating the impact of weather conditions [63, 64, 72, 103, 110] and asymmetrical patterns of vehicle's HLs and TLs [11, 56, 59, 60, 105, 138, 142, 151] on vehicular VLC systems while the impact of solar irradiance has captured only a little attention so far in the literature [66, 152, 153]. The Sun is considered as the strongest shot noise source that significantly limits the performance of VLC system [154]. It has been demonstrated through measurements that the shot noise from the sunlight significantly reduces the achievable data rate of VLC systems [152]. In [153], the impact of the sunlight on a vehicle-to-vehicle VLC system has been investigated using a theoretical calculation. Although, the ideal Lambertian pattern has been assumed for the vehicle source and the PD has been assumed to have a 90° with the Sun, the results demonstrated that the sunlight causes a significant link distance reduction. In [66], the measurements have been conducted to investigate the

impact of solar irradiance on a traffic light-to-vehicle VLC link. The measurements have been carried out in Riverside city, California, USA where the weather was a little cloudy. In addition to, a PD with a narrow FOV was utilized. These make the results useful for only specific location and system parameters.

It should be further emphasized that the aforementioned works in [66, 152, 153] do not consider either the S2P or the S2V links. In such cases, the PD should face upwards which in turns enlarges the amount of received irradiance from the Sun. In addition to, the mobility of the vehicles and pedestrians will affect the link performance which should be taken into account when dealing with outdoor VLC broadcasting systems.

Motivated by this, in this chapter, we explore VLC as a wireless connectivity solution to enable the outdoor broadcasting for public safety systems utilizing the ubiquitous street lights as wireless access points. Taking into account the fundamental differences imposed by the outdoor medium and lightning infrastructure, we investigate the system performance for the links between S2P and S2V. Non-sequential ray tracing approach is used to obtain the CIRs for S2P and S2V links which are then used to calculate the variance of the received signal at the PD. We then utilize the advanced features of OpticStudio and provide a realistic modeling for the solar irradiance calculating the variance of the received background noise at the PD. The received SNR is then obtained for both S2V and S2P links under the mobility condition.

The rest of this chapter is organized as follow. In Section 6.2, we introduce the VLC broadcasting system, explain the sunlight modeling with OpticStudio, and present the SNR calculations. In Section 6.3, we present the broadcasting scenarios under consideration and discuss the numerical results.

6.2 Outdoor VLC Broadcasting System

Streetlight Classifications and Use Cases: LED street luminaries usually have complex intensity profiles because they use optical components that greatly modify the distribution of the light emitted from each LED [155–157]. In general, the radiation pattern

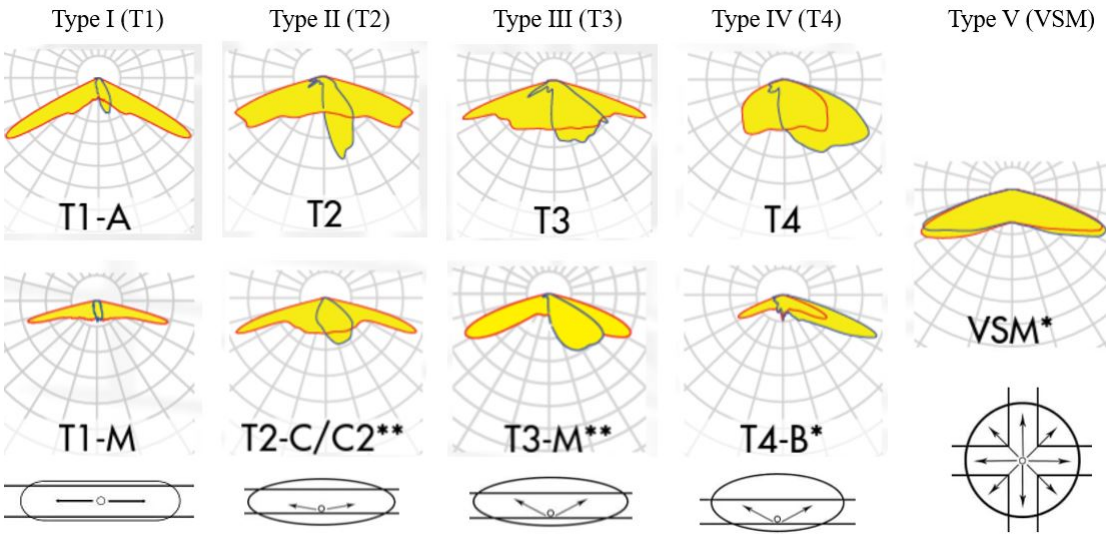

Figure 56: Main types of street lights and their use cases.

of LED luminaries has a "whale tail" shape [158], which is much different about Lambertian pattern. According to the Illuminating Engineering Society of North America (IESNA), there are main five different types of street lighting distribution patterns [159] with different use cases [160] which is shown in Fig. 56 and can be described as the following:

Type I: This type I distribution is a two-way lateral pattern and offers narrow and oval shape of LED distribution. As shown in Fig. 56, bi-directional illumination is uniformity distributed at the two sides of the lighting pole. The preferred lateral angle of this type is 15° in the cone of maximum power. This type street light is applicable for lighting sidewalks, paths, Border lighting, or Narrow walkways.

Type II: This type II distribution have a slightly wider lateral angle of 25°. As shown in Fig. 56, it also maintains the illumination for wider area comparing to type I LED distribution while achieving the uniform bi-directional illumination at the two sides of the lighting pole. Consequently, they are applicable for lighting wide walkways and wide path as well as smaller side streets.

Type III: This type III pattern provides a wider illumination area comparing to either type I or type II distribution. As shown in Fig. 56, It has also asymmetric arrangement but with wider preferred lateral angle of 40°. This Type III patterns are applicable

for lighting Roadways, highways, driveway, General parking lots, sports fields, and garages.

Type IV: This type IV pattern has the same intensity at angles from 90° to 270° and it has a preferred lateral angle of 60° as shown in Fig. 56. This Type IV patterns are applicable for building exteriors, perimeter of parking areas and businesses, wide highways, and suspension bridge.

Type V: This type V pattern distributes light evenly in all sides of the fixture. In other words, as shown in Fig. 56, it produces a circular of 360° distribution with same foot-candles at all viewing angles. Type V LED offers the largest, most even pattern of intensity. Such omni-directional LED distribution is applicable for crossroad, center of the roadway, intersections, Large-commercial parking areas, and center islands of the parkway.

Sunlight Modeling and SNR Calculations: In this part, we provide a realistic characterization for the received irradiance from the sunlight using the advanced features available in OpticStudio simulator. Generally, the received amount of solar irradiance at the PD depends on different parameters such as the position of the Sun with respect to the zenith point, the atmospheric weather condition, and the PD specifications (i.e., orientation, area, etc.). To model the Sunlight in OpticStudio, we define an accurate sunlight source type with suitable spectral, and irradiance characteristics. Specifically, the "Source Radial" object is utilized to represent the Sun where its light spectrum is modeled as a subgroup of the blackbody radiation spectrum considered between two wavelengths, i.e., λ_1 and λ_2.

Since the visible light range is the focus of this paper, we consider the values of λ_1 and λ_2 as 400 nm and 700 nm, respectively. For precise accuracy, we consider the maximum value of discrete spectral points available in OpticStudio which is 100 points. We also consider the blackbody temperature of 5778 K which is the temperature for which the blackbody radiates the same total irradiance as the Sun of 1368 W/m2 [161]. As a worst condition, the clear weather is considered while two cases of the Sun position are investigated and compared. In the first one, the sun is assumed to be at the zenith

(0°) which is the worst-case position. In fact, the amount of solar irradiance in this case is rarely reach the earth's surface [161]. The second case is similar to [152, 154] where the sun is at 60° zenith angle and hence less irradiance can be received.

Our objective is therefore measuring the optical background power received at the PD. To do this, we utilize a PD with an area of A_{PD} = 1 cm^2 while the whole visible range (400 nm-700 nm) is considered in the blackbody spectrum. Since in the visible range, a small variation in the spectrum is existing, one can take the average value over this range as $P_b = \sum_\lambda P_b(\lambda)/\lambda_2 - \lambda_1$. The maximum irradiance in the spectrum which is near 500 nm is also considered for comparison. The received background current assuming a bandwidth of $\Delta\lambda$ can be then given as [154]

$$I_b \;=\; P_b\, \eta \Delta\lambda\, G_{PD}\, q/\hbar v, \tag{6.1}$$

where q, $\hbar$, and v denote respectively electron charge, Planck constant, and the wave frequency. Also, η and G_{PD} denote the the responsivity of the PD and the PD gain, respectively. The variance of the received shot noise at the PD is then computed by [2]

$$\sigma_{sh}^2 = 2qG_{PD}N_F I_b B, \tag{6.2}$$

where N_F and B denote the noise figure of the PD and the bandwidth of the low pass filter, respectively. In addition to the shot noise, the communication system is subjected to the thermal noise with a variance of σ_{th}^2 given as [152, 154]

$$\sigma_{th}^2 = \frac{4KT}{R} N_F B. \tag{6.3}$$

where K, T, and R denote the Boltzmann constant, the temperature in Kelvin, and the load resistance.

For channel modelling, we utilize non-sequential ray tracing approach which was earlier explained in chapter 2 and utilized for vehicular VLC channel modeling in chapters 3-5. Based on this approach, The CIR at the PD can be expressed as

$$h(t) = \sum_{i=1}^{N} P_i\, \delta\,(t - \tau_i), \tag{6.4}$$

where δ is the Dirac delta function, N is the total number of rays reaching the PD for a given distance of d, and P_i and τ_i respectively denote the power and the propagation

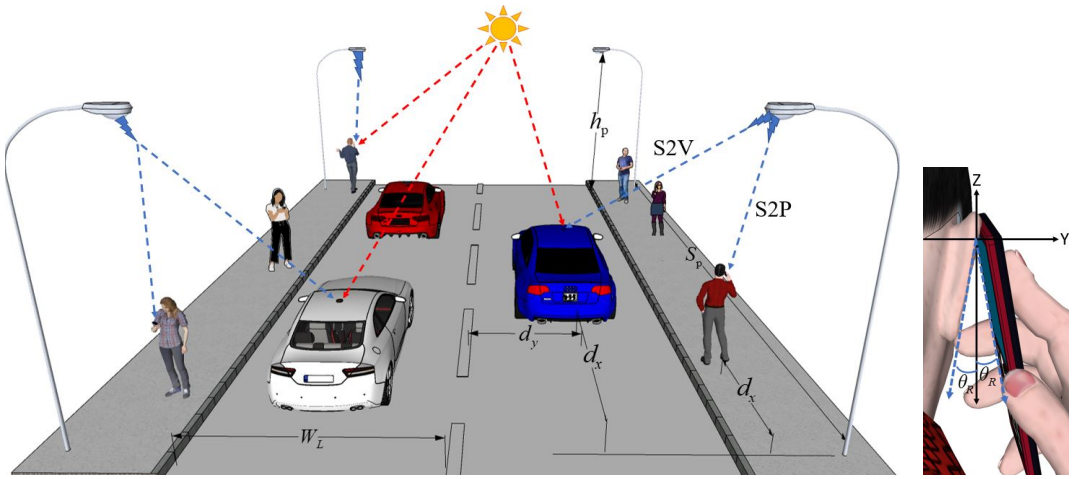

(a) (b)

Figure 57: (a) VLC-based outdoor broadcasting system in roadway case and (b) User equipment rotation angle.

delay of the i^{th} ray, $i = 1, 2, ..., N$ received by the PD. The DC channel gain is then given as [1]

$$H_{dc} = \int_0^{\infty} h(t)\, dt. \tag{6.5}$$

Once the optical DC channel gain is obtained, the variance of the received electrical signal at the PD can be computed by

$$\sigma_{sig}^2 = (\eta G_F P_t H_{dc} G_{PD})^2, \tag{6.6}$$

where G_F and G_{PD} denote the average optical filter transmission over a bandwidth of $\Delta\lambda$ and the avalanche PD gain, respectively.

From Eq. (6.2), Eq. (6.3), and Eq. (6.6), the received SNR can be obtained as [2, 145]

$$\Gamma = \frac{\sigma_{sig}^2}{\sigma_{sh}^2 + \sigma_{th}^2}. \tag{6.7}$$

6.3 Broadcasting Scenarios and Numerical Results

6.3.1 Roadway Scenario

As indicated in Fig. 57, we consider a VLC-based broadcasting system in a two-lane roadway having a lane width of W_L. The streetlight poles (Type II) act as wireless transmitters broadcasting safety information to pedestrian and vehicles along the road. The poles are assumed to be located at both sides of the road (i.e., double sided arrangement)

Table 9: Simulation parameters for VLC broadcasting system

Streetlights	Transmit power (P_t)	22.5 W
	Height (h_P)	8 m
	Spacing (S_P)	22 m
	Number of Poles	4
	Type	II
	Brand	Vestel Ephesus
Receiver	Area (A_{PD})	1 cm^2
	FoV (ψ)	90°
	Responsivity (η)	0.64 A/W
	Bandwidth (B)	5 MHz
Road	Type	R2
	Coating material	Asphalt
	Lane width (W_L)	3.75 m
Vehicle/ Pedestrian	Vehicle length	4.6 m
	Vehicle width	1.8 m
	Vehicle height	1.4 m
	Vehicle material	Glossy paint
	Pedestrian height	1.7 m
	Pedestrian material	Cotton

and they are uniformly separated from each other with a spacing of S_P. Each streetlight pole has a height of h_P and an optical transmit power of P_t. The vehicle moves at a longitudinal distance of d_x with respect to the streetlight pole and has a possible lateral shift of d_y with respect to the road center. Also, the pedestrian moves on the road pavement at a longitudinal distance of d_x where his/her cell phone can rotate with a rotation angle of θ_R as shown in Fig. 56.b. To receive the signal, the vehicle is equipped with a PD located at its top while the pedestrian is assumed to use a cell phone where the PD located on. The PD has an area of A_{PD}, a responsivity of η, and a FoV angle of ψ.

Results and Discussions: In this section, we present some numerical results to quantify the impact of solar irradiance on the performance of VLC-based broadcasting

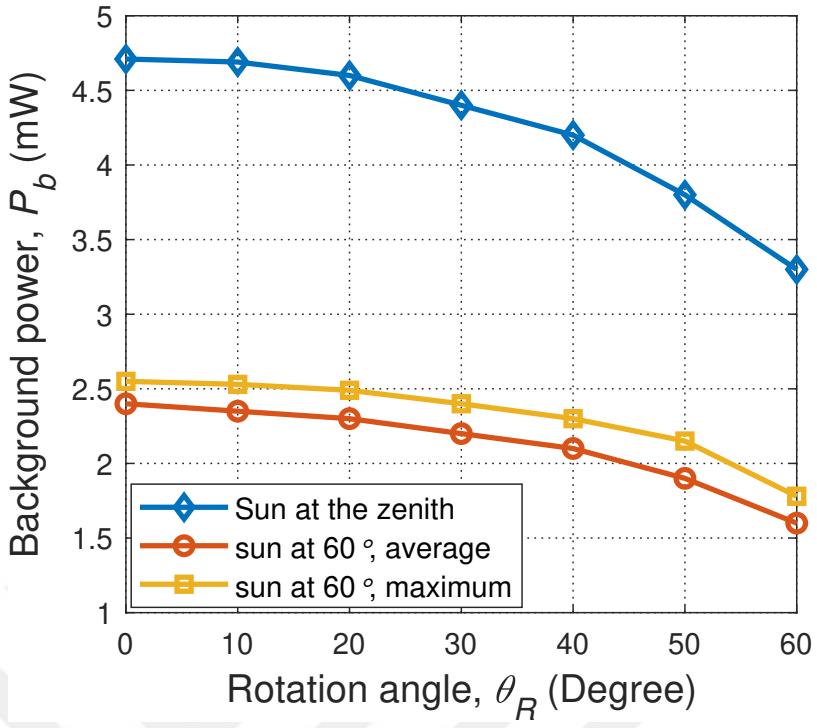

Figure 58: Received optical power from the Sun versus the rotation angle of the PD assuming the clear weather condition and a blackbody temperature of 5778 K.

system assuming the clear weather condition. A two-lane road with a lane width of W_L = 3.75 m is considered where the streetlight poles are located at both sides of the road and separated from each other with a spacing distance of S_P = 22 m. The values of h_P, η, $\Delta\lambda$, and P_t are given as 8 m, 0.64 A/W, 30 nm, and 22.5 W, respectively. It can be noted that the spacing between the streetlight poles can be taken as 2.5-3 times the pole height (i.e., $S_P = 2.75 \times 8 = 22$ m). A commercial streetlight LED from Vestel ephesus-m4s-68 is adopted in our simulation which has asymmetrical radiation pattern given in Fig. 42.d. Other simulation parameters are listed in Table 9.

In Fig. 58, we present the results of the optical background power received by the PD versus the rotation angle of the PD for the two Sun positions. It is observed a significant power reduction when the position of the Sun changes by 60° from its zenith. It is also observed that the maximum power can be received when the PD is facing upwards to the Sun. Any rotation results in a reduction in the received background power as shown in Fig. 58. The results in Fig. 58 further reveal that taking the average irradiance over the visible range is a good approximation to estimate the background

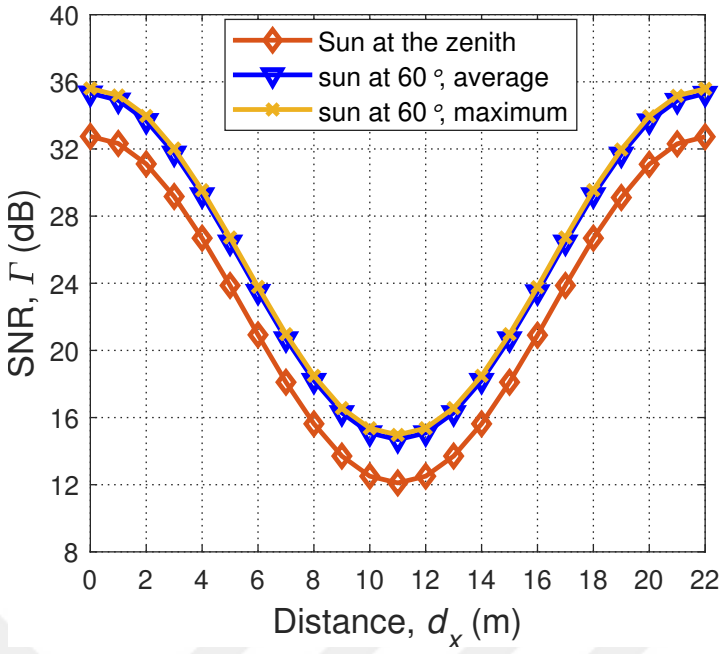

(a)

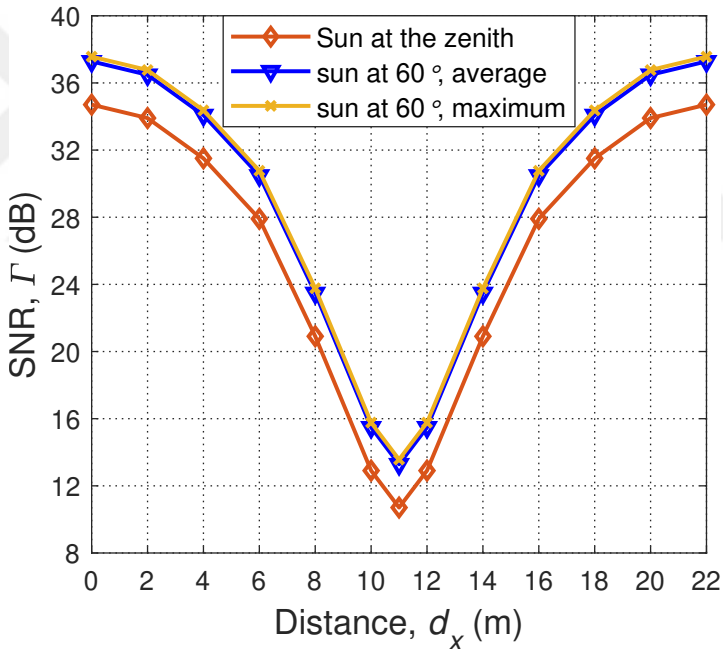

(b)

Figure 59: Received SNR versus distance assuming the two positions of the Sun with respect to the zenith. (a) For S2V link with $d_y = 3$ m and (b) For S2P link with $\theta_R = 0°$.

power for a single wavelength. It is seen that the average and the maximum irradiance values are very close to each other.

In Fig. 59, we present the SNR results for both S2V (see Fig. 59.a) and S2P (see Fig. 59.b) links at the two positions of the Sun assuming the clear weather condition. It is observed a degradation of about 3 dB in the SNR value when the Sun at the zenith

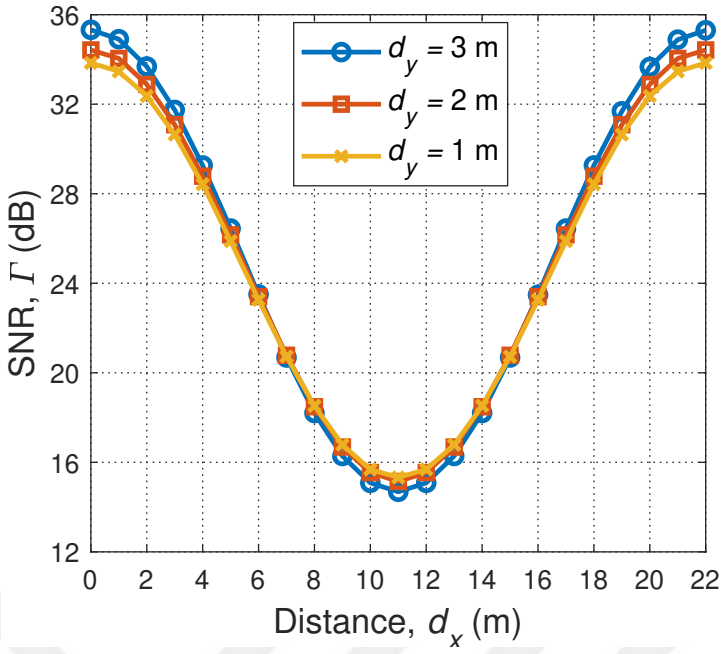

Figure 60: Effect of lateral shift (d_y) on the received SNR for S2V link assuming the Sun at 60° with respect to the zenith.

comparing with the position of 60° from the zenith. On the other side, the SNR value when considering the maximum spectral peak is almost the same as considering the average value over the visible wavelengths.

In the following, we consider the clear weather condition and the Sun at 60° from the zenith to present the SNR results for both S2V and S2P links under the impact of mobility. In Fig. 60, we present the SNR for the S2V link at different values of d_y. It is observed that at shorter distances, the impact of d_y is larger. It is also seen that when d_y increases the SNR increases. Because increasing means that the vehicle becomes closer to the streetlight pole and hence a higher power can be received.

In Fig. 61, we present the SNR results for the S2P link at different θ_R values. Here, we have two cases where it is possible that the rotation occurs into the inner (i.e., positive θ_R) or the outer side (i.e., negative θ_R) of the road. For the first case (i.e., $+\theta_R$), the received SNR reduces with increasing θ_R at shorter distances ($d_x \leq$ 5 m) as shown in Fig. 61.a. When the distance becomes sufficiently large, increase the value of θ_R results in an improvement in the SNR value. This is due to that at shorter distances, the pedestrian is located near the streetlight pole where the maximum

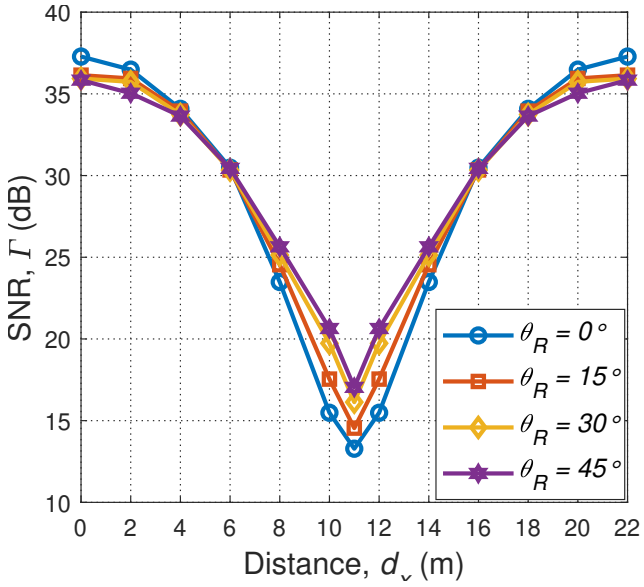

(a)

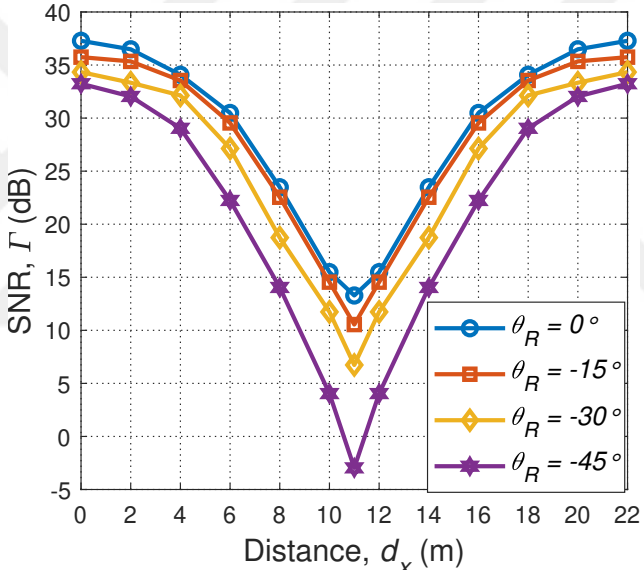

(b)

Figure 61: Effect of rotation angle (θ_R) on the received SNR of S2P link assuming the Sun at 60° with respect to the zenith. (a) The PD rotation is toward the inner road side (b) The PD rotation is toward the outer road side.

contribution of the received power comes from and therefore any rotation reduces this power. At larger distances, however, the pedestrian becomes near to the center between two streetlight poles at a road side where a small amount of the power can be received. Increasing the rotation angle in this case makes the PD able to receive larger power from the streetlights on the other road side and hence the SNR increases. Owing to the second case (i.e., $-\theta_R$), it is observed that the received SNR worsen when the rotation angle increases for any distance under consideration as indicated in Fig. 61.b. This is

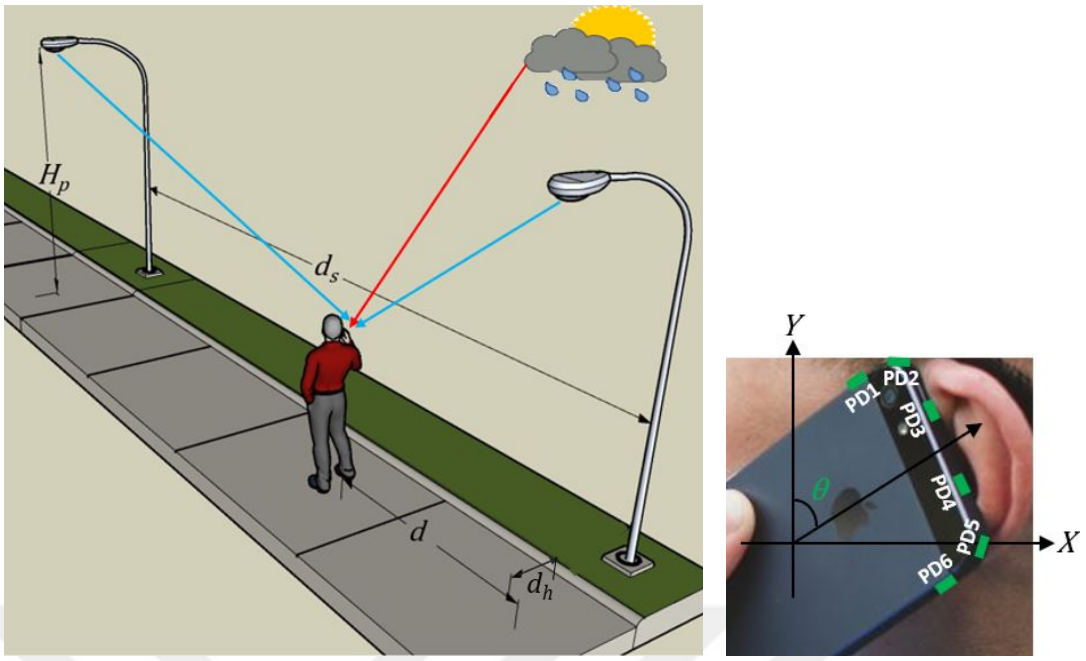

(a) (b)

Figure 62: (a) VLC-based outdoor broadcasting system in sidewalk case and (b) Locations of PDs on the user cellphone.

due to the reduction in the received power when the PD rotates to the outer side of the road. It is also observed that the reduction in the SNR has a nonlinear relation with the rotation angle. For example, consider d_x = 10 m. The SNR degradation for θ_R = -15° is 1 dB comparing with θ_R = 0°. Such reduction is given for θ_R = -30° and θ_R = -45° as 3.8 dB and 11 dB, respectively.

The obtained results from Fig. 59-61 further reveal that when the Sun at 60° from the zenith, the target SNR of 13.6 dB for the both S2V and S2P links can be achieved. However, when the Sun becomes at the zenith or the pedestrian rotates at the outer road side, a significant degradation in the received SNR are noticed particularly at the middle distance between the streetlight poles.

6.3.2 Sidewalk Scenario

As shown in Fig. 62, we consider a VLC broadcasting system in a sidewalk scenario. We assume that a user talks on his cellphone and moves on the sidewalk at a longitudinal distance of d a way from a streetlight pole and with a lateral shift of d_h from the road-edge. The streetlights are separated by a spacing distance of d_s, and each has a height

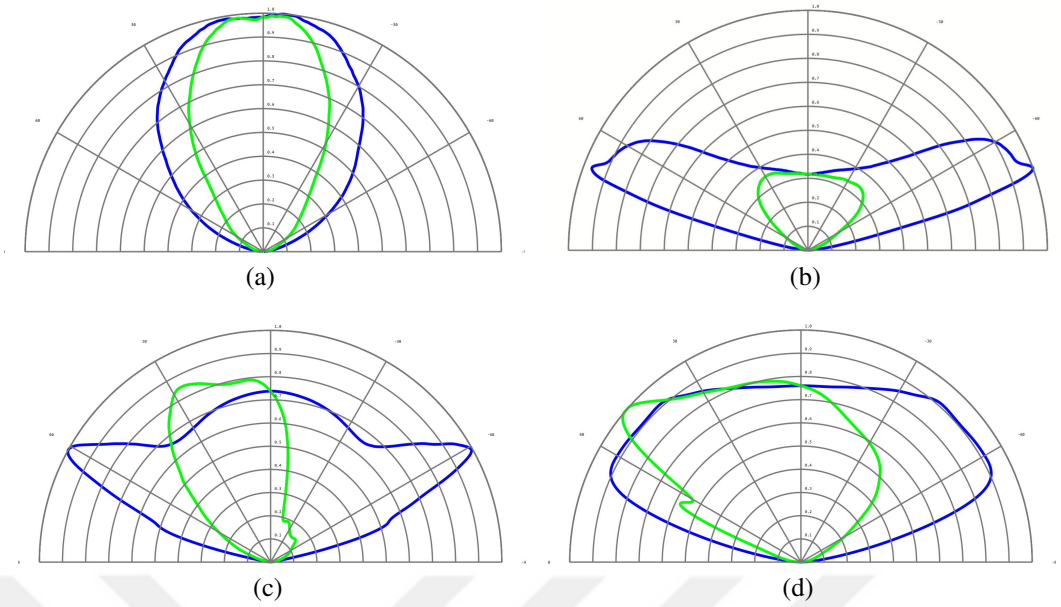

Figure 63: Commercial examples of intensity profiles types (a) Lambertian (b) Type I (c) Type II and (d) Type III.

of H_p. The cellphone is set next to the person's ear with a rotation angle to upward of θ = 45°. It is equipped with a PD to receive the broadcasting signals where six potential locations denoted as PD_i, i = 1,...,6 are considered as shown in Fig. 62.b. For the streetlight type, we first compare the received power for different types (Type I, Type II, and Type III) as well as with the ideal Lambertian profile. Then, we assume Type I, which is commonly considered for the sidewalk and narrow path road (see Section 6.2.1 and Fig. 56), to investigate the effect of user location, PD orientation, weather condition, and sunlight.

Results and Discussions: In the following, we present the numerical results for the VLC broadcasting system in sidewalk scenario. We consider a pole height of H_P = 6 m which is within the standard pole heights for sidewalks that is from 4.5–6 m [162, 163]. The pole spacing is assumed as d_s = 18 m since it should be from 2.5–3 times the height of the pole [162, 163]. We consider the width of the sidewalk as 2 m since the sidewalks usually require a minimum width of 6.0 feet (1.82 m) [164, 165]. We further assume commercial streetlights for Lambertian, Type I, Type II, and Type III [119, 166–168] with illumination profiles given in Fig. 63.

In Fig. 64, we indicate the effect of different pattern types (Type I, Type II, Type

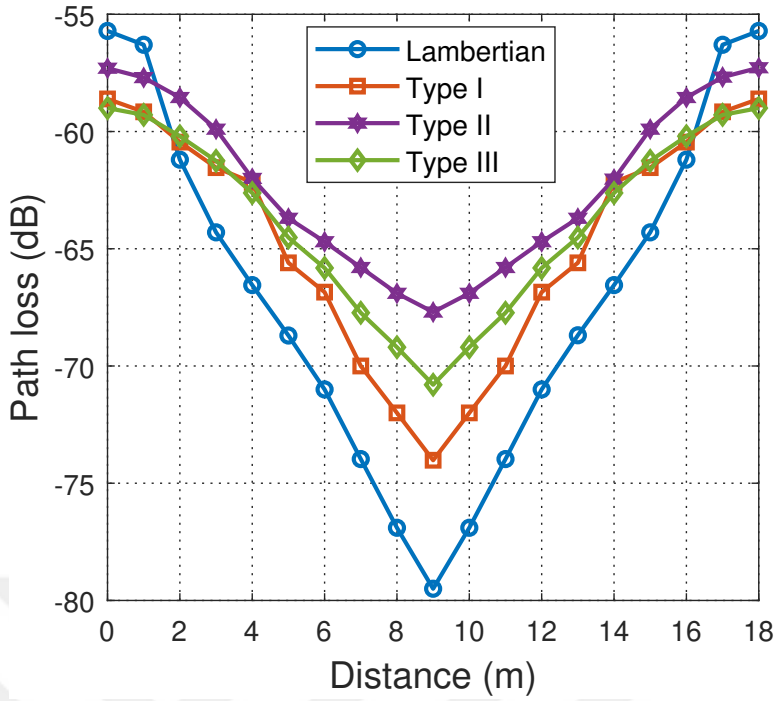

Figure 64: Path loss results versus distance for different streetlight pattern types.

III) on the path loss results. As a benchmark, we include also the results of Lambertian profile. It is observed that the path loss significantly changes with changing the streetlight type as well as the distance from the streetlight pole. It is obvious that Lambertian profile is not suited for illumination the sidewalk path since the received power is significantly reduced with the distance. One can notice also that Type III provides less path loss results comparing with Type II and Type I. This is due it is designed for illuminating larger ranges while here we considered shorter distance for sidewalk scenario.

In the following, we consider Type I and introduce the effect of PD orientation on the cell phone, the user location (both longitudinal and lateral shift), weather conditions, and the sunlight. Fig. 65 shows the effect of PD orientations assuming clear weather, d_h = 0 m. It is observed a significantly change in the path loss results when the orientation of the PD changes since the received power is highly dependent on the geometry of both transmitter and receiver. It can be observed that PD1 and PD2 provides the maximum average received power while PD 6 can collect the minimum amount of the power which is almost fluctuates around -78 dB. This is due to its direction toward the ground and

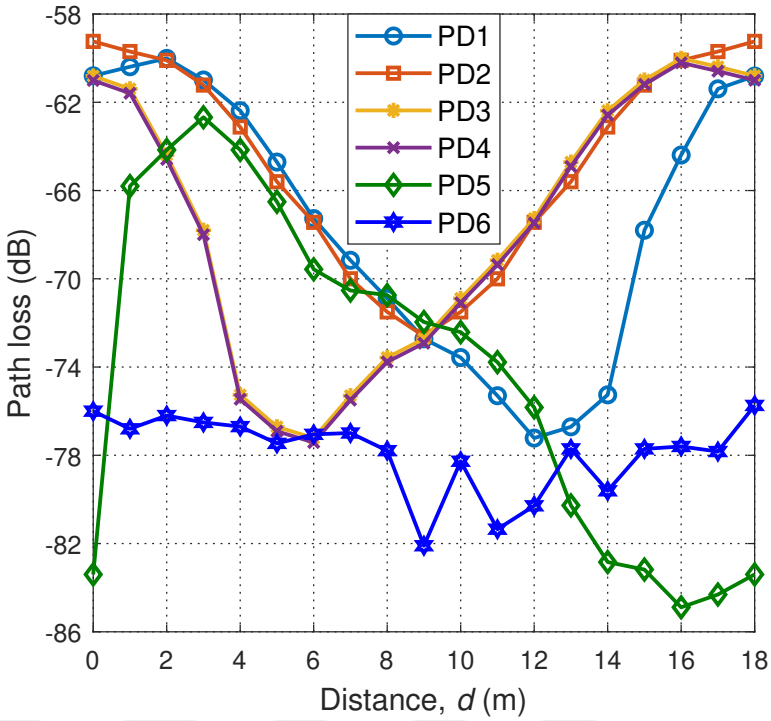

Figure 65: Path loss results versus distance by individual PDs.

therefore, it can collect power only from the reflections. It is also seen the PD 3 and PD 4 has almost the same performance since their locations are near to each other while they have the same orientation angle of 45◦. They have also the reverse behaviour of PD 1. For instant, consider that the user located under the lighting pole (i.e., d = 0 m). The recorded path loss results at PD1, PD2, PD3, PD4, PD5, and PD6 are given as -60.8 dB, -59.2 dB, -60.8, -61 dB, -83.4 dB, and -76 dB, respectively. These values are given at d = 5 m as -64.7 dB, -65.6 dB, -76.7 dB, -76.9 dB, -66.5 dB, -77.46 dB.

In Fig. 66, we present the two-dimensional path loss distributions assuming PD 1 (see Fig. 66.a) and PD 2 (see Fig. 66.b) under the assumption of clear weather. It is observed that when the lateral shift (d_h) increases the path loss increases since the user become farther than the streetlight source and hence less power can be received. The results demonstrate that the middle distance ($d = d_s/2$) with larger lateral shift of $d_h = 2m$ is the worst location in the sidewalk area. On contrast, closer to any streetlight pole with no or less lateral shift provides higher performance.

In Fig. 67, we consider PD1 and illustrate the diverse of weather conditions on the

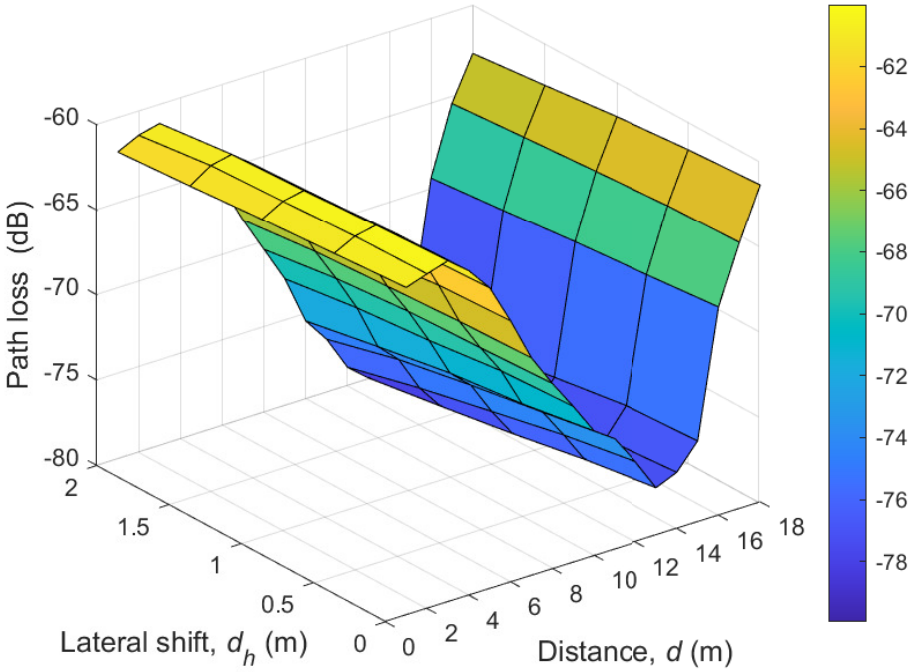

(a)

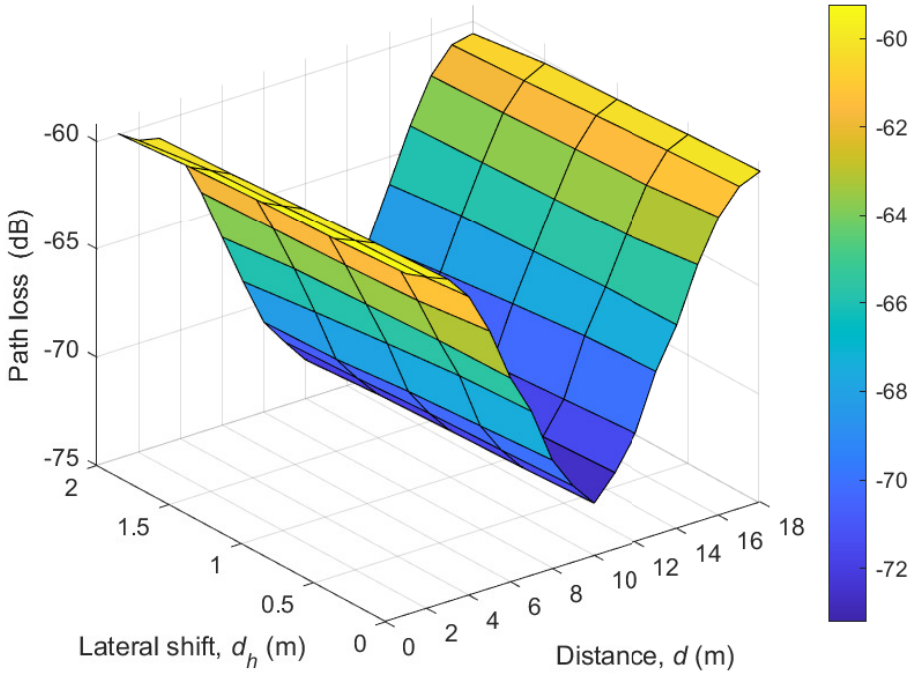

(b)

Figure 66: Spatial path loss distribution as seen by sample of individual PDs (a) PD 1 and (b) PD 2.

path loss results. Specifically, we consider 5 weather condition types; clear, rain, moderate fog (visibility of 500 m), thick fog (visibility of 250 m), and dense fog (visibility

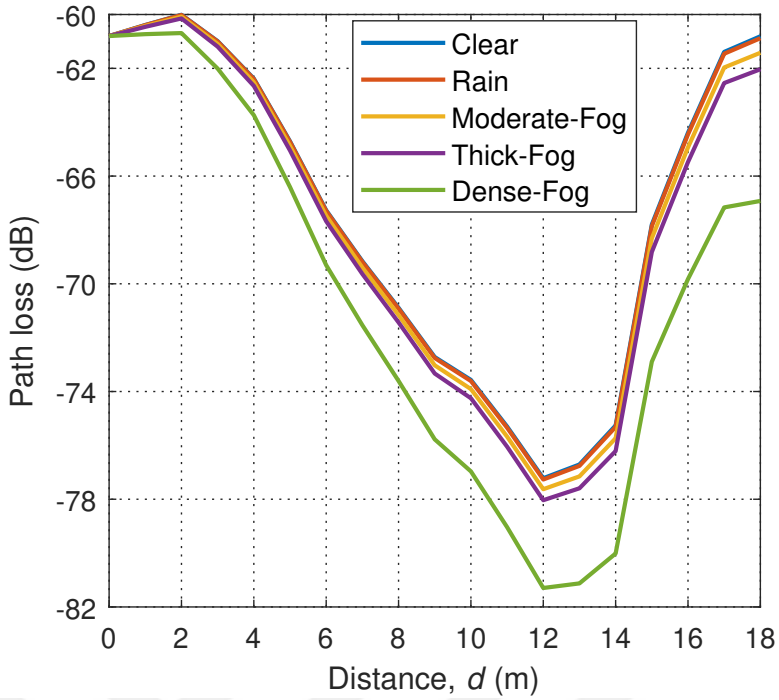

Figure 67: Effect of different weather condition on the path loss assuming PD 1.

of 50 m). It is observed that the rain weather has almost negligible effect on the path loss results. On contrast, the dense fog significantly increase the path loss and hence degrades the performance. For example, consider d = 10 m. The path loss for clear, rainy, moderate fog, thick fog, and dense fog are given as -73.5 dB, -73.6 dB, -73.9 dB, -74.25 dB, and -76.96 dB, respectively.

Lastly, Fig. 68 shows the effect of the sunlight on the received SNR assuming PD1. We consider three different cases as follow; **Case I** which indicates the situation without considering the sunlight effect, **Case II** which indicates the situation with considering the sunlight effect where the Sun is at 60° from the zenith, and **Case III** which illustrates the sunlight effect when the Sun at the zenith. Case III is considered the worst case situation. It is observed a huge SNR difference between Case I (i.e., neglecting the sunlight effect) from one side and Case II and/or Case III (considering the effect of sunlight) from another side. It is also observed that the received SNR is affected by the situation of the Sun with respect to its zenith. For example, consider a distance of d = 2 m. The received SNR for Case I, Case II, and Case III are given as 19 dB, 11 dB, 8.2 dB.

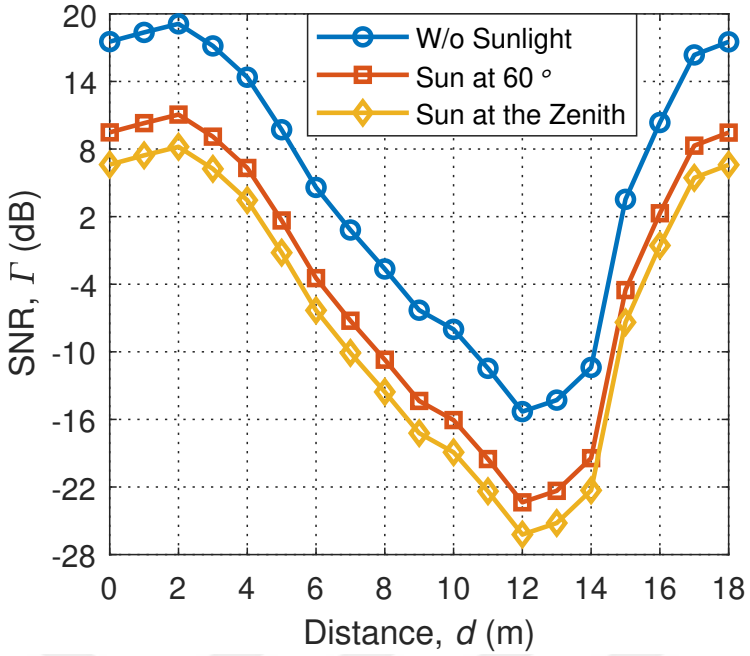

Figure 68: Effect of the sunlight on the received SNR performance assuming PD 1 and different Sun situations.

The obtained results reveal that the sunlight has a significant effect on the system performance. Therefore, when designing VLC based outdoor broadcasting systems, it is important to take into account the effect of user mobility, weather condition same as the impact of sunlight. This will require utilizing effective mitigation and enhancement techniques such as the blue optical filtering and/or angle diversity receiver with different combining techniques which will be considered as future research.

CHAPTER VII

CONCLUSIONS AND FUTURE WORK

In this chapter, we review the entire dissertation objectives and results. We emphasize the contributions that this research made. In the end, we give some perspective points for future work.

7.1 Conclusions

In this dissertation, we have investigated channel modeling of vehicular VLC systems. Our study builds upon the well-established raytracing channel modeling approach. Firstly, we have explained and validated this channel modeling methodology considering different VLC scenarios. Then, we utilized it and proposed closed-form path loss expressions for the V2V link with both HLs and TLs assuming a perfect alignment between the vehicles. Based on the derived path loss models, the V2V system performance was investigated by deriving closed-form expressions for the maximum achievable distance while satisfying a target of BER. We then considered the non-perfect alignment case and derived a closed-form expression for the channel path loss as a function of the lateral shift, weather conditions, and receiver aperture size. For the I2V VLC links, we began with the I2V based traffic light and derived a closed-form path loss expression as a function of longitudinal and lateral distances. Then, we considered the I2V based streetlights and derived a closed-form expression of channel path loss as a function of transceiver and infrastructure parameters, which we then utilized to investigate the system average error rate performance. The reverse channel link, i.e., V2I was then considered, and a closed-form expression for the achievable capacity was derived. Furthermore, we investigated the channel modeling of multi-directional coverage in different road types and traffic scenarios to quantify the capability of receiving signals in several cases and justify the number and locations of the required PDs. In the last part of this dissertation, we considered a practical application of vehicular VLC

by exploring it as a wireless connectivity solution to enable outdoor broadcasting for public safety systems. We considered different broadcasting scenarios and investigated the effect of streetlight type patterns, the orientation of the user equipment, weather type, and solar irradiance. The contributions of this dissertation can be summarized as follows.

In Chapter 2, we explained the utilized channel modeling approach which builds upon advanced non-sequential ray tracing features of OpticStudio software (see Section 2.2). It allowed us to integrate the asymmetrical intensity profiles of vehicular light sources and handle a large number of reflections for better accuracy. We explained how we model the wavelength-dependent reflectance of surface coating for each material in the environment as well as the different types of reflections (specular, diffuse, or mixed). We then explained how we model any weather type based on Mie scattering model. In Section 2.3, since this approach is a simulation-based channel modeling methodology, we have validated it against the measurements in some real scenarios including both the LoS and the NLoS cases. Our results of CIRs, CFRs, and path loss from the two methods were in a good agreement validating the ray tracing approach. The results of this chapter have been published in [100–102, 104].

Chapter 3 can be summarized as follow. In Section 3.2.1, we adopted such a well-established channel modeling approach and investigated V2V link based on HLs transmitters. We proposed a closed-form path loss expression that takes the form of a negative exponential function. Our results demonstrated that the proposed path loss model provides an excellent match to simulation results for larger transmission ranges and under different weather conditions comparing with the linear model. We then utilized this expression to derive the maximum transmission distance for a targeted data rate while satisfying a given value of BER. In Section 3.2.2, we considered V2V based TLs and derived a closed-form path loss expression that works for measured TL radiation patterns of different commercial car models. Utilizing this model, we derived a closed-form expression for the maximum transmission distance under the target BER value. Furthermore, we investigated the RMS delay spread at different V2V density cases.

In the previous models, we considered that the two vehicles travel in the same lane and with a perfect alignment. This means that the dependency of the derived path loss expressions on the system parameters were limited to only the longitudinal and weather type. Therefore, in Section 3.3, we considered the non-perfect alignment case, and developed a comprehensive closed-form path loss expression for the V2V VLC system as a function of link distance, lateral shift, weather type, transmitter beam divergence angle, and receiver aperture diameter. The results demonstrated that proposed path loss expression provided a very good match with the ray tracing results at all scenarios and system parameters under consideration. The results of this chapter have been published in [103, 105, 110, 114].

In Chapter 4, we considered the I2V VLC links where in addition to HLs/TLs, the traffic lights and streetlights were deployed as wireless transmitters. In Section 4.2, we modeled the I2V based on a commercial traffic light and derived a closed-form expression of the path loss as a function of both longitudinal and lateral shift distances. Since the results showed a very good matching between the proposed path loss model and the ray tracing results, we utilized it to derive the optimal power allocation for the hybrid I2V-V2V system. In Section 4.3, we modeled the I2V system with street light transmitters and derived a closed-form expression for the channel path loss as a function of transceiver and infrastructure parameters. These include the pole spacing, the height of both the lighting pole and the vehicle, the longitudinal and lateral distance between the vehicle and the pole, and the aperture size of the PD. Our results demonstrated that the path loss results obtained from the ray tracing and from the derived path loss model were in a good agreement. The effect of transceiver and infrastructure parameters on the system average error rate performance was also investigated [125]. In Section 4.4, we modeled the reverse channel link, i.e., V2I system, where the vehicle communicates with an infrastructure pole deploying its HLs as transmitters, and three PDs located within the traffic pole, adjacent to yellow, red, and green LED luminaries, to act as wireless receivers. Based on the CIRs, obtained from ray tracing, we introduced an

expression for the achievable capacity considering the effect of propagation environment and the LED non-linear characteristics. We further gained from the advantage of deploying the three PDs by employing Equal Gain Combining (EGC) scheme, which resulted in improvements of the overall system capacity. The results of this chapter have been published in [118, 125, 169].

In the previous chapters, we considered the use of one or two PDs, which might be sufficient for establishing a connection between two vehicles cruising in the same straight lane or between the vehicles and infrastructure with clear LoS. In Chapter 5, we investigated the channel modeling of multi-directional coverage for vehicular VLC systems. In Section 5.2, we illustrated the vehicular VLC scenarios under consideration which included different road types (i.e., multi-lane, curved roads), intersections (i.e., T-shaped, Y-shaped intersections) and traffic scenarios (i.e., cruising in the same or different lanes, lane change etc.). In Section 5.3, we indicated the locations of PDs around the vehicle to achieve the required omni-directional coverage for all scenarios. In Section 5.4, we quantified the capability of receiving signals in all scenarios considering both V2V links (in front and back directions) and I2V links (with traffic and street lights). Our results revealed that deployment of nine PDs with carefully determined locations on the vehicle is enough to create the required quasi-omni-directional coverage for V2V and I2V links. We further quantified the contribution of individual PDs to elaborate the usage cases of each PD. The results of this chapter have been published in [142, 151].

In Chapter 6, we considered a practical application of vehicular VLC by exploring it as a wireless connectivity solution to enable outdoor broadcasting for public safety systems. We utilized the ubiquitous streetlights as wireless transmitters taking into account the fundamental differences imposed by the outdoor medium and lightning infrastructure. In Section 6.2, we introduced the outdoor VLC broadcasting system, explained the street light classifications and their use cases, investigated the sunlight modeling with OpticStudio, and presented the SNR analysis. In Section 6.3, we illustrated the broadcasting scenarios under consideration; VLC broadcasting in the roadway and VLC

broadcasting in the sidewalk path. Our results revealed that the sunlight has a significant effect on the system performance. Therefore, when designing VLC based outdoor broadcasting systems, it is important to take into account the effect of user mobility, weather condition, asymmetrical pattern of streetlights same as the impact of sunlight. The results of this chapter have been published in [170].

7.2 Future Work

In Chapter 2, we have validated the ray tracing channel modeling approach in different indoor scenarios including both the Single-Input Single-Output (SISO) and the MIMO cases, and in outdoor scenarios assuming only the V2V link and in the clear weather condition. Validating the racy tracing approach for the V2V link in the presence of different weather conditions as well as for I2V links can be a topic for future work.

In Chapter 3, we have utilized the ray tracing channel modeling approach and proposed closed-form path loss expressions for the V2V links based-on both HLs and TLs while in Chapter 4, we proposed closed-form path loss expressions for the I2V links based-on both streetlights and traffic lights. To further improve the road safety, it is also important to consider the other vehicular links such as the links between the vehicles and pedestrians (V2P) and between the infrastructures and pedestrians (I2P). Therefore, proposing closed-form expression of channel path loss for both V2P and I2P links can be considered as future work.

In Chapter 5, we have investigated the channel modeling of multi-directional coverage for vehicular VLC systems in different road types (i.e., multi-lane, curved roads), intersections (i.e., T-shaped, Y-shaped intersections) and traffic scenarios (i.e., cruising in the same or different lanes, lane change etc.). We further quantified the capability of receiving signals in all scenarios where our results have revealed that deployment of nine PDs with carefully determined locations on the vehicle is enough to create the required quasi-omni-directional coverage for V2V and I2V connectivity. It would be a future research direction whether or not there is a need for additional PDs to enable V2P connectivity.

In Chapter 6, we have considered the vehicular VLC as a wireless connectivity solution to enable outdoor broadcasting for public safety systems. We have utilized the ubiquitous streetlights as wireless transmitters taking into account the fundamental differences imposed by the outdoor medium and lightning infrastructure. Our results revealed that the sunlight has a significant effect on the system performance. Therefore, when designing VLC based outdoor broadcasting systems, it is important to take into account the effect of user mobility, weather condition same as the impact of sunlight. This will require utilizing effective mitigation and enhancement techniques such as the blue optical filtering and/or angle diversity receiver with different combining techniques which will be considered as future research.

In addition to the aforementioned future works, which focus on the channel modeling of vehicular VLC systems, the following research points can be further considered as future works. Since realistic channel path loss models for vehicular VLC systems became available, investigating the system development and the overall network performance (handover, throughput, packet delivery ratio, etc.) becomes accessible. So far, we have considered direct vehicular communication links. To support large communication ranges or to avoid outages due to possible blockages, multi-hop relay systems and the hybridization between different V2V and I2V VLC links can be deployed. Since the demand for high data rate vehicular applications is continuously increasing, the integration of VLC with other emerging V2X solutions (i.e., DSRC, C-V2X, mmWave) becomes strongly required. That will require the development of dedicated channel models and efficient switching algorithms.

Bibliography

[1] T. Komine and M. Nakagawa, "Fundamental analysis for visible-light communication system using LED lights," *IEEE Trans. Consum. Electron.*, vol. 50, no. 1, pp. 100–107, 2004.

[2] J. M. Kahn and J. R. Barry, "Wireless infrared communications," *Proc. IEEE*, vol. 85, no. 2, pp. 265–298, 1997.

[3] S. Arnon, *Visible light communication*. New York, NY, USA: Cambridge Univ. Press, 1st ed., 2015.

[4] S. Dimitrov and H. Haas, *Principles of LED light communications: Towards networked Li-Fi*. Cambridge Univ. Press, Mar. 2015.

[5] Z. Nazari Chaleshtori, Z. Ghassemlooy, H. B. Eldeeb, M. Uysal, and S. Zvanovec, "Utilization of an OLED-based VLC system in office, corridor, and semi-open corridor environments," *Sensors*, vol. 20, no. 23, p. 6869, 2020.

[6] H. B. Eldeeb, M. Al-Nahhal, H. A. Selmy, and F. E. Abd El-Samie, "Continuous phase modulation with chaotic interleaving for visible light communication systems based on orthogonal frequency division multiplexing," *Trans. Emerg. Telecommun. Technol.*, vol. 31, no. 10, p. e4100, 2020.

[7] L. Feng, R. Q. Hu, J. Wang, P. Xu, and Y. Qian, "Applying VLC in 5G networks: Architectures and key technologies," *IEEE Netw.*, vol. 30, no. 6, pp. 77–83, 2016.

[8] A. Boucouvalas, P. Chatzimisios, Z. Ghassemlooy, M. Uysal, and K. Yiannopoulos, "Standards for indoor optical wireless communications," *IEEE Commun. Mag.*, vol. 53, no. 3, pp. 24–31, 2015.

[9] S. Zhang, J. Liu, H. Guo, M. Qi, and N. Kato, "Envisioning device-to-device communications in 6G," *IEEE Netw.*, vol. 34, no. 3, pp. 86–91, 2020.

[10] H. B. Eldeeb, H. A. I. Selmy, H. M. Elsayed, R. I. Badr, and M. Uysal, "Efficient resource allocation scheme for multi-user hybrid VLC/IR networks," in *2019 IEEE Photon. Conf. (IPC)*, pp. 1–2, 2019.

[11] M. Uysal, Z. Ghassemlooy, A. Bekkali, A. Kadri, and H. Menouar, "Visible light communication for vehicular networking: Performance study of a V2V system using a measured headlamp beam pattern model," *IEEE Veh. Technol. Mag.*, vol. 10, pp. 45–53, Dec 2015.

[12] H. B. Eldeeb, E. Yanmaz, and M. Uysal, "MAC layer performance of multi-hop vehicular VLC networks with CSMA/CA," in *2020 12th Int. Symp. Commun. Syst., Netw. and Digit. Signal Process. (CSNDSP)*, pp. 1–6, 2020.

[13] Y.-K. Cheong, X.-W. Ng, and W.-Y. Chung, "Hazardless biomedical sensing data transmission using VLC," *IEEE sensors J.*, vol. 13, no. 9, pp. 3347–3348, 2013.

[14] D. Tagliaferri and C. Capsoni, "High-speed wireless infrared uplink scheme for airplane passengers' communications," *Electron. Lett.*, vol. 53, no. 13, pp. 887–888, 2017.

[15] M. F. Keskin, S. Gezici, and O. Arikan, "Direct and two-step positioning in visible light systems," *IEEE Trans. Commun.*, vol. 66, no. 1, pp. 239–254, 2017.

[16] H. B. Eldeeb, H. A. Selmy, H. M. Elsayed, F. E. Abd El-Samie, and R. I. Badr, "Visible light communication based on CPM-OFDM with chaotic interleaving scheme," in *2017 IEEE Photon. Conf. (IPC)*, pp. 241–242, IEEE, 2017.

[17] J. Gancarz, H. Elgala, and T. D. Little, "Impact of lighting requirements on VLC systems," *IEEE Commun. Mag.*, vol. 51, no. 12, pp. 34–41, 2013.

[18] S.-H. Chen and C.-W. Chow, "Color-shift keying and code-division multiple-access transmission for RGB-LED visible light communications using mobile phone camera," *IEEE Photon. J.*, vol. 6, no. 6, pp. 1–6, 2014.

[19] Z. N. Chaleshtori, S. Zvanovec, Z. Ghassemlooy, H. B. Eldeeb, and M. Uysal, "A flexible OLED VLC system for an office environment," in *2020 12th Int. Symp. Commun. Syst., Netw., and Digit. Signal Process. (CSNDSP)*, pp. 1–5, 2020.

[20] M. S. Islim, R. X. Ferreira, X. He, E. Xie, S. Videv, S. Viola, S. Watson, N. Bamiedakis, R. V. Penty, I. H. White, *et al.*, "Towards 10 Gb/s orthogonal frequency division multiplexing-based visible light communication using a GaN violet micro-LED," *Photon. Research*, vol. 5, no. 2, pp. A35–A43, 2017.

[21] Z. N. Chaleshtori, S. Zvanovec, Z. Ghassemlooy, H. B. Eldeeb, and M. Uysal, "Coverage of a shopping mall with flexible OLED-based visible light communications," *Opt. express*, vol. 28, no. 7, pp. 10015–10026, 2020.

[22] G. A. Mapunda, R. Ramogomana, L. Marata, B. Basutli, A. S. Khan, and J. M. Chuma, "Indoor visible light communication: A tutorial and survey," *Wireless Commun. and Mobile Comput.*, vol. 2020, 2020.

[23] K. Modepalli and L. Parsa, "Dual-purpose offline LED driver for illumination and visible light communication," *IEEE Trans. Ind Appl.*, vol. 51, no. 1, pp. 406–419, 2014.

[24] P. H. Pathak, X. Feng, P. Hu, and P. Mohapatra, "Visible light communication, networking, and sensing: A survey, potential and challenges," *IEEE Commun. Surveys & tuts.*, vol. 17, no. 4, pp. 2047–2077, 2015.

[25] H. B. Eldeeb, H. A. Selmy, H. M. Elsayed, and R. I. Badr, "Interference mitigation and capacity enhancement using constraint field of view ADR in downlink VLC channel," *IET Commun.*, vol. 12, no. 16, pp. 1968–1978, 2018.

[26] M. Kashef, M. Abdallah, K. Qaraqe, H. Haas, and M. Uysal, "Coordinated interference management for visible light communication systems," *J. Opt. Commun. Netw.*, vol. 7, no. 11, pp. 1098–1108, 2015.

[27] H. B. Eldeeb, H. A. Selmy, H. M. Elsayed, and R. I. Badr, "Co-channel interference cancellation using constraint field of view ADR in VLC channel," in *2017 IEEE Photon. Conf. (IPC) Part II*, pp. 1–2, IEEE, 2017.

[28] A.-M. Căilean and M. Dimian, "Current challenges for visible light communications usage in vehicle applications: A survey," *IEEE Commun. Surveys & Tuts.*, vol. 19, no. 4, pp. 2681–2703, 2017.

[29] R. I. Meneguette, R. De Grande, and A. A. Loureiro, *Intelligent transport system in smart cities*. Cham, Switzerland: Springer, 2018.

[30] O. Pribyl, P. Pribyl, M. Lom, and M. Svitek, "Modeling of smart cities based on ITS architecture," *IEEE Intell. Transp. Syst. Mag.*, vol. 11, pp. 28–36, Nov. 2018.

[31] S. H. Bouk, S. H. Ahmed, D. Kim, and H. Song, "Named-data-networking-based ITS for smart cities," *IEEE Commun. Mag.*, vol. 55, pp. 105–111, Jan. 2017.

[32] Z. MacHardy, A. Khan, K. Obana, and S. Iwashina, "V2X access technologies: Regulation, research, and remaining challenges," *IEEE Commun. Surveys Tuts.*, vol. 20, pp. 1858–1877, Feb. 2018.

[33] "Toyota commits big to DSRC." `https://www.adandp.media/blog/post/\toyota-commits-big-to-dsrc`. [Accessed: January 4, 2022].

[34] "Cellular V2X." `https://www.qualcomm.com/invention/5g/cellular-v2x/ecosystem`. [Accessed: January 4, 2022].

[35] P. H. Pathak, X. Feng, P. Hu, and P. Mohapatra, "Visible light communication, networking, and sensing: A survey, potential and challenges," *IEEE commun. Surveys & Tuts.*, vol. 17, no. 4, pp. 2047–2077, 2015.

[36] A.-M. Cailean and M. Dimian, "Impact of IEEE 802.15. 7 standard on visible light communications usage in automotive applications," *IEEE Commun. Mag.*, 2017.

[37] B. M. Masini, A. Bazzi, and A. Zanella, "Vehicular visible light networks for urban mobile crowd sensing," *Sensors*, vol. 18, no. 4, p. 1177, 2018.

[38] H. Zhang, A. Yang, L. Feng, and P. Guo, "Gb/s real-time visible light communication system based on white LEDs using T-bridge cascaded pre-equalization circuit," *IEEE Photon. J.*, vol. 10, no. 2, pp. 1–7, 2018.

[39] M. Ijaz, D. Tsonev, J. J. McKendry, E. Xie, S. Rajbhandari, H. Chun, G. Faulkner, E. Gu, M. D. Dawson, D. O'brien, *et al.*, "Experimental proof-of-concept of optical spatial modulation OFDM using micro LEDs," in *2015 IEEE int. conf. Commun. workshop (ICCW)*, pp. 1338–1343, IEEE, 2015.

[40] M. S. Amjad, C. Tebruegge, A. Memedi, S. Kruse, C. Kress, C. Scheytt, and F. Dressler, "An IEEE 802.11 compliant SDR-based system for vehicular visible light communications," in *2019 IEEE Int. Conf. Commun. (ICC)*, pp. 1–6, IEEE, 2019.

[41] S. Ucar, S. C. Ergen, and O. Ozkasap, "IEEE 802.11 p and visible light hybrid communication based secure autonomous platoon," *IEEE Trans. Veh. Technol.*, vol. 67, no. 9, pp. 8667–8681, 2018.

[42] A. Memedi and F. Dressler, "Vehicular visible light communications: A survey," *IEEE Commun. Surveys & Tuts.*, vol. 23, no. 1, pp. 161–181, 2020.

[43] M. Uysal *et al.*, "IEEE 802.15. 7r1 reference channel models for visible light communications," *IEEE Commun. Mag.*, vol. 55, no. 1, pp. 212–217, 2017.

[44] H. B. Eldeeb, M. Hosney, H. M. Elsayed, R. I. Badr, M. Uysal, and H. A. I. Selmy, "Optimal resource allocation and interference management for multi-user uplink light communication systems with angular diversity technology," *IEEE Access*, vol. 8, pp. 203224–203236, 2020.

[45] M. Akanegawa, Y. Tanaka, and M. Nakagawa, "Basic study on traffic information system using LED traffic lights," *IEEE Trans. Intell. Trans. Syst.*, vol. 2, no. 4, pp. 197–203, 2001.

[46] N. Kumar, D. Terra, N. Lourenco, L. N. Alves, and R. L. Aguiar, "Visible light communication for intelligent transportation in road safety applications," in *2011 7th Int. Wireless Commun. Mobile Comput. Conf.*, pp. 1513–1518, IEEE, 2011.

[47] S. Kitano, S. Haruyama, and M. Nakagawa, "LED road illumination communications system," in *IEEE 58th Veh. Technol. Conf. (VTC Fall)*, vol. 5, pp. 3346–3350, IEEE, Oct. 2003.

[48] N. Zhu, Z. Xu, Y. Wang, H. Zhuge, and J. Li, "Handover method in visible light communication between the moving vehicle and multiple LED streetlights," *Optik*, vol. 125, pp. 3540–3544, July 2014.

[49] F. S. Diana, G. Guth, J. Den Breejen, and I. Black, "Asymmetrical light intensity distribution from luminaire," Sept. 17 2019. US Patent 10,416,370.

[50] "Uniform provisions concerning the approval of motor vehicle headlamps emitting an asymmetrical passing beam or a driving beam or both and equipped with filament lamps." United Nations, Tech. Rep. Regulation No. 112 - Revision 1, Oct. 2006.

[51] L. Cheng, W. Viriyasitavat, M. Boban, and H.-M. Tsai, "Comparison of radio frequency and visible light propagation channels for vehicular communications," *IEEE Access*, vol. 6, pp. 2634–2644, Dec. 2017.

[52] T. Lang, Z. Li, A. Wang, and G. Chen, "Hemispherical lens featured beehive structure receiver on vehicular massive MIMO visible light communication system," in *Int. Conf. on Internet of Veh.*, pp. 469–477, Springer, 2015.

[53] Y. Bao, Y. Wang, J. Yu, and J. Shen, "A visible light communication based vehicle collision avoiding system," in *2016 15th Int. Conf. Opt. Commun. and Netw. (ICOCN)*, pp. 1–3, IEEE, 2016.

[54] H. Farahneh, S. M. Kamruzzaman, and X. Fernando, "Differential receiver as a denoising scheme to improve the performance of V2V-VLC systems," in *2018 IEEE Int. Conf. Commun. Workshops (ICC Workshops)*, pp. 1–6, IEEE, 2018.

[55] Z. Cui, P. Yue, X. Yi, and J. Li, "Research on non-uniform dynamic vehicle-mounted VLC with receiver spatial and angular diversity," in *ICC 2019-2019 IEEE Int. Conf. on Commun. (ICC)*, pp. 1–7, IEEE, 2019.

[56] W. Viriyasitavat, S.-H. Yu, and H.-M. Tsai, "Short paper: Channel model for visible light communications using off-the-shelf scooter taillight," in *2013 IEEE Veh. Netw. Conf.*, pp. 170–173, IEEE, 2013.

[57] S. Lee, J. K. Kwon, S.-Y. Jung, and Y.-H. Kwon, "Evaluation of visible light communication channel delay profiles for automotive applications," *EURASIP j. Wireless Commun. Netw.*, vol. 2012, no. 1, p. 370, 2012.

[58] P. Luo, Z. Ghassemlooy, H. Le Minh, E. Bentley, A. Burton, and X. Tang, "Fundamental analysis of a car to car visible light communication system," in *2014 9th Int. Symp. Commun. Syst., Netw., and Digit. Signal Process. (CSNDSP)*, pp. 1011–1016, IEEE, 2014.

[59] P. Luo, Z. Ghassemlooy, H. Le Minh, E. Bentley, A. Burton, and X. Tang, "Performance analysis of a car-to-car visible light communication system," *Appl. Opt.*, vol. 54, no. 7, pp. 1696–1706, 2015.

[60] A. Memedi, H.-M. Tsai, and F. Dressler, "Impact of realistic light radiation pattern on vehicular visible light communication," in *2017 IEEE Globecom Workshops (GC Wkshps)*, pp. 1–6, IEEE, 2017.

[61] H.-Y. Tseng, Y.-L. Wei, A.-L. Chen, H.-P. Wu, H. Hsu, and H.-M. Tsai, "Characterizing link asymmetry in vehicle-to-vehicle visible light communications," in *2015 IEEE Veh. Netw. Conf. (VNC)*, pp. 88–95, IEEE, 2015.

[62] Y.-H. Kim, W. A. Cahyadi, and Y. H. Chung, "Experimental demonstration of LED-based vehicle to vehicle communication under atmospheric turbulence," in *2015 Int. Conf. Inf. Commun. Technol. Convergence (ICTC)*, pp. 1143–1145, IEEE, 2015.

[63] Y. H. Kim, W. A. Cahyadi, and Y. H. Chung, "Experimental demonstration of VLC-based vehicle-to-vehicle communications under fog conditions," *IEEE Photon. J.*, vol. 7, no. 6, pp. 1–9, 2015.

[64] M. Elamassie, M. Karbalayghareh, F. Miramirkhani, R. C. Kizilirmak, and M. Uysal, "Effect of fog and rain on the performance of vehicular visible light communications," in *IEEE 87th Veh. Technol. Conf. (VTC Spring)*, pp. 1–6, IEEE, 2018.

[65] I. E. Lee, M. L. Sim, and F. W.-L. Kung, "Performance enhancement of outdoor visible-light communication system using selective combining receiver," *IET optoelectronics*, vol. 3, no. 1, pp. 30–39, 2009.

[66] K. Cui, G. Chen, Z. Xu, and R. D. Roberts, "Traffic light to vehicle visible light communication channel characterization," *Appl. opt.*, vol. 51, no. 27, pp. 6594–6605, 2012.

[67] S.-A. Avătămăniţei, A.-M. Căilean, E. Zadobrischi, A. Done, M. Dimian, and V. Popa, "Intensive testing of infrastructure-to-vehicle visible light communications in real outdoor scenario: Evaluation of a 50 meters link in direct sun exposure," in *2019 Global LIFI Congress (GLC)*, pp. 1–5, IEEE, Jun. 2019.

[68] T. Nawaz, M. Seminara, S. Caputo, L. Mucchi, F. S. Cataliotti, and J. Catani, "IEEE 802.15.7-compliant ultra-low latency relaying VLC system for safety-critical ITS," *IEEE Trans. Veh. Technol.*, vol. 68, pp. 12040–12051, Dec. 2019.

[69] N. Kumar, N. Lourenço, D. Terra, L. N. Alves, and R. L. Aguiar, "Visible light communications in intelligent transportation systems," in *2012 IEEE Intell. Veh. Symp.*, pp. 748–753, IEEE, Jun. 2012.

[70] A. I. Petrariu, A. Lavric, and E. Coca, "VLC for vehicular communications: A multiple input multiple output (MIMO) approach," in *2018 Int. Conf. Develop. Appl. Syst. (DAS)*, pp. 134–137, IEEE, May 2018.

[71] M. Seminara, T. Nawaz, S. Caputo, L. Mucchi, and J. Catani, "Characterization of field of view in visible light communication systems for intelligent transportation systems," *IEEE Photon. J.*, vol. 12, pp. 1–16, Aug. 2020.

[72] S.-A. Avătămăniței, A.-M. Căilean, A. Done, M. Dimian, and V. Popa, "Experimental evaluation of traffic light to vehicle visible light communications in snowfall conditions," in *2020 7th Int. Conf. Control Decis. Inf. Technol. (CoDIT)*, vol. 1, pp. 693–696, IEEE, 29 June–2 July 2020.

[73] S. Kitano, S. Haruyama, and M. Nakagawa, "LED road illumination communications system," in *IEEE 58th Veh. Technol. Conf. (VTC Fall)*, vol. 5, pp. 3346–3350, IEEE, Oct. 2003.

[74] N. Kumar, "Smart and intelligent energy efficient public illumination system with ubiquitous communication for smart city," in *Int. Conf. on Smart Structures and Syst. (ICSSS'13)*, pp. 152–157, IEEE, Mar. 2013.

[75] N. Zhu, Z. Xu, Y. Wang, H. Zhuge, and J. Li, "Handover method in visible light communication between the moving vehicle and multiple LED streetlights," *Optik*, vol. 125, pp. 3540–3544, July 2014.

[76] X. You, Y. Zhong, J. Chen, and C. Yu, "Mobile channel estimation based on decision feedback in vehicle-to-infrastructure visible light communication systems," *Opt. Commun.*, vol. 462, p. 125261, May 2020.

[77] V. M. Baeza, M. Sánchez-Fernández, A. G. Armada, and A. Royo, "Testbed for a LiFi system integrated in streetlights," in *European Conf. Netw. and Commun. (EuCNC)*, pp. 517–521, IEEE, June 2015.

[78] P. Arunachalam and N. Kumar, "Visible light communication and radio network for vehicular environment," in *Proc. 2nd Int. Conf. Adv. Electron., Comput. Commun. (ICAECC)*, pp. 1–5, IEEE, Feb. 2018.

[79] J.-H. Lee and S.-Y. Jung, "SNR analyses of the multi-spectral light channels for optical wireless LED communications in intelligent transportation system," in *Proc. IEEE 79th Veh. Technol. Conf. (VTC Spring)*, pp. 1–5, IEEE, May 2014.

[80] S. Lee, J. K. Kwon, S.-Y. Jung, and Y.-H. Kwon, "Evaluation of visible light communication channel delay profiles for automotive applications," *Eurasip J. Wirel. Commun. Netw.*, vol. 2012, p. 370, Dec. 2012.

[81] M. S. Demir, H. B. Eldeeb, and M. Uysal, "CoMP-based dynamic handover for vehicular VLC networks," *IEEE Commun. Lett.*, vol. 24, pp. 2024–2028, Sept. 2020.

[82] "Opticstudio 18.9." `https://www.zemax.com/pages/opticstudio`. [Accessed: January 4, 2022].

[83] A. Al-Kinani, C.-X. Wang, L. Zhou, and W. Zhang, "Optical wireless communication channel measurements and models," *IEEE Commun. Surveys & Tuts.*, vol. 20, no. 3, pp. 1939–1962, 2018.

[84] J. R. Barry, J. M. Kahn, W. J. Krause, E. A. Lee, and D. G. Messerschmitt, "Simulation of multipath impulse response for indoor wireless optical channels," *IEEE J. Sel. Areas Commun.*, vol. 11, no. 3, pp. 367–379, 1993.

[85] F. Lopez-Hermandez and M. Betancor, "DUSTIN: Algorithm for calculation of impulse response on IR wireless indoor channels," *Electronics Lett.*, vol. 33, no. 21, pp. 1804–1806, 1997.

[86] J. B. Carruthers and P. Kannan, "Iterative site-based modeling for wireless infrared channels," *IEEE Trans. Antennas Propag.*, vol. 50, no. 5, pp. 759–765, 2002.

[87] K. Lee, H. Park, and J. R. Barry, "Indoor channel characteristics for visible light communications," *IEEE Commun. Lett.*, vol. 15, no. 2, pp. 217–219, 2011.

[88] J. B. Carruthers and J. M. Kahn, "Modeling of nondirected wireless infrared channels," *IEEE Trans. Commun.*, vol. 45, no. 10, pp. 1260–1268, 1997.

[89] V. Jungnickel, V. Pohl, S. Nonnig, and C. Von Helmolt, "A physical model of the wireless infrared communication channel," *IEEE J. Sel. Areas Commun.*, vol. 20, no. 3, pp. 631–640, 2002.

[90] N. Hayasaka and T. Ito, "Channel modeling of nondirected wireless infrared indoor diffuse link," *Electron. Commun. Japan (Part I: Communications)*, vol. 90, no. 6, pp. 9–19, 2007.

[91] V. Pohl, V. Jungnickel, and C. Von Helmolt, "Integrating-sphere diffuser for wireless infrared communication," *IEE Proc. Optoelectronics*, vol. 147, no. 4, pp. 281–285, 2000.

[92] O. González, S. Rodríguez, R. Pérez-Jiménez, B. R. Mendoza, and A. Ayala, "Error analysis of the simulated impulse response on indoor wireless optical channels using a monte carlo-based ray-tracing algorithm," *IEEE Trans. Commun.*, vol. 53, no. 1, pp. 124–130, 2005.

[93] M. S. Chowdhury, W. Zhang, and M. Kavehrad, "Combined deterministic and modified Monte carlo method for calculating impulse responses of indoor optical wireless channels," *J. Lightw. Technol.*, vol. 32, no. 18, pp. 3132–3148, 2014.

[94] S. Dimitrov, R. Mesleh, H. Haas, M. Cappitelli, M. Olbert, and E. Bassow, "On the SIR of a cellular infrared optical wireless system for an aircraft," *IEEE J. Sel. Areas Commun.*, vol. 27, no. 9, pp. 1623–1638, 2009.

[95] O. González, S. Rodríguez, R. Pérez-Jiménez, B. R. Mendoza, and A. Ayala, "Comparison of Monte Carlo ray-tracing and photon-tracing methods for calculation of the impulse response on indoor wireless optical channels," *Opt. Express*, vol. 19, no. 3, pp. 1997–2005, 2011.

[96] F. Miramirkhani and M. Uysal, "Channel modeling and characterization for visible light communications," *IEEE Photon. J.*, vol. 7, no. 6, pp. 1–16, 2015.

[97] M. Uysal, F. Miramirkhani, O. Narmanlioglu, T. Baykas, and E. Panayirci, "IEEE 802.15. 7r1 reference channel models for visible light communications," *IEEE Commun. Mag.*, vol. 55, no. 1, pp. 212–217, 2017.

[98] M. Uysal, F. Miramirkhani, T. Baykas, N. Serafimovski, and V. Jungnickel, "IEEE 802.11 bb reference channel models for indoor environments," doc: IEEE 11-18-1236-01-00bb, July, 2018.

[99] OSRAM. `https://www.osram.com/os/ecat/OSLUX`. [Accessed: January 4, 2022].

[100] H. B. Eldeeb, M. Uysal, S. M. Mana, P. Hellwig, J. Hilt, and V. Jungnickel, "Channel modelling for light communications: Validation of ray tracing by measurements," in *2020 12th Int. Symp. Commun. Syst., Netw., and Digit. Signal Process. (CSNDSP)*, pp. 1–6, 2020.

[101] H. B. Eldeeb, S. M. Mana, V. Jungnickel, P. Hellwig, J. Hilt, and M. Uysal, "Distributed MIMO for Li-Fi: Channel measurements, ray tracing and throughput analysis," *IEEE Photon. Technol. Lett.*, vol. 33, no. 16, pp. 916–919, 2021.

[102] H. B. Eldeeb, M. Uysal, S. M. Mana, P. Hellwig, J. Hilt, and V. Jungnickel, "Channel measurements and ray tracing simulations for MIMO light communication at 200 mhz," in *2020 IEEE Photon. Conf. (IPC)*, pp. 1–2, 2020.

[103] M. Karbalayghareh, F. Miramirkhani, H. B. Eldeeb, R. C. Kizilirmak, S. M. Sait, and M. Uysal, "Channel modelling and performance limits of vehicular visible light communication systems," *IEEE Trans. Veh. Technol.*, vol. 69, no. 7, pp. 6891–6901, 2020.

[104] H. B. Eldeeb, M. Uysal, S. M. Mana, P. Hellwig, and V. Jungnickel, "Channel modelling for LC in TGbb: Validation of ray tracing models by measurements," tech. rep., IEEE, 2020. doc: IEEE 802.11-12/1234r0, August 2020.

[105] H. B. Eldeeb, E. Eso, M. Uysal, Z. Ghassemlooy, S. Zvanovec, and J. Sathian, "Vehicular visible light communications: The impact of taillight radiation pattern," in *2020 IEEE Photon. Conf. (IPC)*, pp. 1–2, 2020.

[106] M. Uysal, C. Capsoni, Z. Ghassemlooy, A. Boucouvalas, and E. Udvary, *Optical wireless communications: An emerging technology*. Springer, 2016.

[107] S. Hranilovic, *Wireless optical communication systems*. New York, NY, USA: Springer-Verlag, 2005.

[108] P. Colonna, P. Intini, N. Berloco, and V. Ranieri, "Integrated american-european protocol for safety interventions on existing two-lane rural roads," *European transport research review*, vol. 10, no. 1, p. 5, 2018.

[109] Audi A5. `https://www.audiusa.com/models/audi-a5-coupe`. [Accessed: January 4, 2022].

[110] H. B. Eldeeb, F. Miramirkhani, and M. Uysal, "A path loss model for vehicle-to-vehicle visible light communications," in *2019 15th Int. Conf. on Telecommun. (ConTEL)*, pp. 1–5, 2019.

[111] I. C. on Illumination, *Calculation and Measurement of Luminance and Illuminance in Road Lighting: Computer Program for Luminance, Illuminance and Glare*. CIE rapport, Bureau Central, CIE, 1976.

[112] "Aster spectral." `http://speclib.jpl.nasa.gov`. [Accessed: January 4, 2022].

[113] W. Adrian and R. Jobanputra, "Influence of pavement reflectance on lighting for parking lots," 2005.

[114] H. B. Eldeeb, E. Eso, E. A. Jarchlo, S. Zvanovec, M. Uysal, Z. Ghassemlooy, and J. Sathian, "Vehicular VLC: A ray tracing study based on measured radiation patterns of commercial taillights," *IEEE Photon. Technol. Lett.*, vol. 33, no. 16, pp. 904–907, 2021.

[115] J. Poliak, P. Pezzei, E. Leitgeb, and O. Wilfert, "Link budget for high-speed short-distance wireless optical link," in *2012 8th Int. Symp. Commun. Syst., Netw., and Digit. Signal Process. (CSNDSP)*, pp. 1–6, IEEE, 2012.

[116] I. I. Kim, B. McArthur, and E. J. Korevaar, "Comparison of laser beam propagation at 785 nm and 1550 nm in fog and haze for optical wireless communications," in *Optical Wireless Communications III*, vol. 4214, pp. 26–37, International Society for Optics and Photonics, 2001.

[117] "Osram Co." `https://www.osram.com/os/products/product-promotions/`. [Accessed: July 30, 2021].

[118] H. B. Eldeeb, M. Elamassie, and M. Uysal, "Performance analysis and optimization of cascaded I2V and V2V VLC links," in *2021 17th Int. Symp. Wireless Commun. Syst. (ISWCS)*, pp. 1–6, 2021.

[119] "Vestel Co." `https://www.vestelledlighting.com/eu-en/ephesus-m4s-68`. [Accessed: January 4, 2022].

[120] "Solve nonlinear curve-fitting." `https://www.mathworks.com/help/\optim/ug/lsqcurvefit.html`. [Accessed: January 4, 2022].

[121] "Pole arrangement in street lighting." https://www.mocled.com/newsinfo/406576.html. [Accessed: January 4, 2022].

[122] "Photodiodes." http://www.photek.co.uk/products/photodiodes.html. [Accessed: January 4, 2022].

[123] A.-M. Căilean and M. Dimian, "Toward environmental-adaptive visible light communications receivers for automotive applications: A review," *IEEE Sensors J.*, vol. 16, pp. 2803–2811, May. 2016.

[124] J. S. Seybold, *Introduction to RF propagation*. John Wiley & Sons, 2005.

[125] H. B. Eldeeb, M. Elamassie, S. M. Sait, and M. Uysal, "Infrastructure-to-vehicle visible light communications: Channel modelling and performance analysis," *IEEE Trans. Veh. Technol.*, July 2021. Accepted.

[126] M. Abramowitz and I. A. Stegun, "Handbook of mathematical functions with formulas, graphs, and mathematical table," in *US Department of Commerce*, National Bureau of Standards Appl. Math. Ser. 55, 1965.

[127] M. Vaezi, Z. Ding, and H. V. Poor, *Multiple access techniques for 5G wireless networks and beyond*, vol. 159. Springer, 2019.

[128] B. Turan, S. Ucar, S. C. Ergen, and O. Ozkasap, "Dual channel visible light communications for enhanced vehicular connectivity," in *2015 IEEE Veh. Netw. Conf. (VNC)*, pp. 84–87, Dec 2015.

[129] M. I. Petkovic, A. M. Cvetkovic, M. Narandzic, N. D. Chatzidiamantis, D. Vukobratovic, and G. K. Karagiannidis, "Mixed RF-VLC relaying systems for interference-sensitive mobile applications," *IEEE Trans. Veh. Technol.*, vol. 69, pp. 11099–11111, July 2020.

[130] L. Grobe and K.-D. Langer, "Block-based PAM with frequency domain equalization in visible light communications," in *2013 IEEE Globecom Workshops (GC Wkshps)*, pp. 1070–1075, IEEE, 2013.

[131] A. Lapidoth, S. M. Moser, and M. A. Wigger, "On the capacity of free-space optical intensity channels," *IEEE Trans. Inf. Theory*, vol. 55, no. 10, pp. 4449–4461, 2009.

[132] J.-B. Wang, Q.-S. Hu, J. Wang, M. Chen, and J.-Y. Wang, "Tight bounds on channel capacity for dimmable visible light communications," *J. Lightw. Technol.*, vol. 31, no. 23, pp. 3771–3779, 2013.

[133] A. Chaaban, J.-M. Morvan, and M.-S. Alouini, "Free-space optical communications: Capacity bounds, approximations, and a new sphere-packing perspective," *IEEE Trans. Commun.*, vol. 64, no. 3, pp. 1176–1191, 2016.

[134] L. Yin and H. Haas, "Physical-layer security in multiuser visible light communication networks," *IEEE J. Sel. Areas Commun.*, vol. 36, no. 1, pp. 162–174, 2017.

[135] A.-L. Chen, H.-P. Wu, Y.-L. Wei, and H.-M. Tsai, "Time variation in vehicle-to-vehicle visible light communication channels," in *2016 IEEE Veh. Netw. Conf. (VNC)*, pp. 1–8, IEEE, 2016.

[136] B. Aly, M. Elamassie, H. B. Eldeeb, and M. Uysal, "Experimental investigation of lens combinations on the performance of vehicular VLC," in *2020 12th Int. Symp. Commun. Syst., Netw., and Digit. Signal Process. (CSNDSP)*, pp. 1–5, 2020.

[137] A. Al-Kinani, C.-X. Wang, Q. Zhu, Y. Fu, E.-H. M. Aggoune, A. Talib, and N. A. Al-Hasaani, "A 3D non-stationary GBSM for vehicular visible light communication MISO channels," *IEEE Access*, vol. 8, pp. 140333–140347, 2020.

[138] A. Memedi, C. Tebruegge, J. Jahneke, and F. Dressler, "Impact of vehicle type and headlight characteristics on vehicular VLC performance," in *2018 IEEE Vehicular Networking Conf. (VNC)*, pp. 1–8, IEEE, 2018.

[139] Y. Wang, X. Huang, J. Shi, Y.-q. Wang, and N. Chi, "Long-range high-speed visible light communication system over 100-m outdoor transmission utilizing receiver diversity technology," *Opt. Eng.*, vol. 55, no. 5, p. 056104, 2016.

[140] M. Morales-Céspedes, A. A. Quidan, and A. G. Armada, "Experimental evaluation of the reconfigurable photodetector for blind interference alignment in visible light communications," in *2019 27th European Signal Process. Conf. (EUSIPCO)*, pp. 1–5, IEEE, 2019.

[141] S. Yahia, Y. Meraihi, A. B. Gabis, and A. Ramdane-Cherif, "Multi-directional vehicle-to-vehicle visible light communication with angular diversity technology," in *2020 2nd Int. Workshop on Human-Centric Smart Environments for Health and Well-being (IHSH)*, pp. 160–164, IEEE, 2021.

[142] H. B. Eldeeb and M. Uysal, "Vehicle-to-vehicle visible light communication: How to select receiver locations for optimal performance?," in *2019 11th Int. Conf. Electr. and Electron. Eng. (ELECO)*, pp. 402–405, IEEE, 2019.

[143] M. A. Vieira, M. Vieira, P. Louro, and P. Vieira, "Redesign of the trajectory within a complex intersection for visible light communication ready connected cars," *Opt. Eng.*, vol. 59, no. 9, p. 097104, 2020.

[144] M. W. Hancock and B. Wright, "A policy on geometric design of highways and streets," *American Association of State Highway and Transportation Officials, Washington, DC, USA*, 2013.

[145] Z. Ghassemlooy, W. Popoola, and S. Rajbhandari, *Optical wireless communications: system and channel modelling with Matlab®*. CRC press, 2019.

[146] "LUXEON Rebel Automotive." `https://www.lumileds.com/products/auto-\motive-lighting/luxeon-rebel-automotive/`. [Accessed: February 20, 2021].

[147] "Osram Co." `https://www.osram.com/os/products/product-promotions/`. [Accessed: February 20, 2021].

[148] S.-H. You, S.-H. Chang, H.-M. Lin, and H.-M. Tsai, "Visible light communications for scooter safety," in *Proc. 11th Annual Int. Conf. Mobile Syst., APPl., services*, pp. 509–510, 2013.

[149] R. Zhang, M. Biagi, L. Lampe, T. D. Little, S. Mangold, and Z. Xu, "Guest editorial localisation, communication and networking with VLC," *IEEE J. Sel. Areas Commun.*, vol. 36, no. 1, pp. 1–7, 2018.

[150] O. Narmanlioglu, B. Turan, B. Kebapci, S. C. Ergen, and M. Uysal, "Poster: Onboard camera video transmission over vehicular VLC," in *2016 IEEE Veh. Netw. Conf. (VNC)*, pp. 1–2, IEEE, 2016.

[151] H. B. Eldeeb, S. M. Sait, and M. Uysal, "Visible light communication for connected vehicles: How to achieve the omnidirectional coverage?," *IEEE Access*, vol. 9, pp. 103885–103905, 2021.

[152] M. S. Islim, S. Videv, M. Safari, E. Xie, J. J. McKendry, E. Gu, M. D. Dawson, and H. Haas, "The impact of solar irradiance on visible light communications," *J. Lightw. Technol.*, vol. 36, no. 12, pp. 2376–2386, 2018.

[153] D. Cervinka, Z. Ahmad, O. Salih, and S. Rajbhandari, "A study of yearly sunlight variance effect on vehicular visible light communication for emergency service vehicles," in *12th Int. Symp. Commun. Syst. Netw. Digit. Signal Process. (CSNDSP)*, pp. 1–6, IEEE, 2020.

[154] T. Hamza, M.-A. Khalighi, S. Bourennane, P. Léon, and J. Opderbecke, "Investigation of solar noise impact on the performance of underwater wireless optical communication links," *Opt. express*, vol. 24, no. 22, pp. 25832–25845, 2016.

[155] Z. Feng, Y. Luo, and Y. Han, "Design of LED freeform optical system for road lighting with high luminance/illuminance ratio," *Opt. express*, vol. 18, no. 21, pp. 22020–22031, 2010.

[156] H.-C. Chen, J.-Y. Lin, and H.-Y. Chiu, "Rectangular illumination using a secondary optics with cylindrical lens for LED street light," *Opt. express*, vol. 21, no. 3, pp. 3201–3212, 2013.

[157] R. Wu, K. Li, P. Liu, Z. Zheng, H. Li, and X. Liu, "Conceptual design of dedicated road lighting for city park and housing estate," *Appl. Opt.*, vol. 52, no. 21, pp. 5272–5278, 2013.

[158] I. Moreno, M. Avendaño-Alejo, T. Saucedo-A, and A. Bugarin, "Modeling LED street lighting," *Appl. Opt.*, vol. 53, no. 20, pp. 4420–4430, 2014.

[159] "Streetlight classifications." `https://www.ledil.com/street-lighting-optics-guide`. [Accessed: January 4, 2022].

[160] "Streetlight classifications." `https://intrans.iastate.edu/app/uploads/sites/15/2018/09/Chapter_11-2016.pdf`. [Accessed: January 4, 2022].

[161] C. Mobley, E. Boss, and C. Roesler, "Ocean optics web book (2016).," *http://www. oceanopticsbook.info/*, 2016.

[162] "Lighting design guidance." https://globaldesigningcities.org/publication/global-street-design-guide/utilities-and-infrastructure/lighting-and-technology/lighting-design-guidance/. [Accessed: January 4, 2022].

[163] "Streetlight pole spacing." https://www.thaisolid.com/en/what-is-the-distance-between-street-light-pole/. [Accessed: January 4, 2022].

[164] "Minimum width and buffer requirements for sidewalks." https://sustainablecitycode.org/brief/minimum-width-and-buffer-requirements-for-sidewalks/. [Accessed: January 4, 2022].

[165] "Downtown design guide city of san antonio." https://perma.cc/QJC8-4Z9Q. [Accessed: January 4, 2022].

[166] "Orion streetlight LED flga3." https://files.orionlighting.com/resources/PRODUCT/HARRIS/data%20sheets/HARRIS%20FLGA3.pdf. [Accessed: January 4, 2022].

[167] "Vestel S3-78-L6." http://www.vestelledlighting.com/files/vestel-sardes-street-light-l6_DAE255997472.png. [Accessed: January 4, 2022].

[168] "Orion streetlight LED ALLED3." https://files.orionlighting.com/resources/PRODUCT/HARRIS/data%20sheets/HARRIS_AreaSiteLight_ALLED3.pdf. [Accessed: January 4, 2022].

[169] H. B. Eldeeb, M. Elamassie, and M. Uysal, "Vehicle-to-infrastructure visible light communications: Channel modelling and capacity calculations," in *12th Int. Symp. Commun. Syst., Netw., and Digit. Signal Process. (CSNDSP)*, pp. 1–6, IEEE, 2020.

[170] H. B. Eldeeb and M. Uysal, "Visible light communication-based outdoor broadcasting," in *2021 17th Int. Symp. Wireless Commun. Syst. (ISWCS)*, pp. 1–6, 2021.

VITA

Hossien Eldeeb received the B.Sc. and the M.Sc. degree in electronics and electrical communication engineering from Menoufia University and Cairo University, Egypt, in 2008 and 2018, respectively. He joined the Communication Theory and Technologies (CT&T) Research Group as a research and teaching assistant in 2018 working toward his doctorate under the supervision of Prof. Murat Uysal at Özyeğin University, Istanbul, Turkey. He has several practical experiences, having served as a Research Engineer for the EU H2020 Marie Skłodowska-Curie Innovative Training Network (MSCA ITN) and an Instrumentation, Control, and Operation Engineer at Cairo Electricity Production Company, Cairo, Egypt. His current research interests include photonics and optical wireless communications, 6G/mmWave communications, indoor and vehicular visible light communications, channel modeling and measurements.

During his Ph.D., he has 7 accepted/published IEEE journal papers and 12 conference/workshop papers. He also contributed to IEEE standardization task group activities on VLC in a joint work with HHI Fraunhofer. One of his conference papers received the Best Student Paper Award in 12th IEEE/IET International Symposium on Communication Systems, Networks and Digital Signal Processing (CSNDSP), in 2020. He is a member of the IEEE society and IEEE Photonics society.